ADVANCED OPTICAL TECHNIQUES FOR HIGH CAPACITY TRANSMISSION

YAK WAN ANDY LEE

Doctor of Philosophy

ASTON UNIVERSITY

October 2003

ASTON UNIVERSITY

ADVANCED OPTICAL TECHNIQUES FOR HIGH CAPACITY TRANSMISSION

YAK WAN ANDY LEE

Doctor of Philosophy

October 2003

ABSTRACT

This thesis presents several advanced optical techniques that are crucial for improving high capacity transmission systems. The basic theory of optical fibre communications are introduced before optical solitons and their usage in optically amplified fibre systems are discussed. The design, operation, limitations and importance of the recirculating loop are illustrated.

The crucial role of dispersion management in the transmission systems is then considered. Two of the most popular dispersion compensation methods – dispersion compensating fibres and fibre Bragg gratings – are emphasised. A tunable dispersion compensator is fabricated using the linear chirped fibre Bragg gratings and a bending rig. Results show that it is capable of compensating not only the second order dispersion, but also higher order dispersion. Stimulated Raman Scattering (SRS) are studied and discussed. Different dispersion maps are performed for all Raman amplified standard fibre link to obtain maximum transmission distances. Raman amplification is used in most of our loop experiments since it improves the optical signal-to-noise ratio (OSNR) and significantly reduces the nonlinear intrachannel effects of the transmission systems.

The main body of the experimental work is concerned with nonlinear optical switching using the nonlinear optical loop mirrors (NOLMs). A number of different types of optical loop mirrors are built, tested and implemented in the transmission systems for noise suppression and 2R regeneration. Their results show that for 2R regeneration, NOLM does improve system performance, while NILM degrades system performance due to its sensitivity to the input pulse width, and the NALM built is unstable and therefore affects system performance.

KEY WORDS

Optical fibre, optical solitons, dispersion management, fibre Bragg gratings, Raman amplifiers, Stimulated Raman Scattering, optical signal-to-noise ratio (OSNR), nonlinear optical loop mirrors (NOLMs), 2R regeneration

ACKNOWLEDGEMENTS

I would like to acknowledge some of the many people who have, in their own individual ways, contributed to this thesis.

Firstly, I would like to thank my supervisor, Igor Khrushchev, for much needed guidance, support, encouragement and discussions that he provided during my three and a half years at Aston University.

During the early part of this project, I owe a great deal to my ex-team-mates Wladek Forysiak, Paul Harper, Steve Alleston and Nick Doran, who have all gone to Marconi's Solstis, for accepting the opportunities of 'showing me the ropes' in optical fibre communications.

Thanks to all the members of the Photonics Research Group who have helped me at one time or another. Special thanks go to Zhijian Huang, Ashley Gray, Yicheng Lai, Michael Dubov, Keith Blow and Robin Ibbotson for their consistence advice, help and invaluable discussions during this period. Domenico Giannone for providing the chirped gratings for tunable dispersion compensation.

Finally, I'd like to thank my wife Hwee Ping for her continuous emotional support, understanding and patience over the past few years when I was very busy with my research work.

Content

1 Introduction to optical fibre communications 11
1.1 Introduction 11
1.2 Properties of single mode fibres 12
1.2.1 Optical losses 14
1.2.2 Chromatic dispersion 16
1.2.3 Fibre birefringence 20
1.2.4 Fibre nonlinearities 22
1.3 Optical amplifier 25
1.4 RZ, NRZ and soliton 29
1.5 The soliton solution 30
1.5.1 The NLSE with loss – the average soliton 34
1.6 Soliton system design considerations 37
1.6.1 Soliton-Soliton interactions 38
1.6.2 Gordon-Haus jitter 41
1.6.3 The required signal-to-noise ratio 44
1.6.4 Soliton system design 45
1.7 Thesis overview 46
Reference 48

2 The recirculating loop and experimental techniques 52
2.1 Introduction 52
2.2 Design considerations and principle of operation 56
2.3 Burst measurement techniques 62
2.3.1 Clock recovery 63
2.3.2 Q measurement 64
2.4 Pulse width measurement using autocorrelator 67
2.5 Chapter summary 69
References 70

3 Transmission over dispersion managed standard fibre 73
3.1 Introduction 73
3.2 Dispersion profiling 74
3.3 Dispersion compensation 75
3.3.1 40Gbit/s experimental results on dispersion managed systems (EDFA-based system) 79
3.4 Chirped fibre Bragg grating as tunable compensator 82
3.5 Stimulating Raman Scattering (SRS) 88
3.5.1 Feature of the fibre Raman amplifier 92
3.5.2 40Gbit/s experimental results on all-Raman amplified dispersion managed system 97
3.6 Chapter summary 103
References 105

4 Nonlinear Optical Loop Mirror (NOLM) and its application 110
4.1 Introduction 110
4.2 The Nonlinear Optical Loop Mirror (NOLM) 112
4.2.1 The Nonlinear-Imbalanced Loop Mirror (NILM) 117
4.2.2 The Nonlinear-Amplifying Loop Mirror (NALM) 118
4.3 Autosoliton propagation over standard fibre guided by in-line NOLM 121
4.3.1 10Gbit/s autosoliton propagation, BER, eye-diagram and results 123
4.3.2 40Gbit/s autosoliton propagation, BER, spectral evolution and discussion 124
4.4 NILM experiments 126
4.4.1 10Gbit/s results 127
4.4.2 40Gbit/s results 131
4.5 NALM experiments 133
4.5.1 10Gbit/s results 136
4.5.2 40Gbit/s demultiplexing 138
4.6 Chapter summary 141
References 143

5 Thesis conclusion 146

A Publications and patent 152

List of Figures

Figure 1.1:	Cross-section of an optical fibre with the corresponding refractive index profile	13
Figure 1.2:	Typical loss characteristics of single mode optical fibre	15
Figure 1.3:	The material dispersion parameter (Dm), the wavelength dispersion parameter (Dw) and the total dispersion parameter (D) as a function of wavelength for a conventional single-mode fibre	18
Figure 1.4:	Evolution of light polarisation through a birefringent fibre	22
Figure 1.5:	Schematic of an erbium-doped fibre amplifier	26
Figure 1.6:	(a) Absorption spectrum of erbium; (b) Erbium energy diagram	27
Figure 1.7:	EDFA operating characteristics: (a) ASE spectrum; (b) Gain and noise figure as a function of output power at $\lambda = 1545$nm	28
Figure 1.8:	Schematic representation of the pattern 1001110 for (a) NRZ encoding and (b) RZ encoding	30
Figure 1.9:	Variation of the soliton energy with propagation distances over 4 amplifier spans. Due to loss in the fibre, the energy decreases exponentially before restored at each amplifier. The average energy is equal to 1, which is the energy of a fundamental soliton in a lossless fibre	36
Figure 1.10:	Evolution of a soliton pair over 90 dispersion lengths showing the effects of soliton interaction for four different choices of amplitude ratio r and relative phase θ. Initial spacing $q_o = 3.5$ for all four cases	40
Figure 2.1:	Schematic diagram of the recirculating loop	56
Figure 2.2:	Loop timing diagram	60
Figure 2.3:	Clock recovery Set-up. VCO: Voltage Controlled Oscillator, PLL: Phase Locked Loop	63
Figure 2.4:	A typical Q value measurement. Mean and standard deviations of the one level is found in the calculation of the Q	66

Figure 3.1:	Dispersion map, pulse width and spectral width over two map periods of DMS	77
Figure 3.2:	Schematic representation of the recirculating loop transmission experiment	81
Figure 3.3:	BER against propagation distance	82
Figure 3.4:	Eye diagrams of demultiplexed 10Gbit/s data pattern (a) Back-to-back performance (b) Propagation after 1160km	82
Figure 3.5:	(a) Photograph and (b) schematic diagram and working principle of the multipoint mechanical system used to change the dispersion of a linearly chirped FBG	84
Figure 3.6:	Characteristic of time delay verses wavelength of the original chirped grating	85
Figure 3.7:	Experimental set-up used to test the recompression capability of the tuneable FBG on dispersed optical pulse streams at 10 and 40Gbit/s	85
Figure 3.8:	Autocorrelator traces of a 10Gbit/s pulse stream as seen from the Pritel laser (dashed line) and after optimum recompression by the tuneable FBG (bold line). (Inset, the recompressed pulse stream at 40Gbit/s).	86
Figure 3.9:	Chromatic dispersion D and dispersion slope S for the strained grating at 1550nm	87
Figure 3.10:	Figure 3.10: Measured Raman-gain spectrum for fused silica at a pump wavelength $\lambda p = 1\ \mu m$. From reference [40]	90
Figure 3.11:	Signal excursion over distance	94
Figure 3.12:	Typical scheme of fibre Raman amplifier	95
Figure 3.13:	Fibre span configurations	100
Figure 3.14:	(a) OSNR and (b) Q factor of signals after 6 loops of recirculation against pump power of Raman laser 2	102
Figure 3.15:	(a) BER performance and (b) OSNR evolution for different types of span configuration when the longest error free propagation distance was reached	102

Figure 3.16: Eye diagram of 40Gbit/s and demultiplexed 10Gbit/s data stream for a type A span configuration. Upper: after 1970km propagation, Lower: back-to-back 103

Figure 4.1: Schematic of a nonlinear optical loop mirror (NOLM) with coupling coefficient α 113

Figure 4.2: Transmitted power as a function of input power for a nonlinear fibre loop mirror (NOLM), where f = α = coupling coefficient 114

Figure 4.3: (a) Conceptual operation of a dispersion-imbalanced loop mirror (b) Plots of the peak intensity for pulse input as a function of distance along the two propagation directions, counter clockwise (CCW) and clockwise (CW) 117

Figure 4.4: Schematic diagram of a nonlinear amplifying loop mirror (NALM), with gain from an erbium–doped fibre amplifier (EDFA) 118

Figure 4.5: Variation of transmitted power with input power in the NALM, with Gss=20dB, α = 0.5 and L= $\lambda A_{eff}/n_2$ = 1. The saturation power P_{sat} was 5xPs, 2,5xPs and 1.8xPs 120

Figure 4.6: Experimental setup for NOLM to be used as 2R regenerator 122

Figure 4.7: 10Gb/s experiment. (a) propagation in the system with and without the in-line NOLMs. Eye diagrams taken at (b) 4,300 km without in-line NOLM; (c) 11,000 km with in-line NOLM 123

Figure 4.8: 40Gb/s measurements. (a) BER vs distance (b) Q-factor vs distance (c) Eye-diagrams of received 40Gb/s and demultiplexed 10Gb/s signal after i) 2,500 km ii) 4,000 km iii) 6,000 km and iv) 7,500 km 125

Figure 4.9: Spectral evolution of 40Gb/s signal (a) without NOLM 151 (b) with NOLM 126

Figure 4.10: Eye diagrams for 10Gb/s signal. Top eye diagram is the input to DILM, bottom eye diagram is the output from DILM 127

Figure 4.11: Transmission power as a function of input power for a NILM 128

Figure 4.12: Schematic diagram of experimental setup showing the 40Gbit/s data generator, and 40Gbit/s to 10Gbit/s demultiplexer 129

Figure 4.13:	BER vs Receiver Power (dBm) for a filtered and unfiltered 10Gbit/s demultiplexed channel	130
Figure 4.14:	Eye diagrams result for a filtered and unfiltered 10Gbit/s demultiplexed channel	130
Figure 4.15:	Experimental setup. PC: polarisation controller, TA: tunable attenuator, DSF: dispersion-shifted fibre, DCF: dispersion-compensating fibre	131
Figure 4.16:	Switching curves for NILM at 10Gbits and 40Gbit/s	132
Figure 4.17:	Eye diagram for 80 km SMF transmission (a) without DILM and (b) with DILM	133
Figure 4.18:	BER vs received power for back-to-back, output of DILM, 85 km SMF and 85 km SMF + DILM	133
Figure 4.19:	Schematic diagram of a Nonlinear Amplifying Loop Mirror (NALM)	134
Figure 4.20:	Transmitted power as a function on input power for the NALM	136
Figure 4.21:	Experimental setup. PC: polarization controller, ISO: isolator, TA:tunable attenuator, DSF: dispersion-shifted fibre, H.EDFA: high power erbium-doped fibre amplifier	137
Figure 4.22:	(a) Input spectrum before NALM, (b) Output spectrum after NALM	137
Figure 4.23:	Comparison of BER vs threshold voltage for input and output of NALM	138
Figure 4.24:	Eye diagram for (a) BTB, (b) with NALM	139
Figure 4.25:	Comparison of BER vs threshold voltage for input and output of NALM (one recirculating loop, 300 km), triangular – without NALM, squares and circles – with NALM	139
Figure 4.26:	(a), (c) and (e) show the eye diagrams for 1, 2 and 3 recirculating loops without NALM. (b), (d) and (f) show the eye-diagrams for 1, 2 and 3 recirculating loops with NALM	140
Figure 4.27:	Spectrum for 1, 2 and 3 recirculating loops with NALM	141

List of Tables

1	Autocorrelation conversion factors and time bandwidth products for two common pulse shapes	68
2	Fibre parameters	100

Chapter 1

Introduction to optical fibre communication

1.1 Introduction

The phenomenon of total internal reflection, responsible for the guiding of light in optical fibres, has been known since 1854 [1]. Although glass fibres were made [2] – [4] in the 1920s, they became practical only in the 1950s, when the use of a cladding layer led to considerable improvement in their guiding characteristics [5] – [7]. Before 1970, optical fibres were used mainly for medical imaging over short distances [8]. Their usefulness in communication purposes were considered impractical because of the high loss (~ 1000 dB/km). However, the situation changed drastically in 1970 when, following an earlier

suggestion [9], the loss of optical fibres was reduced to about 20dB/km [10]. Further progress resulted by 1979, in a loss of only 0.2 dB/km near the 1.55μm spectral region [11]. Fibre can now be routinely manufactured with a loss, as low as 0.18dB/km at certain wavelength, which is close to the fundamental limit set by Rayleigh scattering. The availability of low-loss fibres led to a revolution in the field of lightwave technology and started the era of optical fibre communications. This low loss allows propagation of optical signal over large distances (~400km) [12] before amplification is required. It also allows nonlinear phenomena to be observed at moderate power levels due to the long interaction lengths which can be achieved [13].

Using all optical systems have allowed the bit rate of trans-oceanic systems to reach 40Gb/s and this data is likely to keep increasing with the demand for new broadband services either through direct increase in the data rate, multiple wavelength channels or a combination of both of these methods.

1.2 Properties of single mode fibres

At the heart of a lightwave communication system, is the optical fibre, which acts as the transmission channel carrying the light beam, loaded with data patterns. The most common type of fibre being used is the step-index fibre (SIF) shown in Figure 1.1. It consists of a dielectric core (usually doped silica) of high refractive index surrounded by a lower refractive index cladding. Other types of fibre include the graded-index fibre, where the refractive index of the core decreases gradually from center to the core boundary, and the multiple cladding fibre, where more than one cladding layer is used.

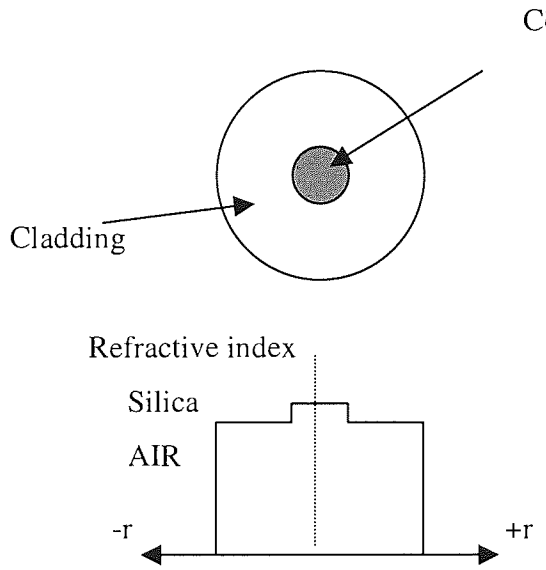

Figure 1.1: Cross-section of an optical fibre with the corresponding refractive index profile

Dopants such as G_eO_2 and P_2O_5 increase the refractive index of pure silica and are suitable for the core, while materials such as boron and fluorine are used for the cladding since they decrease the refractive index of silica. Two very useful parameters that characterise the fibre are the relative core-cladding index difference Δ defined by

$$\Delta = \frac{n_1 - n_2}{n_1} \tag{1.1}$$

and the normalised frequency V defined by [14, 15]

$$V = \frac{2\pi a}{\lambda}\sqrt{n_1^2 - n_2^2} \tag{1.2}$$

where a is the core diameter, λ is the operating wavelength, n_1 is the refractive index of the core, n_2 is the refractive index of the cladding. The normalised frequency V defines the number of modes that are able to propagate within the fibre, although the numbers of modes which are supported also depend on the wavelength of the light. A step-index fibre will support only the fundamental mode (LP_{01}) provided $V < 2.405$. The fibres designed to satisfy this condition are called single mode fibre. If V is above this value,

multimode fibres will occur since more modes will be guided. The main difference between the single mode and multimode fibres is the size of the core. For single mode fibre, the core radius is in the range of 2 – 4 μm. The multimode fibre has a core radius of around 25 – 30 μm. Standard single mode fibre has a refractive index difference of Δ ~ 0.003. In this thesis, whenever the word 'fibre' is being mentioned, it is understood to be single mode and the wavelength of the signal is ~ 1550 nm.

1.2.1 Optical losses

An important fibre parameter is the measure of power loss during transmission of optical signals inside it. The loss of a fibre, α is defined as

$$\alpha = -\frac{1}{L}\ln\frac{P_0}{P_i} \tag{1.3}$$

where P_i is the input power, P_0 is the output power and L is the fibre length. It is customary to express the fibre loss in units of dB/km using the relation

$$\alpha_{dB} = -\frac{10}{L}\log\frac{P_0}{P_i} \tag{1.4}$$

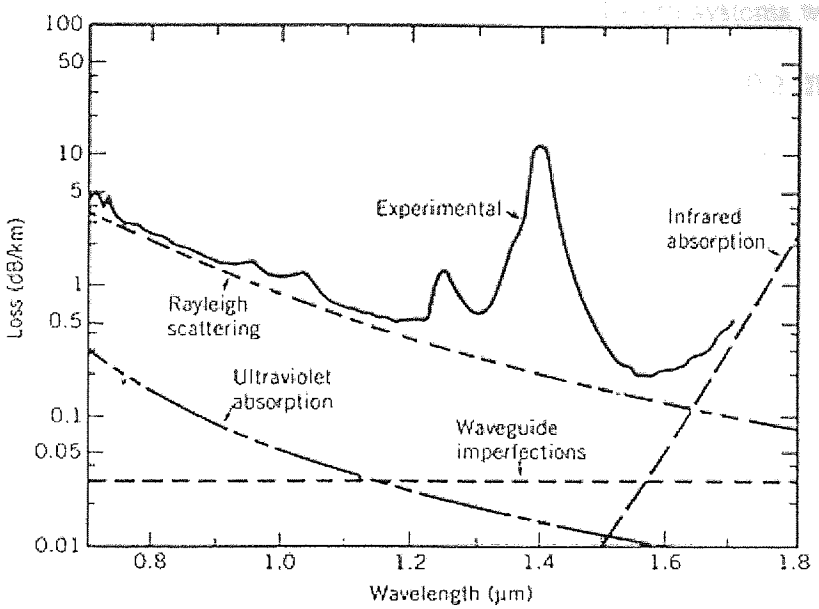

Figure 1.2 Typical loss characteristics of single mode optical fibre. From reference [11]

Figure 1.2 shows the loss spectrum for single mode fibre, together with some of the calculated loss mechanisms. Fibre loss can be caused by intrinsic or extrinsic absorption, Rayleigh scattering, bending losses, and nonlinear effect [14]. Rayleigh scattering is the most dominant intrinsic loss mechanism in modern silica fibres, and is caused by microscopic non-uniformity of refractive index of glass. A ray of light is scattered into many directions, thus some light energy will be lost. Rayleigh scattering is proportional to λ^{-4}, therefore it only dominates at shorter wavelengths. Other intrinsic losses are due to absorption caused by interactions between S_iO_2 and G_eO_2 components within the glass structure which results in electronic absorption in the ultra-violet wavelength region and photon absorption in the infra-red region. Extrinsic absorption is caused by the unwanted materials or impurities within the fibre. Water (OH-ions) is the most dominant absorber in most modern fibres, causing peaks in optical loss at 1.25 μm and 1.39 μm. Modern manufacturing methods are capable of reducing these effects to almost zero. The earliest systems operated in the ~ 0.85 μm region where the loss is ~ 10 dB/km due to the

availability of sources and detectors in this wavelength. Modern systems will use the 1.5 μm region (third communication window) due to its lowest loss ~ 0.2 dB/km and the availability of suitable optical amplifiers at this wavelength. The total loss of a fibre link in optical communication systems also includes splice loss that occurs when two fibres are being joined together. Advances in the fibre technologies have reduced splice loss to as low as ~0.01 dB when joining the same type of fibre.

1.2.2 Chromatic dispersion

In general the response of a dielectric to the interaction of electromagnetic radiation with the bound electrons of the medium depends upon the frequency of the wave. This phenomena is referred to as chromatic dispersion and manifests itself through the frequency dependence of the refractive index, $n(\omega)$. Mathematically, it is accounted for by expanding the mode propagation constant, $\beta = 2\pi n / \lambda$, in a Taylor series about the centre frequency [16], ω_0:

$$\beta(\omega) = n(\omega)\frac{\omega}{c} = \beta_0 + \beta_1(\omega - \omega_0) + \frac{1}{2}\beta_2(\omega - \omega_0)^2 + \ldots + \frac{1}{m!}\beta_m(\omega - \omega_0)^m \qquad (1.5)$$

Where

$$\beta_m = \left(\frac{d^m \beta}{d\omega^m}\right)_{\omega=\omega_0} \qquad \text{m} = 0, 1, 2, \ldots \text{n}$$

Fibre dispersion plays a vital role in the propagation of short optical pulses [15] since different spectral components travel at speeds given by $c/n(\omega)$. The pulse envelop moves with group velocity, $v_g = \mathrm{d}\omega/\mathrm{d}\beta$, and is broadened due to second order dispersion, $\mathrm{d}^2\beta/\mathrm{d}\omega^2$. The wavelength at which the second order dispersion is zero is referred to as the zero dispersion wavelength, λ_0. At this condition, higher order dispersions will then dominate the systems.

The material dispersion referred above relates to that of bulk silica. When silica is used to form a fibre, dielectric waveguiding occurs [16]. The effective mode index is slightly lower than the material index $n(\omega)$ and this reduction is wavelength dependent. Generally, the waveguide contribution to β_2 is negligible except near the zero-dispersion wavelength λ_0 where the two become comparable. The main effect of waveguide dispersion is to shift λ_0 slightly from that of bulk silica. Most of the installed fibre in inland communications networks are step index fibre, SIF, which has λ_0 in the 1300 nm window. However, by changing the refractive indices profile and the core radii, waveguide dispersion of respective fibre can be easily changed. Hence, the design of different types of fibre such as dispersion-shifted fibre (DSF), dispersion-compensated fibre (DCF), etc can be readily produced. All these fibres will have different dispersions and will be discussed later in this section.

Total fibre dispersion is shown in Figure 1.3. It is the sum of material and waveguide dispersion. The total dispersion passes through zero at λ_0, which in standard single-mode fibre is 1.3 μm, the second telecommunication window. The main contribution to the dispersion of standard fibre comes from the dispersion of the fibre material. The sign changes of the dispersion give rise to two distinct regimes, the normal regime where D is negative and the anomalous regime where D is positive. In the anomalous dispersion regime short wavelengths travel faster than long wavelengths and so light propagated through a fibre with anomalous dispersion will emerge with the blue end of the spectrum leading the red. The opposite is true for normal dispersion regime.

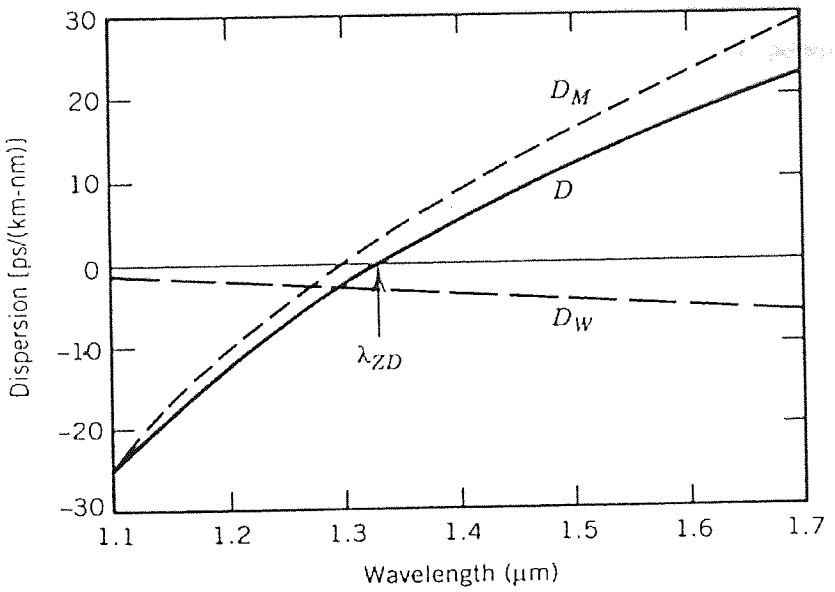

Figure 1.3: The material dispersion parameter (Dm), the wavelength dispersion parameter (Dw) and the total dispersion parameter (D) as a function of wavelength for a conventional single-mode fibre. From reference [11]

From Figure 1.3, it is shown that in the low loss region of 1.55 μm, standard fibre has a high dispersion of ~ +17 ps/nm/km. This will cause problems to the transmission systems since at this wavelength pulse will be broadening significantly due to the high dispersion. Dispersion shifted fibres (DSFs), which has λ_0 in the 1.55 μm region, have therefore been developed for use at this wavelength. However, DSF is not the ultimate solution due to nonlinearity effect namely Four Wave Mixing (FWM), which will occur at low dispersion with high power. Moreover, since most of the existing installed fibres are mainly standard fibres, it will be very expensive and time consuming to change all of them. Other methods of reducing the dispersion is done by including a length of dispersion compensating fibre (DCF) with zero-dispersion wavelength beyond 1.6 μm or using fibre Bragg gratings. Both of these methods will be mentioned in chapter 3 under the section on dispersion management.

Research in fibre area has been very active recently and many new fibres have been developed. A new type of optical transmission line known as dispersion-managed fibre (DMF) has been recently proposed [17] – [19]. It consists in alternately disposed fibre trunks exhibiting positive and negative local dispersion values so that zero dispersion is achieved on the average at the end of the link. Efficient reduction of the FWM penalties has been proven. Most of the recent 40Gbit/s WDM transmissions of multi-Tbit/s capacity for classical long-haul terrestrial application have been achieved using non-zero dispersion shifted fibre (NZDSF) types with chromatic dispersion ranging from 6 to 10 ps/nm/km [20] – [22] in the wavelength range of transmission. Dense channel spacing favours high dispersion values to minimise cross phase modulation (XPM) and four wave mixing (FWM). However, fibre dispersion has to be low enough to reduce the amount of dispersion compensating fibre (DCF) and to manage intra-channel distortion for future very high bit-rates ($\geq$ 40Gbit/s). Photonics crystal fibres (PCFs) are glass optical fibres in which unusual waveguiding effects are created by incorporating an array of air holes running down the fibre length [23]. Modification of group velocity dispersion (GVD) in extruded PCFs has been demonstrated [24].

Finally, a comment on the notation used for GVD. Throughout the derivation above, the group velocity dispersion parameters β_2 was used. However, there is a second notation used throughout much of the rest of this thesis, that of the group delay dispersion D_2 which tends to be a more useful quantity in practical terms. The difference between them is that group delay dispersion D_2 is the second derivation of the refractive index with respect to wavelength rather than frequency. The simple relation between group delay and group velocity dispersion is

$$D_2 = \frac{-2\pi c}{\lambda^2}\beta_2 \qquad (1.6)$$

where D_2 has the units ps/nm/km, and β_2 has the units ps^2/nm.

An important parameter when considering fibre dispersion is known as the dispersion length L_D. L_D is defined as the length over which a transform-limited gaussian pulse will double in width, and is given by [13]:

$$L_D = \tau_0^2 / |\beta_2| \qquad (1.7)$$

where τ_0 is the input 1/e half width of the pulse, related to the full width at half maximum (FWHM) pulse width by:

$$\tau_{FWHM} = 2(\ln 2)^{1/2}\tau_0 = 1.665\,\tau_0 \qquad (1.8)$$

1.2.3 Fibre birefringence

Single-mode fibres are not truly single mode since it can support two degenerate modes polarised in two orthogonal directions [13]. Under ideal conditions of perfect cylindrical geometry and isotropic material, a mode excited with its polarisation in the x-direction will not couple with a mode in the orthogonal y-polarisation. Practically, it is extremely difficult to fabricate a fibre with a perfect geometry, and hence mixing of the polarisation states occurs. Changes in the dimensions of the fibre cross section from a circular to an elliptic symmetry result in differing refractive indices for the two axes, hence both field components will then propagate with different group velocity. This leads to a polarisation dependent group delay, where propagation along one axis is faster than the other; this is known as fast axis. The other axis is known as slow axis. The power between the two modes is exchanged periodically, with the period of evolution referred to as the beat length L_B. In standard single-mode fibre, L_B is typically 1 metre. Therefore, light that is launched into a fibre with a linear polarisation will quickly reach an arbitrary

state of polarisation. While this is not generally a problem for single polarisation transmission, the net difference in the group velocities of the fast and slow axes of the two orthogonal polarisation states can, if large enough, result in a pulse splitting for a randomly orientated input polarisation components. This effect, known as polarisation mode dispersion (PMD), is not often a significant problem with new optical fibre due to the improvements in the manufacturing process. However, since majority of the installed fibres are old fibres, PMD can have a very significant effect and make upgrading to higher data rates with NRZ formats extremely difficult [25]. Although PMD's effects resemble those of chromatic dispersion, there is an important difference. Chromatic dispersion is a relatively stable phenomenon. The total chromatic dispersion of a telecommunications system can be calculated from the sum of its parts, and the location and value of dispersion compensators can be placed in advance. In contrast, the PMD of single mode fibre at any given signal wavelength will not be stable, forcing system designers to make statistical predictions of the effects of PMD.

When considering old fibres and other devices, another polarisation effect known as polarisation dependent loss (PDL) becomes very important. PDL occurs when the loss through a device depends on the input state of polarisation. Small flexures in an optical fibre can dramatically change the polarisation transfer function of a fibre. A component with PDL will convert these polarisation fluctuations into the system and change the loss. In particular, lithium-niobate modulators, used to impose data on a pulse stream, tend to be highly polarisation sensitive due to the waveguiding used for these slab devices, with PDL values around 10 dB quite common. Generally such high polarisation dependent losses must be avoided, with polarisation controllers used to set the appropriate state for minimum loss for a single polarisation signal. Although the deviations of the two

refractive indices from each other are low, the birefringence cannot be neglected if long transmission distances are to be realised.

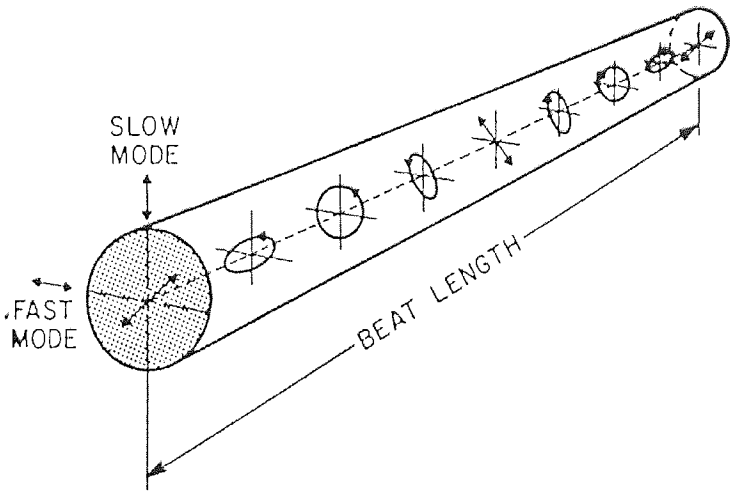

Figure 1.4: Evolution of light polarisation through a birefringent fibre. From reference [13]

Polarisation-maintaining fibre intentionally introduces a large amount of birefringence so that small random birefringence fluctuations do not significantly affect the polarisation. If the polarisation axis of the launched light coincides with the slow or fast axis of the fibre, the polarisation will remain unchanged during propagation. If the polarisation axis makes an angle with these axes, the polarisation changes continuously along the fibre in a period equal to the beat length. A possible application of this fibre is to allow the capacity of systems to be doubled by using different polarisation states to carry different data channels. This method is called polarisation division multiplexing (PDM) [26].

1.2.4 Fibre nonlinearities

In the previous section the linear fibre characteristics that must be accounted for when designing an optical transmission system was highlighted. These limitations may be easily overcome by the use of periodic signal boosting to offset the loss and by operating the system at zero-dispersion wavelength to reduce the pulse broadening effect due to

chromatic dispersion. However, since the response of any dielectric to light will become nonlinear for intense electromagnetic fields, optical fibre will be no exception. This slight nonlinearity can cause severe pulse distortion on systems even when operating on zero-dispersion wavelength. In general, nonlinear effects will cause system impairments and many attempts have been made to avoid or minimise them. However, under certain circumstances, they can be very useful in enhancing system performances. Some of the examples include pulse compression [27], balance the effects of nonlinearity with dispersion to produce optical solitons that allow distortion free transmission over long distances [28], perform nonlinear optical switching by using nonlinear fibre-loop mirror for pulse regeneration and demultiplexing. As a result, nonlinearity in optical fibre transmission has received increasing attention in laboratories worldwide since the last decade. At low power levels the fundamental phenomenological equation that describes the response of a dielectric medium to an optical field is [13]

$$P(\omega) = \varepsilon_0 \chi(\omega) E \tag{1.9}$$

where P is the induced polarisation, E is the electric field, χ is the susceptibility and ε_0 is the vacuum permittivity. At optical frequencies, the polarisation is established by the displacement of electrons relative to the atomic nuclei, so that each atom becomes a dipole oscillating at the frequency of the optical wave. For fields that are considered small compared to that which binds an electron, the induced oscillations are essentially harmonic resulting in a constant χ. At higher power levels the applied field causes harmonic motion of the bound electrons and the relationship between the polarisation vector and the applied field becomes nonlinear and is given by [13]

$$P = \varepsilon_0 \left[\chi^{(1)} E + \chi^{(2)} EE + \chi^{(3)} EEE + \ldots \right] \tag{1.10}$$

The linear susceptibility $\chi^{(1)}$ represents the dominant contribution of P. The second–order susceptibility $\chi^{(2)}$ is zero for symmetric molecule such as silica. The third-order susceptibility is responsible for effects such as four-wave mixing (generation of new frequencies due to phase matching), self-phase modulation (self-induced phase shift when propagating in the fibre) and cross-phase modulation (nonlinear phase shift causing by interaction between two waves propagating along the same fibre.). An important characteristic of cross-phase modulation is that for equally intense optical fields, the contribution of cross-phase modulation (XPM) to the nonlinear phase shift is twice compared with that of self-phase modulation (SPM).

So far, all the nonlinear effects governed by the third-order susceptibility $\chi^{(3)}$ are elastic in the sense that no energy is exchanged between the electromagnetic field and the dielectric medium. A second class of nonlinear effects results from stimulated inelastic scattering in which the optical field transfers part of its energy to the nonlinear medium. Two important effects in optical fibres fall in this category and both of them are related to the vibrational excitation modes of silica. These phenomena are known as stimulated Raman scattering (SRS) and stimulated Brillouin scattering (SBS) and they were among the first nonlinear effects studied in optical fibres [29, 30]. The main difference between the two is that optical phonons participate in SRS while acoustic phonons participate in SBS. In a simple quantum-mechanical picture applicable to both SRS and SBS, a photon of the incident field (often called the pump) is annihilated to create a photon at the downshifted Stokes frequency and a phonon with the right energy and momentum to conserve the energy and the momentum. Of course, a higher-energy photon at the so-called anti-Stokes frequency can also be created if the phonon of right energy and momentum is available. Even though SRS and SBS are very similar in their origin,

different dispersion relations for acoustic and optical phonons lead to some basic differences between the two. A fundamental difference is that SBS in optical fibres occurs only in the backward direction whereas SRS dominates in the forward direction.

1.3 Optical amplifier

Optical amplifiers allow the direct amplification of light without the need for optical to electrical conversion. They provide the amplification necessary to overcome the loss associated with optical transmission. Before the discovery of EDFA, periodically, spaced electronic repeaters were being used to overcome the effects of loss and pulse dispersion. In these repeaters, the input optical signal is first detected and then converted to electrical signals. These electrical signals were then processed (reshaped and retimed) to remove the effects of pulse dispersion and then amplified to drive an optical source, thus regenerating the pulse train. Such repeaters are also being referred to as 3R repeaters (retiming, reshaping and regenerating). Hence the signal emerging from the optical source at the repeater is almost as good as the start of the link and can be sent through the next segment of the link. However, the 3R repeaters have some major setbacks. They are very expensive to implement and maintain, work only at designated bit-rate, limit to the speed of the system due to its conversion between optical to electrical domain, and the electronic processing are required in an electrically regenerated system. An important application for long-haul telecommunication systems consists of replacing these 3R repeaters with optical amplifiers. Such a replacement can be carried out as long as the cumulative effects of dispersion and spontaneous emission, which will be discussed later in this section, do not limit the system performance.

Optical amplification may be achieved from the transmission fibre by several different methods namely Brillouin [31] or Raman effects (see chapter 3), from

semiconductor devices [32, 33] or from fibre doped with earth elements. The preferred choice for application in the 1550 nm window of transmission fibre is the erbium-doped fibre amplifier (EDFA) due to its wide gain in this region. The configuration of a typical EDFA is shown in Figure 1.5.

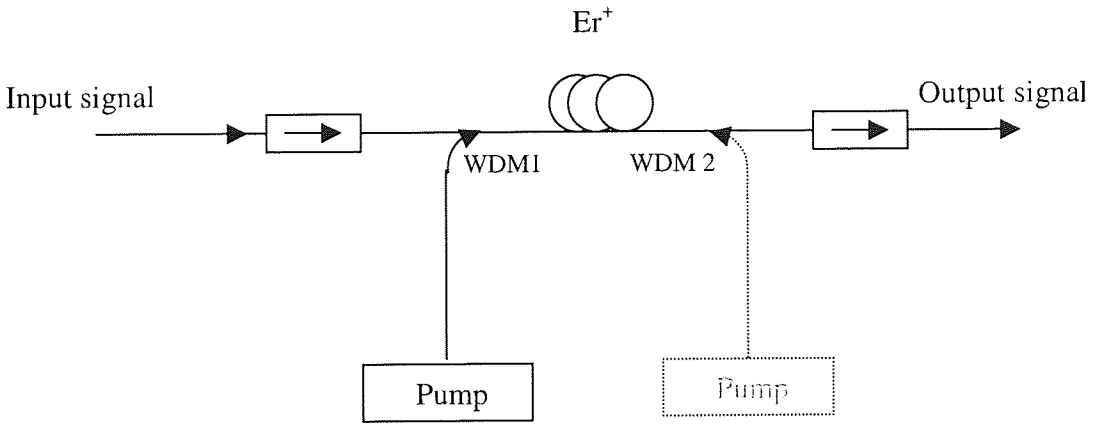

Figure 1.5: Schematic of an erbium-doped fibre amplifier

An EDFA consists of a length (~25m) of erbium-doped fibre, an optical pump laser to provide the necessary population inversion, an optical isolator to prevent any instability from back reflections, and a wavelength division multiplexing (WDM) coupler to combine the signal and pump in the amplifying fibre. Using such an EDFA, gains as large as 30 – 35dB can be readily achieved. The behaviour and performance of erbium-doped fibre amplifiers are determined by a large number of parameters, which have to be optimised according to the needs of each application. If the pump and signal propagate in the same direction, then the amplifier is said to be forward pumped [34]. Amplifiers with this type of configuration have the best characteristics in term of noise figure and optical gain at a fixed pump power, but suffer from low saturated output power. If the pump and signal propagate in the opposite direction, then a higher saturated output power can be achieved and this is known as backward pumping [34]. However, in order to achieve high gain, low noise figure and high-saturated output power, the amplifier can be bi-

directionally pumped [34]. For a given amplifier length L, amplifier gain initially increases exponentially with pump power, but this increment becomes much smaller when the pump power exceeds a certain value. Furthermore, for a given pump power, amplifier gain becomes maximum at an optimum value of L and drops sharply when L exceeds this optimum value. The reason is because the end portion of the amplifier will remain unpumped and absorb the amplified signal.

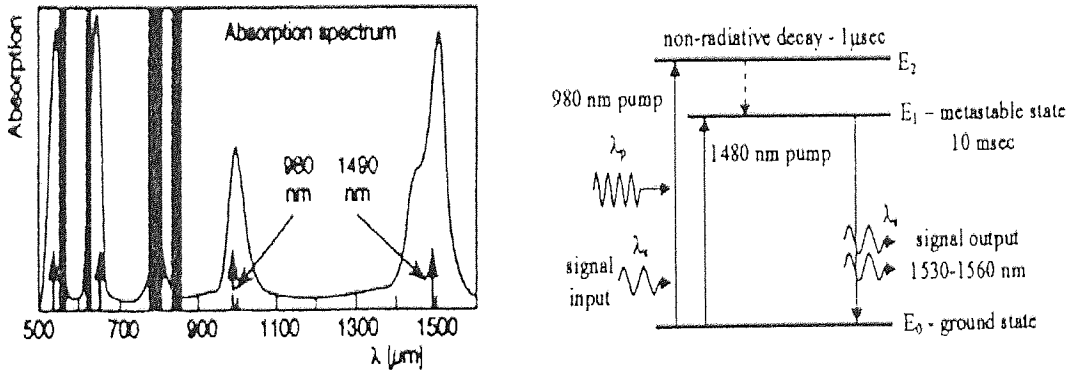

Figure 1.6: (a) Absorption spectrum of erbium; (b) Erbium energy diagram. From reference [35]

Figure 1.6a shows the absorption spectrum of erbium with a number of possible pumping wavelengths for achieving the required population inversion. Highest gain is achieved by pumping at either 980 nm or 1480 nm. The shaded bands indicate regions of excited state absorption where the multiplicity of energy levels of Er^{3+} ions sitting on energy level E_2 can also be absorbed by the pump radiation and get excited to higher level, hence pump efficiency is significantly reduced [35].

The principle of operation can be understood by referring to Figure 1.6b, which shows an energy level diagram of the erbium ion. Considering pumping at 1480 nm, the incoming pump wavelength excites electrons from the ground state E_0 to the higher energy metastable state E_1, creating population inversion. A photon is then emitted when a transition occurs between the metastable state E_1 and the ground state E_0. This can be

caused by either random spontaneous decay (causing optical noise) or it can be due to stimulated emission from the signal photon in the 1550 – 1560 nm wavelength band. A pump photon at 980 nm causes excitation to a higher energy state E_2, from which it decays down to the metastable state E_1, losing energy as it does so. Transitions from the metastable state are similar to the 1480 nm pumping mentioned above. For low pump power, although Er^{3+} ions are getting excited to the E_1 level, population inversion may not exist because of spontaneous emission. Then the signal beam at 1550 nm will get attenuated (due to absorption) rather than amplified. For high pump power, the rate of excitation increases and at some power level, population inversion between E_0 and E_1 can then be achieved, hence signal around 1550 nm will be amplified rather than absorbed.

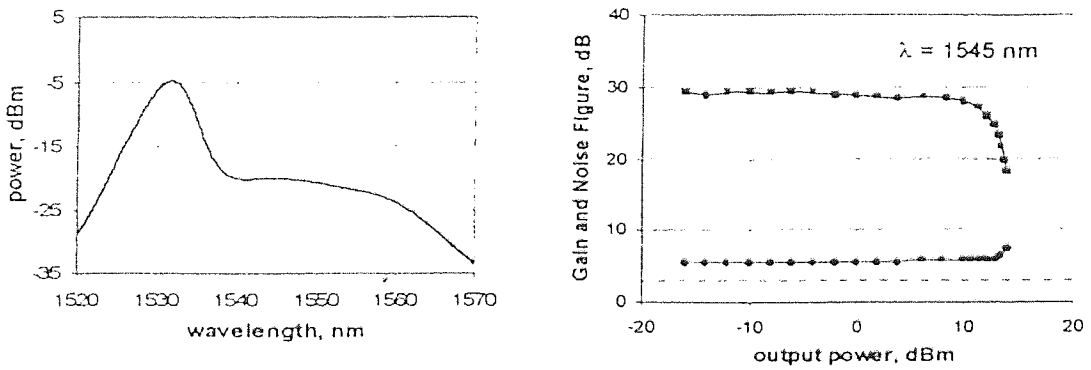

Figure 1.7: EDFA operating characteristics: (a) ASE spectrum; (b) Gain and noise figure as a function of output power at λ = 1545nm. From reference [34]

Typical gain characteristics are shown in Figure 1.7. Erbium amplifiers are typically polarisation insensitive, have gains of > 25dB, saturated output power of > 10dBm, and a noise figure of 3 – 7 dB depending on the pump wavelength and configuration [36]. Nonlinear amplifying loop mirror, which makes use of the amplifier to introduce asymmetry within the loop so as to create a differential phase shift, is being built and tested in chapter 4 for noise suppression and 2R regeneration.

1.4 RZ, NRZ and soliton

In a linear or non-return-to-zero (NRZ) modulation format (Figure 1.8), the optical intensity is turned on-off with the bit-period equal to the inverse of the electrical modulation rate or bit-rate. Any appreciable fibre dispersion (due to the wavelength-dependent mode shape and variation of the refractive index) leads to pulse spreading and energy spill over into the following bit-period, resulting in transmission penalties. The competing technology, the transmission of return-to-zero (RZ) pulses (Figure 1.8), whose duration is much less than the bit-period, say by a factor of 3 – 5, was initially considered a solution to nonlinear interactions, and specifically self-phase modulation induced distortion. These soliton-like pulses balance the effects of self-phase modulation and fibre dispersion to allow long-distance transmission without pulse broadening, which is sometimes referred to as nonlinearity-supported transmission. RZ pulse generation itself is the subject of some considerable research, and RZ pulses are a prerequisite for OTDM transmission, since a number of pulses must be time interleaved within the bit-period to generate a much higher aggregate signal as in chapters 3 and 4. In fact, RZ pulses may or may not evolve into soliton pulses, depending on their energies and total transmission distance. Strictly speaking, a soliton is a pulse that does not spread in time or frequency on transmission, independent of distance. Later in this chapter, soliton solution will be discussed in more detail.

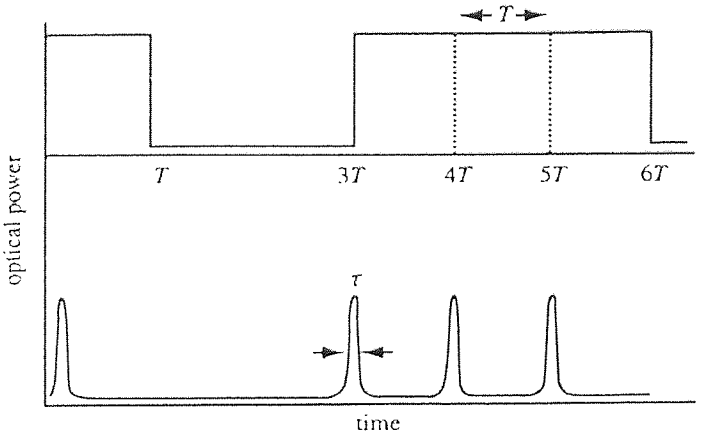

Figure 1.8: Schematic representation of the pattern 1001110 for (a) NRZ encoding and (b) RZ encoding. From reference [14]

Both NRZ and RZ are amenable to wavelength multiplexing; with the RZ format obviously more spectrally demanding, given much shorter initial pulses, which require greater channel spacing. Therefore, there has been a great debate as to which format will be more effective for wavelength division multiplexing (WDM) systems, but this will not be discussed here as it is not within the scope of this thesis, which mainly concentrates on single channel OTDM transmission systems.

1.5 The soliton solution

The combined effects of GVD and SPM lead to a significantly different variation in the pulse dynamics from either case separately. It is possible that under certain conditions, SPM and GVD will co-operate in such a way that they exactly cancel each other, and the optical pulse will then be able to propagate undistorted in the form of a soliton. Initially, we shall look at the lossless case where the governing equation is the Nonlinear SchrÖdinger Equation (NLSE) with the loss coefficient $\alpha = 0$ giving [13]

$$i\frac{\partial A}{\partial Z} = \frac{1}{2}\beta_2\frac{\partial^2 A}{\partial T^2} - \gamma|A|^2 A \tag{1.11}$$

To normalise this equation we use

$$u = N\frac{A}{\sqrt{P_0}}, \xi = \frac{Z}{L_D}, \tau = \frac{T}{\tau_0} \tag{1.12}$$

where N is defined as

$$N^2 = \frac{L_D}{L_{NL}} = \frac{\gamma P_0 \tau_0^2}{|\beta_2|} \tag{1.13}$$

to give

$$i\frac{\partial u}{\partial \xi} + \frac{1}{2}\frac{\partial^2 u}{\partial \tau^2} + |u|^2 u = 0 \tag{1.14}$$

where we have taken the case for the anomalous dispersion regime (sgn (β_2) = -1). For the normal dispersion regime, the second derivative with respect to time will be a minus sign. This equation has been solved by the inverse scattering method in terms of eigenvalues.

The method was first proposed by Gardner et al. [37] and was used to solve the NLSE by Zakharov and Shabat [38]. The inverse scattering method which will not be discussed here is similar to the inverse Fourier transform method used to solve linear partial differential equations. While higher order solutions do exist (N > 1), the solution of most interest here is the single eigenvalue solution which corresponds to N = 1 and has the general form of

$$u(\xi, \tau) = 2\eta_1 \sec h(2\eta_1 \tau) \exp(2i\eta_1^2 \xi) \tag{1.15}$$

The eigenvalue η_1 determines the soliton amplitude. The canonical form of the fundamental soliton is obtained by choosing u(0, 0) = 1 so that $2\eta_1 = 1$. Hence Equation (1.15) becomes

$$u(\xi, \tau) = \sec h(\tau) \exp(i\xi / 2) \tag{1.16}$$

This equation shows that if a hyperbolic-secant pulse whose width τ_0 and the peak power P_0 are chosen such that N = 1, is launched inside an ideal lossless fibre, the pulse will propagate undistorted without any change in shape for arbitrary long distances. It is this feature of the fundamental solitons that makes them attractive for information transmission in optical communication systems. Although it must be mentioned that the pulse does acquire a phase that increases linearly with propagation but this phase has no temporal dependence and so the pulse does not become chirped as it propagates. Therefore no change will occur to the pulse spectrum. There are further solutions to the NLSE and of particular interest are the higher order solitons that have the initial form

$$u(0,\tau) = N \sec h(\tau) \tag{1.17}$$

where N is an integer that denotes the soliton order. The peak power necessary to launch the Nth-order soliton is obtained from Equation (1.13) and is N^2 times of that required for the fundamental soliton with the same pulse width. Unlike fundamental solitons, the higher order soliton undergoes a complicated evolution, with the pulse splitting as it propagates but it is periodic and the soliton returns to the original form at $z = m\pi/2$ where m is an integer [13], or in physical units as

$$Z_0 = \frac{\pi}{2} L_D = \frac{\pi}{2} \frac{|\tau_0^2|}{|\beta_2|} = 0.322 \frac{\pi \tau_{FWHM}^2}{2|\beta_2|} \tag{1.18}$$

This soliton period is frequently used as a length scale for describing the evolution of a soliton under various effects and perturbations. For a 10ps (FWHM) pulse, the soliton period is ~2.5km in standard fibre and ~25km in DSF. An alternative way to consider the formation of solitons as found from the NLSE is to consider the chirps that are imposed on a pulse by GVD and SPM. The sign of the GVD induced chirp depends on dispersion parameter β_2, whilst that from the SPM is always the same. In the normal dispersion

regime this leads to a combined and detrimental effect. But in the anomalous dispersion regime the signs of these two chirps oppose each other. The formation of a soliton can thus be thought of as the pulse shape that gives the correct frequency chirp balance between GVD and SPM, with the pulse width and power chosen such that the SPM chirp contribution exactly balances the GVD chirp. As such there is no build up of any temporal chirp across the pulse and hence no temporal spectral broadening.

Another important feature of solitons is their resilience to perturbations. If the soliton width or spectrum is slightly changed, the soliton will try to adjust itself so as to remain soliton-like. This resilience of solitons does gives rise to unusual and undesirable effect such as Gordon-Haus timing jitter which will be discussed later. It is also possible to excite a soliton even if the pulse launched into the fibre is not of the exact shape, power or chirp required for a soliton. This is because the pulse will ultimately evolve into a soliton after propagation with the excess energy being shed as dispersive radiation [39] – [42]. In a soliton communication system, this shedding has to be minimised or avoided as much as possible since the dispersive radiation would add to the background noise and degrade the signal to noise ratio. Hence, it is therefore very important to use the correct power and pulse shape in soliton systems.

This simple analysis has shown that optical solitons have many of the attributes of the ideal pulses for optical communications systems. They are stable against perturbation; have a stable pulse width and spectrum on propagation and owe their existence to an interplay between the troublesome effects of GVD and SPM. However, in the above we have made several omissions including one particularly important one, the effect of fibre attenuation, which will be considered next.

1.5.1 The NLSE with loss – the average soliton

The major problem for solitons in an optical fibre resulting from the loss is that the decrease in the power of the pulse results in decays in the nonlinear effect it experiences, removing the balance between dispersive and nonlinear chirps. If an N = 1 soliton is launched into the optical fibre this decay in the nonlinear effect results in pulse broadening as the GVD chirp gradually becomes dominant over that from the SPM. In order to balance up the effect of loss, the power must be re-amplified periodically before the signal is lost to the noise propagating with it [43]. For soliton systems, this can be done optically with EDFAs since changes to the pulse shape will not be too significant. However, they have to ensure that dispersion will not destroy the soliton [44] – [46]. This has led to the concept of the *average soliton*, which has a major impact on the propagation of solitons in real optical fibres. In discussing the average soliton, we shall see that the EDFA has been instrumental in the elevation of solitons to a practical transmission format for optical communications. However, EDFAs do introduce noise to the optical signal. (This will be addressed later in this chapter under the section on Gordon-Haus jitter.) We consider the effects of distributed loss and periodic discrete gain have on soliton propagation. The EDFA can be taken as a discrete amplifier as its length (typically in a few metres) is short compared to the fibre transmission length between amplifiers (a few 10's of kilometres). We return to the NLSE with loss and normalise as before Equation (1.11) to obtain

$$i\frac{\partial u}{\partial \xi}+\frac{1}{2}\frac{\partial^2 u}{\partial \tau^2}+|u|^2 u=-i\Gamma u \tag{1.19}$$

where u represents the electric-field amplitude and Γ represents the normalised loss

$$\Gamma=\frac{\alpha}{2}L_D \tag{1.20}$$

The amplifier power gains are $G = e^{2\Gamma\xi_a}$, where ξ_a is the normalised amplifier spacing. After introduction of the transformation $u(\xi,\tau) = \Lambda(\xi)R(\xi,\tau)$, Equation 1.19 becomes

$$i\frac{\partial R}{\partial \xi} + \frac{1}{2}\frac{\partial^2 R}{\partial \tau^2} + \Lambda^2(\xi)|R|^2 R = 0 \tag{1.21}$$

where

$$\Lambda^2(\xi) = \Lambda^2(0)e^{-2\Gamma\xi} \tag{1.22}$$

Thus, the exponential energy variation in the NLSE is equivalent to an exponential variation, $\Lambda^2(\xi)$, in the nonlinear coefficient of the lossless NLSE. If the period of $\Lambda^2(\xi)$ is short on the characteristic length scale of the soliton evolution ($L_a << Z_0$, or equivalent $\xi_a << \pi / 2$), its average is a good approximation in Equation (1.21) and called *average soliton model* [44, 46, 48]. By averaging the variation of $\Lambda^2(\xi)$ over first amplifier span and equating it to the desired normalised average value of 1

$$\left\langle \Lambda^2(\xi) \right\rangle = \frac{1}{\xi_a}\int_0^{\xi_a} \Lambda^2(\xi)d\xi = 1 \tag{1.23}$$

gives

$$\Lambda^2(0) = \Lambda_0^2 = \frac{2\Gamma\xi_a}{1 - e^{-2\Gamma\xi_a}} \tag{1.24}$$

$$= \frac{G\ln G}{G-1} \tag{1.25}$$

where Λ_0^2 is the peak amplitude of the input average soliton. The peak power of the average soliton is then given by

$$P_0 = \Lambda_0^2 \frac{|\beta_2|}{\gamma\tau_0^2} \tag{1.26}$$

which is a factor Λ_0^2 higher than the peak power for a fundamental lossless soliton. By analogy with the equation for the peak power of higher order solitons, Λ_0^2 is often written

as N^2 but for an average soliton N, it is not necessarily an integer as is the case for lossless higher order solitons. As an example consider a 40km span of fibre with a loss of 0.2dB/km. α is then 0.046km^{-1} and so G = exp (0.046 x 40) = 6.3. This gives $\Lambda_0^2 \sim$ 1.8 and so the power of the average soliton is 1.8 times that of the fundamental soliton.

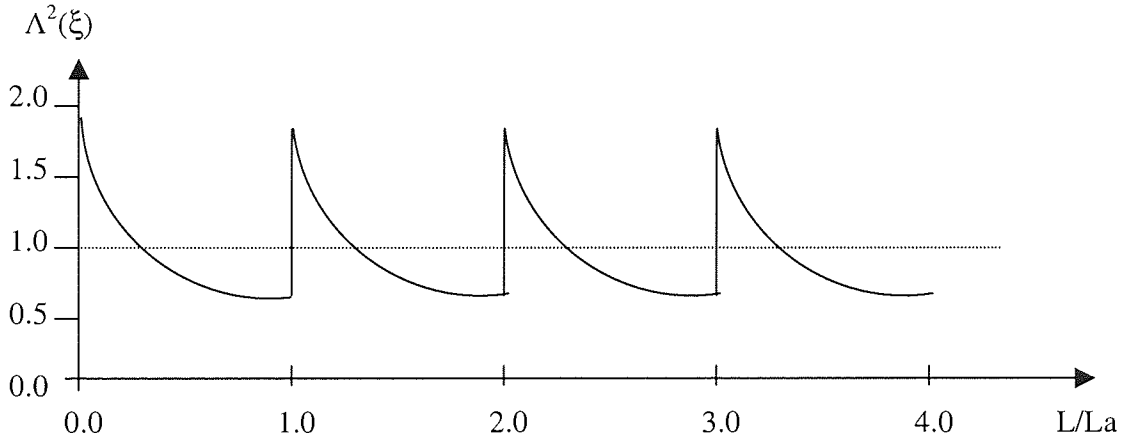

Figure 1.9: Variation of the soliton energy with propagation distances over 4 amplifier spans. Due to loss in the fibre, the energy decreases exponentially before restored at each amplifier. The average energy is equal to 1, which is the energy of a fundamental soliton in a lossless fibre. From reference [47]

Average solitons can propagate along real systems, which have distributed loss and periodic amplification, with little distortion provided that the amplification period is much shorter than the soliton period. Moreover, the input amplitude must be set correctly and the amplifiers must compensate exactly for the total loss of the preceding span (this total loss comprising the fibre loss and losses due to the components).

Figure 1.9 shows the variation in the soliton energy on propagation along a few amplification periods of such a system. Essentially, the average soliton model balances the excess nonlinear chirp of the initial sections of propagation between amplifiers with the excess dispersive chirp of the second part so that on average the dispersion and nonlinearity balance. Diagrammatically, this is equivalent to the area above and below the $\Lambda^2(\xi) = 1$ line being equal.

It must be mentioned that the way soliton reacts to the energy loss strongly depends on the normalised loss Γ and the amplifier spacing L_a. If the amplifier spacing is much smaller than the dispersion length L_D, the soliton shape is not distorted significantly despite the energy loss. The reason is that optical amplifiers boost the soliton energy to the input level locally over a relatively short distance without allowing for gradual recovery of the fundamental soliton. The amplified soliton adjusts its width dynamically in the fibre section following the optical amplifier. However, it also sheds a part of its energy as dispersive waves during their adjustment phase. This dispersive wave can accumulate to significant levels over a large number of amplification stages and must be avoided.

1.6 Soliton system design considerations

Now that the properties and effects of optical fibre transmission and solitons have been introduced, we can consider the requirements for designing an optical soliton transmission system. Various trade-off are necessary to design any given system for its competing requirements. In general, soliton system design falls into two main areas namely short and long haul. Short haul systems are taken here to mean distances of hundreds of kilometres and long haul systems are taken to be trans-oceanic lengths (thousands of kilometres). The length of system changes the emphasis of the design constraints as discussed below. One very important consideration for any length of soliton system is that of the average soliton limit to the amplifier spacing, $L_a << Z_0$.

Typically systems designers take a factor of 10 for safety to mean "much less than" the full soliton period ($8Z_0 = 2\pi$), giving this limit as $La < 8/10Z_0$ [49]. The other

problems considered here are those of soliton interactions, random timing jitter and the signal-to-noise ratio (SNR) requirements.

1.6.1 Soliton-soliton interactions

For high speed transmission system it is desirable that solitons be placed as close together as possible in order to maximise the possible data rate achievable. It is therefore important to assess how closely two solitons can be placed without detrimental effects. Unfortunately the nonlinearity of the optical fibre that leads to the existence of solitons also provides the mechanism for interaction between the solitons. This topic has attracted a great deal of interest over the last few years [50] – [52], as have potential methods of dealing with the problem [53] – [55]. There are two main cases to consider when studying soliton interactions. The first applies to solitons in optical time-division multiplexed (OTDM) systems where interactions of solitons occur in equal frequency. A pair of solitons at the input to a transmission fibre can be described as [13] pp.171

$$u(0,\tau) = \sec h(\tau - \frac{T_R/2}{\tau_0}) + r\sec h\left(r(\tau\frac{T_R/2}{\tau_0}\} \right) e^{i\theta} \qquad (1.27)$$

where $T_R = 1/R$ is the initial separation (R is the data rate), r is the relative amplitude and θ is the relative phase of the two input pulses. The solutions for this input to the NLSE have been calculated by the inverse scattering method, perturbation theory, as well as numerical simulations [56]. It has been shown that two solitons in phase ($\theta = 0$) and of equal amplitude (r = 1) will periodically be attracted and collapsed upon propagation, as shown in Figure 1.10. If the separation is comparatively large compared with the pulse width ($T_R >> 2T_0$) the pulses will collapse and separate with a period [13]

$$Z_p = Z_0 \exp\left(\frac{T_R/2}{\tau_0}\right) = Z_0 \exp\left(\frac{1}{2R\tau_0}\right) \qquad (1.28)$$

In the lossless case, the first collapse will occur at the midpoint of this period and so in order to avoid problems associated with the soliton collapse, system length must be less than $Z_p/2$. Alternatively, and more frequently used, if the solitons are separated by a sufficient mark-to-space ratio, the exponential of Equation (1.16) will be large enough to avoid interaction over global distances. Generally the mark-to-space ratio is between 1:6 and 1:10. Referring to Equation (1.18), since the collapse length is proportional to the square of the pulse width and inversely proportional to dispersion, hence low dispersion for the system is much more desirable, as is the case of Gordon-Haus effect, which will be discussed in detail later. If the pulses are out of phase ($\theta = \pi$), the interaction becomes repulsive even for small values of θ and soliton separate, as shown in Figure 1.10. While repulsion may initially seem to be more desirable for soliton system design to avoid any pulse collapse of in-phase solitons, but there will not however be a complete cancellation. Since there will be empty bit slots in the data stream representing zero leading to uneven forces on some of the solitons. When $\theta = \pi/2$ or $3\pi/2$, there is no interaction between the solitons but this point is very unstable and is inappropriate for real systems. So far we have only considered pulses of equal amplitude ($r = 1$). The case where the amplitudes are unequal has attracted a certain amount of interest [57] – [59], and the effect of soliton interaction is greatly reduced due to the intensity difference leads to a difference in the phase evolution rates for the two pulses and so attractive and repulsive forces are largely cancelled. This effect has been used successfully to propagate solitons for 11500 km at 20 Gbit/s [56] and 500 km at 80 Gbit/s [59].

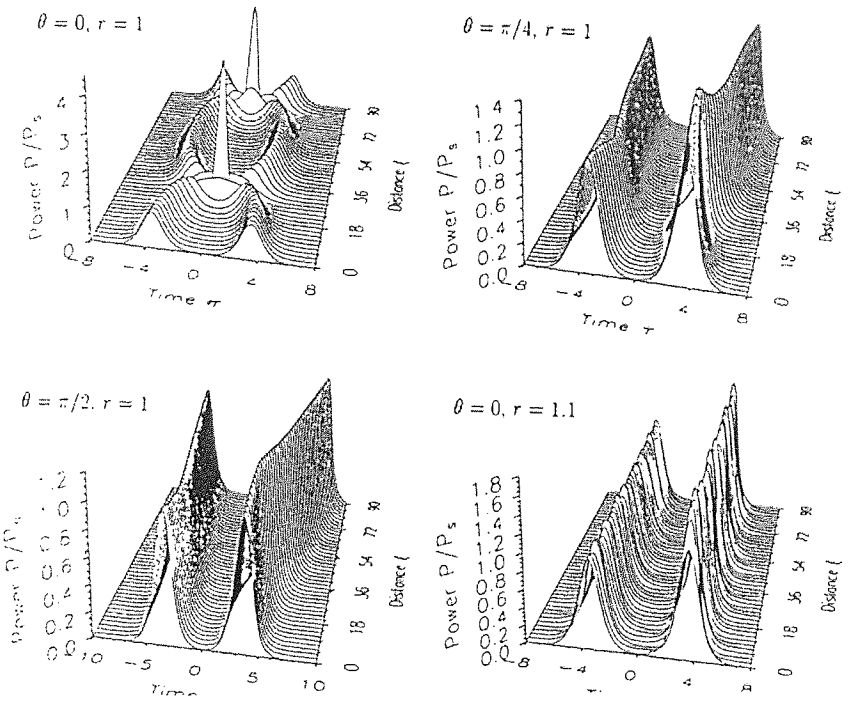

Figure 1.10: Evolution of a soliton pair over 90 dispersion lengths showing the effects of soliton interaction for four different choices of amplitude ratio r and relative phase θ. Initial spacing q_o = 3.5 for all four cases. From reference [52]

The other distinct soliton interaction case is that of solitons of different frequencies, as used in a wavelength-division multiplexed (WDM) communication system [56], [60] – [62]. For this case, solitons from different channels will travel at different speed due to the difference in GVD and hence will collide and interfere periodically when they are in conjunction. After such a collision, pulses from different channels emerge intact but there is a modification to the relative temporal positions of the pulses due to the temporal change in the refractive index [49, 60]. Due to the random data imposed on the communication system, the pulses of one channel will not always encounter a pulse from the other channel, thus resulting in a random number of temporal shifts for any given pulse encounters. Over a long-haul communication system, the temporal shift can become significant and thus limit how closely WDM channels can be placed. As only

single channel propagation is considered here, interactions between solitons of different frequencies will not be considered in our systems design and discussion.

1.6.2 The Gordon-Haus jitter

It was mentioned above that solitons are resilient to perturbations, as they will try to re-attain the stable soliton solution if perturbed. This can lead to somewhat unusual consequences, such as random timing jitter solitons experience in long transmission systems, known as the Gordon-Haus jitter as the solitons propagate [49, 63]. The Gordon-Haus effect is a result of the ASE noise introduced by the EDFAs to the propagating signal. This noise affects all four parameters required to define a soliton, namely temporal position, spectrum, pulse width and phase, but the most important perturbation is found to be that experienced by the soliton spectrum [64]. The soliton will absorb the random noise spectrum of the EDFA while maintaining a soliton nature, leading to a random frequency shift at each amplification stage. While the interaction between the soliton and noise is small, the combined effect of many amplifiers can lead to a significant frequency shift at the end of the system. Through the effect of GVD, which causes different frequencies to travel at different speed along the fibre, this random frequency shift is translated into a random timing shift of the soliton from the centre of the allotted timing slot in the data stream. Over a long propagation distance, this will result in difference in the arrival time of the pulse from the centre of its nominal bit slot. It is this random time shift that is known as Gordon-Haus timing jitter.

Briefly, Gordon-Haus timing jitter comes from the change in the group delay of a pulse over one amplifier span L_a of $\Delta t_g = \beta_2 L_a \Delta\omega$ for a frequency change $\Delta\omega$. By considering an assemble of pulses and summing their variation over the full system

length an estimate of the standard variation of the pulse arrival time $<t_N^2>^{1/2}$ can be derived as [63]

$$<t_N^2>=\frac{2\pi n_2 N_{sp}|\beta_2|hc(G-1)L^3}{9\tau_0\lambda^2 A_{eff}\Lambda_0^2 L_a} \tag{1.29}$$

where N_{sp} is the spontaneous emission factor of the amplifiers, h is Planck's constant, G is the amplifier gain and τ_0 is the pulse width. This equation shows that the deviation of the pulse position and hence jitter experienced is dependent on the system length by $L^{3/2}$. For short systems this will mean that the jitter is low (depending on other parameters) and is not a significant problem, but for longer system lengths the jitter may become significant and can be the limiting factor in long distance systems design. In order to prevent the detector at the end of a system from receiving an error, the pulse must arrive within a time window $\pm t_\omega$ around its input position. Assuming Gaussian statistics, obtaining a typically acceptable bit-error rate (BER) of less than 10^{-9} requires that the variance allowable is [49, 63]:

$$<t_N^2>=\left(\frac{t_\omega}{6.1}\right)^2 \tag{1.30}$$

Through Equations (1.29) and (1.30), we can find the maximum transmission distance allowed for a given set of parameters and this error ratio as

$$L_{max}^3 \le 0.1372\frac{\tau_{fWHM} t_\omega^2 A_{eff} L_a \Lambda_0^2}{N_{sp} n_2 D_2 h(G-1)} \tag{1.31}$$

where we have used the experimentally useful units D_2 and $\tau_{fWHM}=2\ln(1+\sqrt{2})\tau_0=1.763\tau_0$, the full-width at half-maximum width for a soliton. Thus we see that there is a limit to the length of any soliton transmission system due to the ASE noise shifting the frequency of the signal and hence the arrival time of the pulse

through the interaction of the pulse with dispersion. We mentioned earlier that filters could reduce the ASE noise introduced to an optical signal by EDFAs. However, by filtering the noise away from the solitons will reduce the bandwidth of the noise and hence the shift in frequency experienced. It also introduces an additional loss to the wings of the soliton. In practice, filters also have a finite insertion loss across the whole bandwidth. In order to compensate their losses, the gain of the amplifier must be increased. This again leads to an increase in the jitter. As the ASE noise introduced to the signal increases with gain [63], the noise at the centre of the soliton spectrum that cannot be filtered will increase and hence degrade the signal-to-noise ratio. Thus a balance must be struck between the bandwidth of the filtering and gain to an acceptable condition [65]. One other possible way to reduce the Gordon-Haus jitter would appear from Equation (1.29) to be that of reducing the dispersion of the fibre link. Whilst this method does provide some benefit, reducing the dispersion reduces the power required to support a fundamental soliton. If the dispersion is taken too low the energy in per pulse will be insufficient for the detector to distinguish the signal from the noise resulting in errors at the receiver. There are other problems that can be encountered by solitons in low dispersion systems, particularly the effects of higher order dispersion and polarisation mode dispersion (PMD) which limit how low the dispersion can be taken. Optimisation must be performed to find the exact dispersion required.

As this timing jitter appears to limit the possibility of long distance soliton transmission and the data rates of such systems, a great deal of work has been directed to reducing or eliminating this effect [66] – [69]. There is an overlap here to other soliton work towards an optical fibre "soliton storage ring" where pulses can be maintained for long times (and hence long distances) in order to provide an optical buffer or memory

[70] – [72] which obviously suffers similar problems to soliton transmission. One novel result has returned solitons to the fore again. It has been shown that this resilience could lead to a substantial reduction in the ASE noise build-up and accumulation of timing jitter, by forcing the solitons to follow a change in their central wavelength [73] – [75]. By gradually changing the central wavelength of the filters in transmission line away from the input wavelength, the solitons are forced to slide to the new central wavelength. However as noise is linear, it cannot follow the shifting wavelength and will eventually be attenuated by the filters. This "sliding-guiding" filter technique has been used to great effect to propagate solitons of 20 Gbit/s over 14,000 km error-free [75]. The advantages found from this form of filtering by far outweigh the disadvantages of the extra gain requirement. There are still concerns however over this filtering technique regarding its implementation in a real system where supervisory system is required, such as its compatibility with optical time-domain reflectometers (OTDRs).

1.6.3 The required signal-to-noise ratio

Another consequence of noise for optical communication systems is the requirement that the signal-to-noise ratio (SNR) be maintained at a level that is acceptable at the detector. The SNR from signal-spontaneous beat noise is given by [76]

$$SNR = \frac{< i_{sig}^2 >}{< i_{sig-spon}^2 >} = \frac{(eP_{out}/(h\nu))^2}{(2e/(h\nu))^2 P_{out} F_{out} N_a} = \frac{P_{out}}{4F_{out} N_a} \tag{1.32}$$

where P_{out} is the signal power out of the amplifiers, h is Planck's constant, ν is the signal frequency, e is the electronic charge, N_a is the number of amplifiers and F_{out} is the ASE noise power of the amplifier within a bandwidth, B.

$$F_{out} = (G-1)\mu h\nu B \tag{1.33}$$

where μ is the inversion factor of the amplifiers ($\mu = 1$ for perfect amplifier) and G is the amplifier gain. As the power required to support fundamental soliton is a function of the dispersion of the optical fibre, this requirement can limit how low the dispersion can be taken in trying to eliminate effects such as Gordon-Haus jitter.

1.6.4 Soliton system design

In designing a possible soliton system, the main considerations are the required system length and the operating data rate. System parameters such as pulse width, dispersion and amplifier span must then be chosen such that error free operation of the system is possible with a built in safety margin to take account of system aging. This is a difficult process since many of the physical effects have different requirements and thus a balance must be found between them. For example, Gordon-Haus jitter and the average soliton constraint require a large pulse width whilst the SNR and soliton-soliton interaction requirements need a short pulse width.

In addition to the physical effects, there is another very important constraint – system cost. As telecommunications systems are commercial ventures, the cost in developing the system must be carefully controlled. One implication of this is that the number of amplifier stages (which are expensive) must be kept low and so a long amplifier span is desirable. In order to find a compromise between all the requirements, it is useful to construct a system design program which plots the pulse width requirements for each of the various effects versus amplifier span with the dispersion remain constant [77]. Possible windows of operation can then be determined.

1.7 Thesis overview

For transmission at 40Gbit/s, system performance is mainly degraded by pulse distortion and amplitude noise. The high dispersion value of the standard single-mode fibre leads to signal degradation through pulse interactions due to the large pulse broadening. Many advance optical techniques can be used to improve systems performance. In this thesis, we emphasised three of the most popular and effective methods to overcome these impairments. The first two methods are using the dispersion compensated fibre (DCF) to compensate for the chromatic dispersion and the distributed Raman amplification (DRA) to lower the average signal power in the fibre span, thus suppressing the effect of pulse interactions and improve the transmission performance. The third method is using the NOLM to allow partial regeneration of pulse amplitude and shape. As a result, noise in the zeros is almost completely suppressed by it and noise in the ones is also slightly reduced, hence it further enhances the system performance. All these will be shown step-by-step in the following chapters of my thesis.

Chapter 2 describes the operation and design of the recirculating loop used in conducting all the transmission experiments in this thesis. The experimental measurement techniques that were used are also explained.

In chapter 3, we begin by introducing the dispersion management technique since it is one of the most important concepts for dispersion managed systems. One of the most important methods of dispersion management – whereby different types of optical fibres are combined to compensate and give a desirable average dispersion of the system is being mentioned, performed and studied in detail. With the ever-increasing bit-rate and narrowing of pulse width, higher order dispersion becomes very critical to systems performance. A tunable dispersion compensator was fabricated by using a non-uniformly

strained chirped fibre grating to compensate for this detrimental defect. The fundamental concepts of Raman amplification will also be shown. An experiment on 40Gbit/s dispersion managed system was demonstrated for different dispersion maps to study the transmission performance.

The main goal and objective of this thesis are covered in the experimental work in chapter 4, where different types of loop mirrors are being discussed for high capacity transmission systems. It begins by showing how different types of nonlinear optical loop mirrors (NOLM) can be used to improve the transmission performance by suppressing the amplified spontaneous noise and reducing the timing jitters and pulse-to-pulse interactions, thus acting as saturable absorbers and strong filters. Furthermore, we have included the techniques of dispersion management, Raman amplification and NOLM to demonstrate in the experimental results that their usage in 2R-regeneration (re-amplified and re-shaped) within the recirculating loop far outweighs their performance in noise suppression before the receiver. This performance can be further improved by taking appropriate environmental measures. Finally, all the findings and future work on this thesis will be concluded, studied and discussed in chapter 5.

References

[1] J. Tyndall, Proc. *Roy. Inst.* 1, 446 (1854).

[2] J.L.Baird, *British Patent* 285,738 (1927).

[3] C.W.Hansell, *U.S. Patent* 1,751,584 (1930).

[4] H. Lamm, Z. *Instrumentenk.* 50, 579 (1930).

[5] A.C.S. van Heel, *Nature* 173, 39 (1954).

[6] B.I. Hirschowitz, L.E. Curtiss, C.W. Peters, and H.M. Pollard. *Gastroenterology* 35, 50 (1958).

[7] N.S. Kapany. *J. Opt. Soc. Am.*, 49, 779 (1959).

[8] N.S. Kapany, Fiber Optics: Principles and applications. *Academic Press*, San Diego, CA, 1967.

[9] K.C. Kao and G.A. Hockham, Dielectric-fibre surface waveguides for optical frequencies. *Proc. of the IEE*, 113:1151-1158, 1966

[10] F.P. Kapron, D.B. Keck, and R.D. Maurer. Radiation losses in glass optical waveguides. *Appl. Phys. Lett.* 17(6):423-426, 1970.

[11] T. Miya, Y. Terunuma, T. Hosaka, and T. Miyoshita. Ultimate low-loss single-mode fibre at 1550nm. *Electron. Lett.* Vol. 15, pp. 106,1979.

[12] E. Saintdizier, E. Brandon, J-P. Blondel, and J-F. Vinchant. 2.5Gb/s unrepeatered transmission with direct modulated laser and without dispersion compensating fibre over 385 km (412 km with FEC) of pure silica core fibre. *Electron. Lett.*, 32(15): 1383-1384, 1996.

[13] G.P. Agrawal. Nonlinear Fibre Optics. *Academic Press*, San Diego, 1995.

[14] J.M. Senior. Optical Fibre Communications - Principles and Practice. *Prentice Hall,* New York, 1992.

[15] P.S. Henry. Lightwave Primer. *IEEE J. Quantum Electronics*, 21(12):1862-1879, 1985.

[16] A.W. Snyder and J.D. Love. Optical waveguide theory. *Chapman and Hall*, United Kingdom, 1983.

[17] V.A. Bhagavatula. Novel fibres for dispersion-managed high-bit-rate systems. *In Opt. Fib. Comm.* (OFC'98), San Jose, California, 1998.

[18] H.S. Chung. 640Gbit/s (32 x 20 Gbit/s) WDM transmission with 0.4 (bits)/Hz spectral efficiency using short-period dispersion managed fibre (Perfect cable^{TM}). *In Opt. Fib. Comm.* (OFC'01), Anaheim, CA, 2001.

[19] L. Provost, C. Moreau, G. Melin, X. Rejeaunier, and L. Gasca. Dispersion-managed fiber with low chromatic dispersion slope. *In Opt. Fib. Comm.* (OFC'03), Georgia, Atlanta, 2003.

[20] A.H. Gnauck. 2.5Tbit/s (64 x 42.7Gbit/s) transmission over 40x100km NZDSF using RZ-DPSK format. *In Eur. Conf. of Opt. Comm.* (ECOC-2002) – Copenhagen, Denmark, 2002.

[21] B. Zhu. 3.3 Tbit/s (80 x 42.7Gbit/s) transmission over 20x100km of non-zero dispersion fiber with simultaneous C+L band dispersion compensation. *In Opt. Fib. Comm.* (OFC'02), Anaheim, California, 2002.

[22] S. Bigo. Transmission of 125 WDM channels at 42.7Gbit/s (5Tb/s capacity) over 12x100km of TeraLight^{TM} Ultra fibre. *In Eur. Conf. of Opt. Comm.* (ECOC-2001) – Amsterdam, PD.M.1.1, IEE, 2001.

[23] J.C. Knight, T. A. Birks, P. St. J. Russell, and D. M. Atkin. All-silica single-mode optical fiber with photonic crystal. Opt. Lett., 21(19):1547-1055, 1996.

[24] V.V.Ravi, A.K. George, W.H. Reeves, J. Knight, and P. Russell. Modified group-velocity dispersion in extruded photonics crystal fiber. *In Opt. Fib. Comm.* (OFC'03), Atlanta, Georgia, 2003.

[25] C.D. Poole, R.W. Tkach, A.R. Chraplyvy, and D.A. Fishman. Fading in lightwave systems due to polarisation mode dispersion. *IEEE Photon. Tech. Lett.*, 3(1):68-70, 1991.

[26] S.G. Evangelides, L.F. Mollenauer, J.P. Gordon, and N.S. Bergano. Polarisation multiplexing with solitons. *IEEE J. Lightwave Technol.*, 10(1):28-35, 1992.

[27] E.G. Bryant, S.F. Carter, A.D. Ellis, W.A. Stallard, J.V. Wright and R. Wyatt. Unrepeatered 2.4 Gb/s transmission over 250 km of step index fibre using erbium power amplifier. *Electron. Lett.*, 26(8):528-529, 1990.

[28] L.F. Mollenauer and R.H. Stolen. Solitons in optical fibres. *Fibreoptic technology journal*, 193-198, 1982.

[29] R.H. Stolen, E.P. Ippen and A.R. Tynes. Raman Oscillation in glass optical waveguide. *Appl. Phys. Lett.*, vol. 20, pages 62, 1972.

[30] R.G. Smith. Optical power handling capacity of low loss optical fibres as determined by stimulated Raman and Brillouin Scattering. *Appl. Opt.* 11, pages 2489-2492, 1972

[31] Y. Aoki. Properties of fibre Raman amplifiers and their applicability to digital optical communication systems. *IEEE J. Lightwave Technol.*, 6(7):1225-1239, 1988.

[32] M.J. O'Mahony, I.W. Marshall, and H.J. Westlake. Semiconductor laser amplifiers for optical communications systems. *BT Technol. J.*, 5(3):9-18, 1987.

[33] M.J. O'Mahony. Semiconductor laser optical amplifiers for use in future fibre systems. *IEEE J. Lightwave Technol.*, 6(4):531-543, 1988.

[34] E. Desurvire. Erbium-Doped Fibre Amplifiers – Principles and Applications. *John Wiley & Sons*, New York, 1994.

[35] I. Bennion. Lecture notes on Erbium-Doped Fibre Amplifiers. Lecture Course: E585, Department of Electronic Engineering and Applied Physics, *Aston University*, Birmingham, England.

[36] R.G. Smart, J.L. Zyskind, J.W. Sulhoff, and D.J. Digiovanni. An investigation of the noise figure and conversion efficiency of 0.98 μm pumped erbium-doped fibre amplifiers under saturated conditions. *IEEE Photon. Technol. Lett.*, 4(11):1261-1264, 1992.

[37] C.S. Gardener, J.M. Green, M.D. Kruskal, and R.M. Miura. Method for solving the Kortrweg-deVries equation. *Phys. Rev. Lett.*, 19(19):1095, 1967.

[38] V.E. Zakarov and A.B. Shabat. Exact theory of two-dimensional self-focusing and one-dimensional self-modulation of waves in nonlinear media. *Sov. Phys. JEPT.*, 34(1):62-69, 1972.

[39] C. Desem and P.L.Chu. Effect of chirping on solution propagation in single-mode fibres. *Opt. Lett.*, 11(4):248-251, 1986.

[40] D. Anderson, M. Lisak, and T. Relchel. Asymptotic propagation properties of pulses in a soliton-based optical fibre communication system. *J. Opt. Sov. Am. B*, 5(2):207-210, 1988.

[41] K.J. Blow, N.J. Doran, and D. Wood. Generation and stabilisation of short soliton pulses in the amplified nonlinear schrodinger equation. *J. Opt. Soc. Am. B*, 5(2):381-391, 1988.

[42] S.V. Chernikov, J.R. Taylor, and R. Kashyap. Experimental demonstration of step-like dispersion profiling in optical-fibre for soliton pulse generation and compression. *Electron. Lett.*, 30(5):433-435, 1994.

[43] H. Kubota and M. Nakazawa. Long distance optical soliton transmission with lumped amplifiers. *IEEE J. Quantum Electron.*, 26(4):692-700, 1990.

[44] A. Hasegawa and Y. Kodama. Guiding-center soliton in optical fibres. *Opt. Lett.*, 15(24):1443-1445, 1990.

[45] L.F. Mollenauer, S.G. Evangelides, and H.A. Haus. Long distance soliton propagation using lumped amplifiers and dispersion shifted fibre. *IEEE J. Lightwave Technol.*, 9(2):194-197, 1991.

[46] N.J. Smith, K.J. Blow, and I. Andonovic. Sideband generation through perturbations to the average soliton model. *IEEE J. Lightwave Technol.*, 10(10):1329-1333, 1992.

[47] K.J. Blow and N.J. Doran. Average soliton dynamics and operation of soliton systems with lumped amplifiers. *IEEE Photon. Technol. Lett.*, 3(4):369-371, 1991.

[48] A. Hasegawa and Y. Kodama. Guiding-centre soliton. *Phys. Rev. Lett.*, 66:161-164, 1991.

[49] A.F. Mitchell, J.V. Wright, S.F. Carter, A.D. Ellis, A. Lord, J. Lyle, and J.M. Scott. The future of optically amplified submarine systems. *In Techn. Digest of 2nd Intern. Conf. on Optical Fibre Submarine Telecommun.* System, Versailles, France, pp.49-54, 1993.

[50] J.P. Gordon. Interaction forces among solitons in optical fibres. *Opt. Lett.*, 8(11):596-598, 1983.

[51] Y. Kodama and K. Nozaki. Soliton interaction in optical fibres. *Opt. Lett.*, 12(12):1038-1040, 1987.

[52] F.M. Mitschke and L.F. Mollenauer. Experimental observation of interaction forces between solitons in optical fibres. *Opt. Lett.*, 12(5):355-357, 1987.

[53] Y. Kodama and S. Wabnitz. Reduction of soliton interaction forces by bandwidth limited amplification. *Electron. Lett.*, 27(21):1931-1932, 1991.

[54] T. Georges and F. Favre. Modulation, filtering and initial phase control of interaction solitons. *J. Optical society of America.* B, 10(10):1880-1889, 1993.

[55] P.-L. Francois and T. Georges. Reduction of average soliton interaction forces by amplitude modulation. *Opt. Lett.*, 18(8):583-585, 1993.

[56] C. Desem and P.L. Chu. *Optical solitons – theory and experiment, chapter soliton-soliton interactions*, pages 107-151. Press syndicate of the University of Cambridge, 1992.

[57] M. Suzuki, N. Edagawa, H. Taga, H. Tanaka, S. Yamamoto, and S. Akiba. 10Gbit/s, over 12200 km soliton data transmission with alternating-amplitude solitons. *IEEE Photon. Technol. Lett.*, 6(6):7557-7559, 1994.

[58] K. Suzuki, N. Edagawa, H. Taga, M. Takaya, S. Yamamoto, and Akiba. Feasibility demonstration of 20 Gbit/s single channel soliton transmission over 11500 km using alternating-amplitude solitons. *Electron. Lett.*, 30(13):1083-1084, 1994.

[59] M. Nakazawa, E. Yoshida, E. Yamada, K. Suzuki, T. Kitoh, and M. Kawachi. 80 Gbit/s soliton data transmission over 500 km with unequal amplitude soliton for timing clock extraction. *Electron. Lett.*, 30(21):1777-1778, 1994.

[60] P.A. Andrekson, N.A. Olsson, J.R. Simpson, T. Tanbun-EK, A. Logan, and K.W. Wecht. Observation of collision induced temporary soliton carrier frequency shifts in ultra-long fibre transmission systems. *IEEE J. Lightwave Technol.*, 9(9):1132-1135, 1991.

[61] A. Mecozzi and H.A. Haus. Effect of fibres on soliton interactions in wavelength-division-multiplexing systems. *Opt. Lett.*, 17(14):988-990, 1992.

[62] S. Chakravarty, M.J. Ablowitz, J.R. Sauer, and R.B. Jenkins. Multisoliton interactions and wavelength-division multiplexing. *Opt. Lett.*, 20(2):136-138, 1995.

[63] D. Marcuse. An alternative deviation of the Gordon-Haus effect. *IEEE J. Lightwave Technol.*, 10(2):273-278, 1992

[64] A. Hasegawa and Y. Kodama. Solitons in optical communications. *Clareadon Press*, Oxford, 1995.

[65] A. Mecozzi, J.D. Moores, H.A. Haus, and Y. Lai. Soliton transmission control. *Opt. Lett.*, 16(23):1841-1843, 1991.

[66] Y. Kodama and A. Hasegawa. Generation of asymptotically stable optical solitons and suppression of the Gordon-Haus effect. *Opt. Lett.*, 17(1):31-33, 1992.

[67] D. Marcuse. Simulations to demonstrate the reduction of the Gordon-Haus effect. *Opt. Lett.*, 17(1):34-36, 1992.

[68] W. Forysiak, K.J. Blow, and N.J. Doran. Reduction of Gordon-Haus jitter by post-transmission dispersion compensation. *Electron. Lett.*, 29(13):1225-1226, 1993.

[69] H. Kubota and M. Nakasawa. Soliton transmission control in time and frequency domains. *IEEE J. Quantum Electron*, 29(7):1289-1297, 1993.

[70] H.A. Haus and A. Mecozzi. Long-term storage of a bit stream of solitons. *Opt. Lett.*, 17(21):1500-1502, 1992.

[71] S. Wabnitz. Suppression of interactions in a phase-locked soliton optical memory. *Opt. Lett.*, 18(8):601-603, 1993.

[72] C.R. Doerr, W.S. Wong, H.A. Haus, and E.P. Ippen. Additive-pulse mode-locking/limiting storage ring. *Opt. Lett.*, 19(21):1747-1749, 1994.

[73] L.F. Mollenauer, J.P. Gordon, and S.G. Evangelides. The sliding frequency guiding filter: an improved form of soliton jitter control. *Opt. Lett.*, 17(22):1575-1577, 1992.

[74] P.V. Mamyshev and L.F. Mollenauer. Stability of soliton propagation with sliding-frequency guiding filters. *Opt. Lett.*, 19(24):2083-2085, 1994.

[75] L.F. Mollenauer, P.V. Mamyshev, and M.J. Neubelt. Measurement of timing jitter in filter-guided soliton transmission at 10 Gbit/s and achievement of 375Gbit/s-Mm, error-free, at 12.5 and 15 Gbit/s. *Opt. Lett.*, 19(10):704-706, 1994.

[76] Yariv. Signal to noise consideration in fibre links with periodic or distributed optical amplification. *Opt. Lett.*, 15(19):1064-1066, 1990.

[77] J.W. Wright and S.F. Carter. Constraints on the design of long-haul soliton systems. *In conf. on Nonlinear Guided-Wave Phenomena* (NLGW'91), MA2-1, pages 6-9, 1991.

Chapter 2

The recirculating loop and experimental techniques

2.1 Introduction

Circulating loop experiments were performed as early as 1977 to study pulse propagation in multi-mode fibre [1], jitter accumulation in digital fibre systems [2], optical soliton pulse propagation [3], and pulse propagation in single-mode fibre [4]. Loop transmission experiments became useful for optical amplifier feasibility demonstrations after techniques were developed to measure the bit error ratio (BER) of long pseudo-random data patterns [5]. The potential transmission capacity of long systems that use Erbium-

doped Fibre-Amplifier (EDFA) repeaters was understood early on [6, 7]; however, experimental verification would take several years from the first amplifier demonstrations. For undersea cable applications, the untested optical amplifier technology was at odds with strict design requirements of submarine systems. Developing an EDFA cable system would involve extensive resources in both the people and equipment. Before resources could be committed, an experimental proof that could demonstrates high data rate, long-length transmission at low BER was needed. This created a dilemma: A transoceanic length experiment would require more equipment than could be supplied without a major development, and a development could not be justified without proof of the feasibility of EDFA technology. The solution was a loop experiment where the BER could be measured at transoceanic lengths by circulating data through a much shorter amplifier chain. Feasibility was demonstrated by measuring a BER lower than 10^{-9} for a 2.5 Gbit/s NRZ signal over a transmission distance of 9000 km, using a 120 km amplifier chain with four EDFAs [8]. After the first demonstration of measuring BER in the loop, the loop technique became widely accepted, as evidence by many reports on the subject itself [9] – [24].

Since the last decade, loop techniques play an important role in the development of long-haul transmission system by providing a flexible platform for transmission measurement [25]. Since the time of initial feasibility studies using recirculating loop experiments, several long testbed experiments have been reported, where hundreds of amplifiers were combined to form amplifier chains up to 10,000 km long [26, 27]. These experiments provided invaluable information on many of the design parameters in a long-haul system. However, given the amount of equipment involved, in-line systems tend to

be expensive and inflexible. A recirculating loop is a simplified transmission system, which consists of one or few amplifiers and a corresponding number of fibre spans. Recirculating loops can be used to perform long distance (1000s of km) propagating experiments by propagating a signal many times round the loop until the required propagation distance has been achieved and then results taken. Reconfiguration of a loop is extremely easy compared to a full in-line system due to the reduction in the number of components and fibre spans. This flexibility is a major advantage when several experiments are to be performed which require comparison of fibres or components, changing amplifier positions or dispersion maps as in chapter 3.

Recently, H. Xu et al. [28] has demonstrated that even with new low-PMD fibre, loop-synchronous scrambling is necessary for a recirculating loop to correctly emulate a long-haul WDM terrestrial system. Without loop scrambling, by simply adjusting a PC in the loop, the bit error ratio BER, which will be discussed later in this chapter, can vary over four orders of magnitude due to large variations in the amount of PMD and PDL induced waveform distortion. With loop scrambling, the BER varies over two orders of magnitude and polarisation effects no longer dominate the behaviour of the system. Consequently, one must use loop scrambling to make accurate measurements quantifying the effects that chromatic dispersion, nonlinearity, and noise from optical amplifiers have on the system performance.

Most of the propagation experiments in the thesis were performed using the recirculating loop but without loop-synchronous scrambling due to its unavailability. The recirculating loop can only give an indication of what would happen in a real system. The maximum error-free distances (usually defined as the maximum distance which a

data signal can be propagated with fewer than one error per 10^9 bits) for a loop and an in-line experiment may differ significantly. The reason for this is that in a recirculating loop experiment, there are little variations in parameters such as amplifier span, component characteristics, average dispersion and loss per span. The problem is particularly pronounced when a single span loop is used where there is only one fibre span, amplifiers and set of components. While these factors could be expected to give a falsely high propagation distance, there are other effects associated with the use of a loop that have a detrimental effect and may lead to loop experiments giving a pessimistic impression of system performance. When a loop is used, the loss per amplifier span is in general higher than an in-line experiment since components such as isolators and filters have to be included more frequently. As a result, the number of spans in the loop determines the maximum spacing of components. Therefore a single span loop fare badly as all the components to be used must contain within a single amplifier span. Furthermore, an additional loss is encountered since a portion of the signal must be coupled out of the loop to allow measurements to be taken. The optical amplifiers in the loop must be able to compensate for all these losses. Unfortunately increasing the amplifier gain will always lead to system degradation, since more noise will be introduced into the system. To give a good indication of system performance, state of the art recirculating loops now contain up to twenty fibre spans [24]. However, it must be mentioned that even in its simplest form, a recirculating loop is an indispensable tool in the initial stage of long haul system development. This chapter will discuss the basic operation and design of a single span recirculating loop for easy understanding. The loop operation and other experimental techniques used will also be described.

2.2 Design considerations and principle of operation

A single span recirculating loop that consists of only one amplifier, one fibre span and one set of components has obvious economic advantages but it does provide restrictions since all the optical components used must be included in every amplifier span. Thus, experiments such as investigating the effect of filtering or dispersion compensating every x^{th} amplifier cannot be done with a single span loop. However, chapter 3 and 4 have shown that recirculating loop experiments are still very important and reliable by performing an enormous variety of experiments. Results obtained are a good indication of the real system performance.

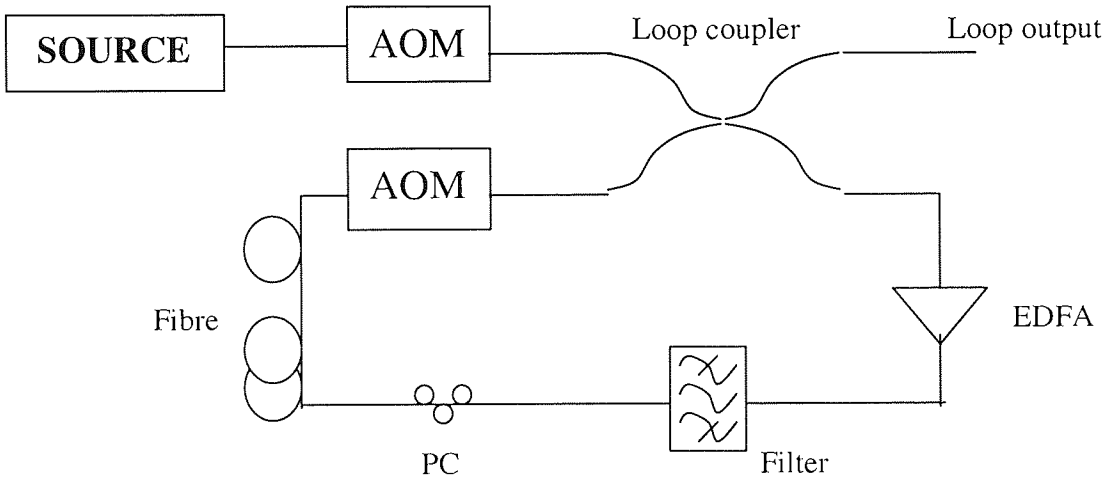

Figure 2.1: Schematic diagram of the recirculating loop

A schematic diagram of a typical single span recirculating loop is shown in Figure 2.1. Before it can be propagated in the loop, the signal from the source must be gated into the loop using a switch such as an AOM (Acousto-optic modulator) and a fibre coupler. To compensate for the losses of these devices, it is usually necessary to amplify the source to give the required power level in the loop. The purposes of the two AOMs are to allow

data to be flowing into the amplifier chain (the load state) and circulate in the loop (the loop state). These functions are accomplished with two AOMs and a single 3dB coupler. The data circulates for a specific time, after which the state of the experiment toggles, and the load/loop cycle is repeated.

If the loop is not completely filled, the ASE noise level from the amplifier can build up in the unfilled section. However, if the AOM is left open for too long and the loop is overfilled, pulses that have already propagated once round the loop will arrive back at the coupler while signal is still being coupled into the loop. This can obviously lead to degradation of the signal, as the two sets of pulses will interfere. AOM is being used for this application because it has a relatively fast switching time, as pulses that are incident on the switch during the transitions will be partially transmitted. An AOM, which has a very high extinction ratio of 60 – 70 dB, is required so that when the switch is opened to stop signal from passing into the loop, there is no leak-through. This is very important, as any leakage into the loop would appear as noise in the system, and this is obviously undesirable. In addition to these specific requirements, low insertion loss and low polarisation dependence are also desirable. Input AOM works by splitting the input beam into a straight through and a deflected beam by passing it through a standing wave pattern that is set up inside the device using acoustic waves. This standing wave pattern acts as a grating leading to the diffraction of the input beam. By switching the power to the device so that diffraction only occurs at the required time, the input to the loop can be switched by ensuring that only the diffracted beam is coupled into the loop input coupler. The straight through signal is always present and must not be coupled into the loop. As

the diffraction process is not 100% efficient, there is always loss when using an AOM. The device used here had a total insertion loss of 2.5 dB

The choice of the coupler is also important, especially in the case of a single span loop because portion of the signal is coupled out of the loop through this coupler after each round trip of the loop. Using a 50:50 coupler therefore leads to an additional 3dB loss per round trip. If too large a fraction of the signal is coupled out of the loop after each round trip, system performance will be compromised since higher loop amplifier gain will be required. However if too small a fraction is coupled out, the loop output signal requires high gain amplification before measurements can be done. There is also the problem that the same coupler must be used for both coupling into and out of the loop. Therefore a compromise must be reached and hence, different experiments may require different coupling ratios.

Once the signal is coupled into the loop, it is first of all amplified. This is necessary since the signal power coupled into the loop is generally low. The design of the amplifier is crucial to the loop performance as there is only one amplifier and any imperfections will be magnified by the many recirculations involved in propagation experiments. The gain of the amplifier must be sufficiently high enough to exactly compensate for all the losses in the loop. The round-trip gain must be in unity so that the signal power and hence pulse power remain the same after each amplification.

The filter in the system is to reduce the rate of Gordon-Haus timing jitters in the system and it has a loss of around 2 dB with a bandwidth of 3nm. A polarisation controller (PC) allowed the polarisation state of the signal to be altered before launching into the transmission fibre. This gave a greater degree of controllability in loop

experiments since the same amplifier and components are being used repeatedly. This is another problem that can lead to discrepancies in the propagation distance achievable in loop experiments and in-line systems. The PC does impose an additional loss of ~ 0.5 dB. When an experiment was being performed, the polarisation state of the signal would be altered as required using the PC before beginning, and left unaltered throughout the duration of the experiment in order to give consistent results.

In early stage of this technology, the typical loop length was 30 – 40 km. But nowadays, the fibre length is 10 times longer than that and it is not only applicable for soliton systems. However, in any given soliton experiment, the average power which must be launched into the fibre is determined by the average soliton power given by Equation (1.26), the dispersion map [29, 30], the data pattern being used and the data rate. In order to fine tune the power launched into the transmission fibre, adjusting the current of the pump diode could alter the EDFA gain and output power.

The loop was completed with a fibre coupler as described above. The portion of the signal that remains in the loop is re-amplified and continues to circulate in the loop until the required numbers of recirculations (corresponding to the desired propagation distance) are reached. Thus, after the first circulation, there is a continuous output from the loop coupler. This output will then be further split to give continuous monitoring as well as the main loop output. For continuous monitoring, we used a slow photo-diode and an oscilloscope to give an indication of the loop performance. When a set of results was actually being taken, the loop had to be completely filled so that the noise level could not be monitored. A second monitor output could also be used to test the electrical spectrum of the propagating signal using an electrical spectrum analyser.

Once the required propagation distance has been achieved, the signal circulating in the loop must be removed before the loop can be re-started. A common way of doing this is to include a second AOM in the loop, which can be switched, to either pass or block the circulating signal. It must be noted that the loop timing for the input AOM and loop AOM switching are directly opposite.

In general, measurements are only taken when required propagation distance has been achieved. This means that switching is required to select a measurement window covering only the section of the continuous output that has propagated for the required distance, which is the final recirculating loop. One electronic delay generator controls the timing of this switching window. The measurement window could be easily adjusted so that data at the beginning and end of the recirculation could be rejected.

The timing of the propagation and measurement cycle can be understood with reference to Figure 2.2.

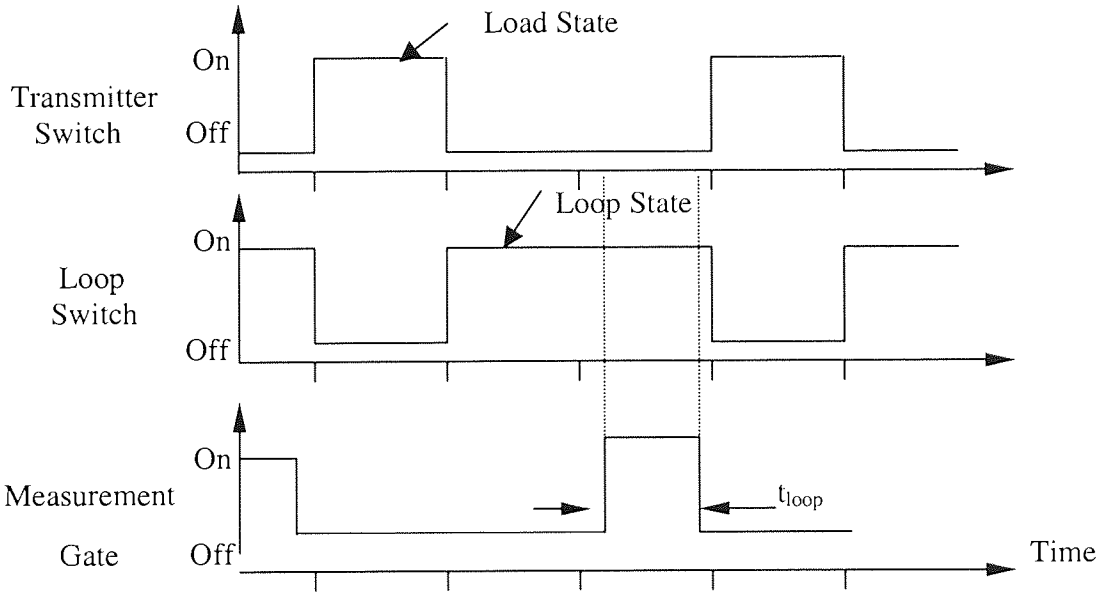

Figure 2.2: Loop timing diagram

The loop cycle begins by opening the input AOM to allow signal to pass into the loop. When the loop is filled, the input AOM will be closed. When this happens, loop AOM will start to open so that signal can propagate for the required distance. When this distance is reached, the measurement switch starts to open and a burst measurement can then be performed. The cycle will then be repeated by re-opening the input AOM to allow another burst of signal to be admitted into the loop. All these measurements will be controlled by a single electronic delay generator.

As an example, for a recirculating loop that is 127km long, the round trip time is approximately

$$\text{Round trip time (s)} = \frac{\text{Length of loop (m)} \times \text{Refractive index of fibre}}{\text{speed of light (m/s)}} \qquad (2.1)$$

$$= (127 \times 1000) \times 1.46 / 3 \times 10^{8}$$

$$= 618\mu s$$

To transmit over 3000 km in a 127 km loop requires 24 circulations (24 x 127 km = 3048 km)

$$\text{Propagation time} = 24 \times 618\mu s + 50\mu s \qquad (2.2)$$

$$= 14.882 \text{ ms}$$

where 50μs is taken as the resynchronised time, the time required for BERT to synchronise to the data pattern.

Finally, the measurement time must stop before the beginning of the 25th circulation. Moreover, it must be less then the round trip time of the loop.

$$\text{Measurement time} = \text{round trip time} - \text{resynchronised time} - \text{switching time} \qquad (2.3)$$

$$= (618 - 50 - 68)\ \mu s$$

$$= 500\ \mu s$$

where switching time is the time required for the AOM switches.

Lastly, before performing an experiment, the source has to be checked to ensure that the quality of the pulses in the data stream is acceptable. This can be done by confirming that the back-to-back performance (i.e. the system performance with the data pass straight through to the receiver without any recirculation in the loop) of the system is optimised. A fixed propagation distance will then be set and the EDFA gain, the loop delays, the filter and the polarisation controller are adjusted by checking the continuous monitors to ensure that the loop is performing as required. An experiment could then be commenced with the propagation distance being adjusted as required.

2.3 Burst measurement techniques

A disadvantage of using a recirculating loop is that burst measurements must be taken. Unlike an in-line experiment, where there is a continuous output which can be measured, measurements can only be made for a small fraction of the recirculating loop cycle – the majority of the loop cycle is taken up with the propagation and only the final recirculation can be measured. In addition to increasing the time scale of experiments, there is also problem as to when the loop output must be switched so that only the relevant part of the loop output is to be sampled. For some, a switched optical signal was sufficient but in this case, the electrical trigger has to be switched to initiate all the measurements at the required time.

To give an indication of system performance, the most frequently quoted parameter is the bit error ratio (BER). The BER is defined as the number of errors detected divided by the total number of bits received in the measurement period [31]. For

a system to be defined as "error-free" a BER of 10^{-9} or better is required. To measure the BER, a bit-error-rate-test set (BERTS) which consists of a data pattern generator and an error detector is required. In this thesis, all the BER measurements are done using the BERTS.

2.3.1 Clock Recovery

When measurements are being taken on the bit-error-rate-test set (BERTS) and sampling scope, an electrical trigger signal is required. Basically there are two methods to produce this electrical signal – the first, using a fast photo-diode to give a direct conversion of the optical signal, but this will only be used for low bit rate experiment with a continuous pulse stream. The second method is to use a clock recovery circuit, which is more appropriate for high bit rate experiments, therefore all the remaining loop experiments in this thesis are using this method since we are dealing with 10Gb/s or higher bit rate.

Using a clock recovery circuit, an electrical signal which is synchronous (and stay in synchronisation) with the optical signal can be obtained. The clock recovery set-up is shown schematically in Figure 2.3:

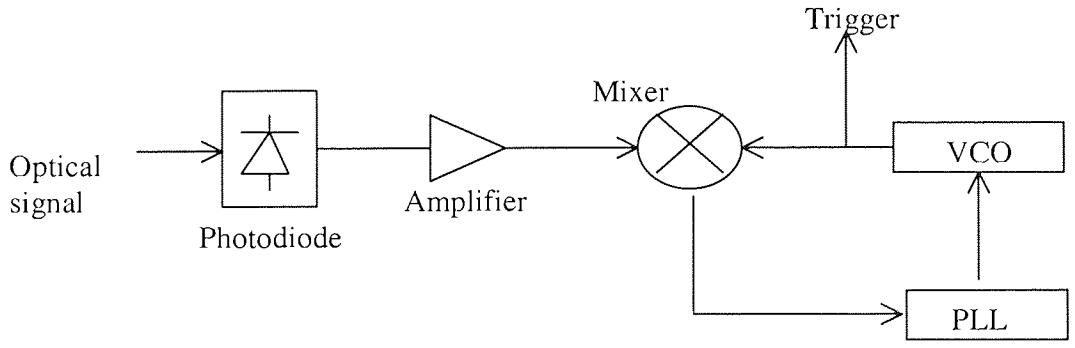

Figure 2.3: Clock recovery Set-up. VCO: voltage controlled oscillator, PLL: phase locked loop

The optical pulse train is first converted into an electrical signal using a photodiode before being electrically amplified and mixed with the signal from a voltage controlled oscillator (VCO) to generate an error signal, which is then fed into a phase locked loop

(PLL) control circuit. This feedback circuit adjusted the VCO frequency so as to minimise the frequency difference between the VCO output and the signal frequency from the photodiode. Thus, by splitting the VCO output, a continuous electrical trigger signal in synchronisation with the optical signal able to be obtained. This electrical signal will then remain in synchronisation with the optical signal even if the optical frequency changes as long as the change in optical signal is not greater than the locking range of the PLL. This locking range is typically ~ 20MHz, which allows the clock recovery circuit to remain locked to the optical frequency for a period of hours. The performance of the clock recovery circuit has a strong influence on the quality of the system performance. Therefore, before starting an experiment, the system performance must be optimised by measuring the back-to-back BER of the system, i.e. the BER where the propagation distance being effectively zeroed.

It must be mentioned that the clock recovery in Figure 2.3 was built by my ex-colleagues. Only the dispersion compensation experiment in section 3.3.1 was done using this clock recovery. We found that sometimes this clock recovery had difficulty in locking to the 10Gbit/s component when performing 40Gbit/s experiments, hence we replaced it by purchasing a new clock recovery subsystem from JDS Uniphase. The model number is: VM10RZCRM-9953. The clock is extracted from the incoming RZ data stream by differentiating to generate spectral energy at 9.953 Gbit/s and 10.664 Gbit/s. A precision narrow-band resonance filter then extracts the clock and eliminates unwanted jitter. The resulting clock is then precisely aligned at the decision circuit to re-time the input data, causing exceptionally low jitter. Therefore, all the rest of the transmission experiments in this thesis were performed using this new clock recovery.

2.3.2 Q measurement

The Q value of a system is defined by [32] – [34]

$$Q = \frac{\mu_1 - \mu_0}{\sigma_1 + \sigma_0} \tag{2.4}$$

where $\mu_{1,0}$ represent the mean values of the ones and zeros in the data stream and $\sigma_{1,0}$ represent their standard deviations.

The Q value gives a measurement of system performance that is related to the bit error ratio (BER) by [35]

$$BER = \frac{1}{\sqrt{2\pi}} \frac{\exp(-Q^2/2)}{Q} \tag{2.5}$$

but can only be measured when a data stream is being used as the propagating signal because it requires measurement of the ones and zeros in the data stream, when a pulse stream is being used all data slots are occupied by ones. A BER of 10^{-9} is generally accepted as representing "error-free" system performance and equivalent to Q value of 6. However, a timing window has to be defined before a Q measurement could be made. Any sampled points within this time window were then used to build up a histogram as shown in Figure 2.4. From this histogram the mean and standard deviations of the one and zero levels could be determined using the statistics facilities of the sampling oscilloscope allowing the Q to be calculated using Equation (2.4). In measuring $\mu_{1,0}$ and $\sigma_{1,0}$ it was necessary to set a decision level with all sampled points above this decision level being taken as representing ones and points below it representing zeros. This decision level was generally taken as being half way between μ_0 and μ_1 but in cases such as that depicted in Figure 2.4, where there was no overlap of the two histograms, the

positioning of the decision level made little difference to the Q value. But when the Q values were lower and there was more overlap of the two histograms, the positioning of the decision level became more critical and it was important that the decision level was consistent throughout the measurements. This leads to a greater error in the measurement of low Q values (~ 4) than high Q's and significantly, for a Q value of 6 (which corresponds to the minimum acceptable value), varying the decision level position led to a variation of Q of less than 0.1.

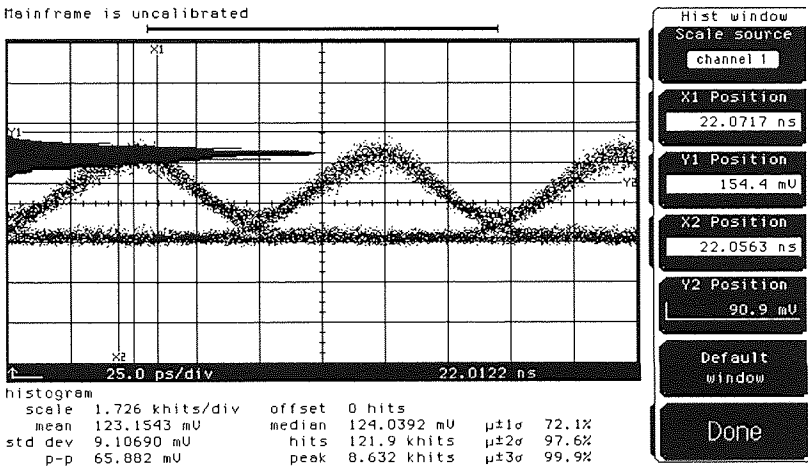

Figure 2.4: A typical Q value measurement. Mean and standard deviations of the one level is found in the calculation of the Q

The eye diagram in Figure 2.4 shows that in a soliton system the one level is defined as the peak pulse height and the zero level corresponds to the baseline. From the definition of Q, it is immediately obvious that any increase in the ASE noise level, timing jitter or amplitude jitter will degrade the system by increasing $\sigma_{1,0}$. Variations in the pulse height can also affect Q as μ_1 will be altered. This has implications for soliton systems as the pulse power (and hence μ_1) depends on the pulse width and so broader pulses will have lower Qs given the same noise conditions. This implies that broader pulses will also give lower BER measurements through Equation (2.5). The reason for the BER being low is

that in taking a BER measurement, a decision level must be set such that the energy detected in a given time interval must be above the decision level for data one to be detected. As a pulse broadens, the pulse energy is spread over a greater time interval and the integrated energy detected in the bit interval may fall below the decision level giving an error.

The main problem found experimentally with taking Q values was that even a small change in the position of the time window on the sampling oscilloscope could lead to a change in Q value. This could give inconsistencies in results as the time position of the pulses on the sampling oscilloscope could vary due to variations in trigger phase as propagation distance was changed. So, it was necessary to reposition the time window when this occurred. The optimum window position was generally with the window centred on the peak of the pulse but this position was often difficult to determine. Thus before measurements were taken, the position of the time window was optimised by taking repeated measurements of the Q value with the position changed.

2.4 Pulse width measurement using autocorrelator

It is frequently necessary to measure the pulse width of the laser being used so that parameters such as pulse width, quality of the pulse, soliton and period duty cycle can be determined. Generally, the pulses that are being used are on the order of 10ps, which is at the limit of the resolution achievable by direct measurement of the pulse width using a fast photodiode with a sampling oscilloscope. The pulses after propagating through the recirculating loops needs to be measured to ensure proper dispersion compensation. Moreover, as bit-rate increases to 40Gbit/s and beyond, pulses as short as femtosecond will need to be used to prevent any pulse-to-pulse interaction. Therefore, an alternative

and very important method of pulse width measurement is required. One of the most common methods is to use the second harmonic signal induced by a nonlinear crystal to determine the autocorrelation width of the input pulse profile being used. From the width of the autocorrelation function, the pulse width can be deduced by assuming the form of the pulse shape.

Second harmonic generation is a nonlinear process and the intensity of the second harmonic signal is

$$I_{2\omega}(t) \quad \alpha \quad \int_{-\infty}^{\infty} I_{\omega}(t)^2 dt \tag{2.6}$$

where I_{ω}(t) is the input intensity and $I_{2\omega}$(t) is the second harmonic intensity. In order to determine the pulse width, the input pulse stream is first split into two parts. A relative time delay, T, is then introduced between the two signals before they are re-aligned and passed through the nonlinear crystal. Assuming the signal is split equally, Equation (2.6) becomes

$$I_{2\omega}(t) \quad \alpha \quad \int_{-\infty}^{\infty} \left[\frac{1}{2} I_{\omega}(t) + \frac{1}{2} I_{\omega}(t-T) \right]^2 dt \tag{2.7}$$

$$\alpha \quad \int_{-\infty}^{\infty} I_{\omega}(t)^2 \, dt + 2 \int_{-\infty}^{\infty} I_{\omega}(t) I_{\omega}(t-T) \, dt \tag{2.8}$$

The first term can be removed from this equation if the non-collinear arrangement is used and in this case the autocorrelation function, G(T), is given by the normalised second harmonic intensity, i.e.

$$G(T) = \int_{-\infty}^{\infty} I_{\omega}(t) I_{\omega}(t-T) \, dt \tag{2.9}$$

In practice, the autocorrelator must be calibrated by changing the delay between the two pulse trains. The FWHM (Full width half maximum) of $G(T)$ can then be found by dividing it with an appropriate conversion factor k. The conversion factor and the time-bandwidth product, $\Delta\nu\Delta t$, of a transform-limited pulse depend on the pulse shape. Values for Gaussian and $sech^2$ pulse shapes are given in Table 1.

Pulse shapes	k	$\Delta\nu\Delta t$
Gaussian	1.41	0.441
$Sech^2$	1.55	0.315

Table 1: Autocorrelation conversion factors and time-bandwidth products for two common pulse shapes

Where pulse width measurements are quoted in the following chapters, it is this method that has been used. After taking an autocorrelation, a curve fit is then being performed on the experimental data to determine the pulse shape so that relevant conversion factor can then be used to calculate the actual pulse width.

2.5 Summary

In this chapter, we have considered the operating principles of the recirculating loop and have highlighted the design considerations and requirements of the various devices required to operate a recirculating loop. The limitations and problems associated with loop experiments in general and of using a single span loop in particular have been discussed. The methods used to monitor the loop's performance and to take propagation results have also been outlined. Recirculating loop experiments are very important for research and initial stage of long haul system development. In fact, most of the transmission experiments performed in this thesis will mainly be using this method.

References

[1] T. Tanifuji and M. Ikeda. Pulse circulation measurement of transmission characteristics in long optical fibres. *Opt. Lett.*, 16(8), 1977.

[2] P.R. Trischitta, P. Sannuti, and C. Chamzas. A recirculating loop experimental technique to simulate the jitter accumulation of a chain of fibre optic regenerators. *IEEE Trans. Commun.* 36(2):205-213, 1988.

[3] L.F. Mollenauer and K. Smith. Demonstration of soliton transmission over more than 4000 km in fibre with periodically compensated by Raman gain. *Opt. Lett.*, 13(8):675-678, 1988.

[4] D. Malyon, T. Widdowson, E.G. Bryant, S.F. Carter, J.V. Wright, and W.A. Stallard. Demonstration of optical pulse propagation over 10,000 km of fibre using recirculating loop. *Electron. Lett.*, 27(2):120-121, 1991.

[5] N.S. Bergano, J. Aspell, C.R. Davidson, P.R. Trischitta, B.M. Nyman, and F.W. Kerfoot. Bit error rate measurements of a 14,000 km 5 Gb/s fibre-amplifier transmission system using a recirculating loop. *Electron. Lett.*, 27(21):1889-1890, 1991.

[6] C.R. Giles, E. Desurvire, J.R. Simpson, and P.C. Becker. 2 Gb/s signal amplification at λ = 1.53 μm in an erbium-doped single-mode fibre amplifier. *IEEE J. Lightwave Technol.*, 7(4):651-656, 1989.

[7] N. Edagawa, S. Yamamoto, Y. Namihira, K. Mochizuki, and H. Wakabayashi. First field demonstration of optical submarine cable system using LD-pumped Er-doped optical fibre amplifier. *Electron. Lett.*, 25(19):1278-1280, 1989.

[8] N.S. Bergano, J. Aspell, C.R. Davidson, P.R. Trischitta, B.M. Nyman, and F.W. Kerfoot. A 9000 km 5 Gb/s and 21,000 km 2.4 Gb/s feasibility demonstration of transoceanic EDFA systems using a circulating loop. *In Opt. Fib. Comm.* (OFC'91), San Diego, CA, 1991.

[9] H. Taga, M. Suzuki, Y. Yoshida, H. Tanaka, S. Yamamoto, and H. Wakabayashi. 2.5 Gb/s optical transmission using electroabsorption modulator over 11,000 km EDFA system. *In Conf. Laser and Elec. Opt.* (CLEO), Baltimore, MD, OSA, 1991.

[10] T. Widdowson and D.J. Malyon. Error ratio measurements over transoceanic distances using recirculating loop. *Electron. Lett.*, 27(24):2201-2202, 1991.

[11] L.F. Mollenauer, M.J. Neubelt, M. Haner, E. Lichtman, S.G. Evangelides, and B.M. Nyman. Demonstration of error-free soliton transmission at 2.5 Gb/s over more than 1400 km. *Electron. Lett.*, 27(22):2055-2056, 1991.

[12] S. Kawai, K. Iwatsuki, K. Suzuki, S. Nishi, M. Suruwatari, K. Sato, and K. Wakita. 10Gb/s optical soliton transmission over 7200 km by using a monolithically integrated MQW-DFB-LD/MQW-EA modulator light source. *Electron. Lett.*, 30(3):251-252, 1994.

[13] H. Taga, M. Suzuki, N. Edagawa, H. Tanaka, Y. Yoshida, S. Yamamoto, S. Akiba, and H. Wakabayashi. Multi-thousand kilometer optical soliton data transmission experiments at 5 Gb/s using an electroabsorption modulator pulse generator. *IEEE J. Lightwave technol.* 12(2):231-236, 1994.

[14] T. Widdowson, D.J. Malyon, X. Shan, and P.J. Watkinson. Soliton without transmission control using a phase-locked Er fibre ring laser. *Electron. Lett.*, 30(8):661-663, 1994.

[15] H. Toda, H. Yamagishi, and A. Hasegawa. 10GHz optical soliton transmission experiment in a sliding-frequency recirculating fibre loop. *Opt. Lett.*, 20(9):1002-1004, 1995.

[16] G. Aubin, T. Montalant, J. Moulu, F. Pirio, J.-B. Thomine, and F. Devaux. 40Gbit/s OTDM soliton transmission over transoceanic distances. *Electron. Lett.*, 32(24):2188-2189, 1996.

[17] A.D. Ellis, T. Widdowson, and X. Shan. Wavelength dependence of 40Gbit/s solitonic transmission over greater distances greater than 2000 km. *Electron. Lett.*, 32(4):381-382, 1996.

[18] L.F. Mollenauer, P.V. Mamyshev, and M.J. Neubelt. Demonstration of soliton WDM transmission at 6x10Gbit/s and 7x10Gbit/s, error-free over transoceanic distances. *IEEE J. Lightwave Technol.*, 32(5):471-474, 1996.

[19] I. Morita, M. Suzuki, N. Edagawa, S. Yamamoto, H. Taga, and S. Akiba. 20Gb/s single-channel soliton transmission over 9000 km without in-line filters. *IEEE Photon. Technol. Lett.*, 8(11):1573-1574, 1996.

[20] M. Nakazawa, K. Suzuki, H. Kubota, and E. Yamada. 60Gbit/s WDM (20 Gbit/s x3 unequally spaced channels) soliton transmission over 10000 km using in-line synchronous modulation and optical filtering. *Electron. Lett.*, 32(18):1686-1688, 1996.

[21] T. Matsuda, A. Naka, and S. Saito. 4 x 10 Gbit/s RZ-signal transmission over 5.040 km in anomalous regime with optimally dispersion compensated WDM channels. *In Eur. Conf. on Opt. Comm.* (ECOC'97) – Edinburgh), pages Vol.2, 5-8, 1997.

[22] E.A. Golovchenko, J.M. Jacob, A.N. Pilipetskii, C.R. Menyuk, and G.M. Carter. Dispersion-managed solitons in a fibre loop with in-line filtering. *Opt. Lett.*, 22(5):289-291, 1997.

[23] M. Nakazawa, E. Yamada, H. Kubota, T. Yamamoto, and A. Sahara. Numerical and experimental comparison of soliton, RZ pulse and NRZ pulses under two-step allocation. *Electron. Lett.*, 33(17):1480-1482, 1997.

[24] T. Terahara, T. Naito, N. Shimojoh, T. Chikama, and M. Suyama. 85Gbit/s WDM transmission of 16 5.3 Gbit/s RZ data signals over 7931 km using accurate gain equalisation and pre-compensation of group velocity dispersion. *Electron. Lett.*, 33(7):603-605, 1997.

[25] H. Taga, M. Suzuki, Y. Yoshida, S. Yamamoto, and H. Wakabayashi. Bit-error-rate characterisation of IM-DD ultra long-distance optical communication systems with Er-doped fibre amplifiers using a recirculating loop. *IEEE J. Lightwave Technol.* 11(12):2100-2104, 1993.

[26] N.S. Bergano, C.R. Davidson, G.M. Homsey, D.J. Kalmus, P.R. Trischitta, J. Aspell, D.A. Gray, R.L. Maybach, S. Yamamoto, H. Taga, N. Edagawa, Y. Yoshida, Y. Horiuchi, T. Kawazawa, Y. Namihira, and S. Akiba. 9000 km, 5Gb/s NRZ transmission experiment using 274 erbium-doped fibre-amplifiers. *In Opt. Amp. and Their Appl. Topical Meet*, Santa Fe, NM, 1992.

[27] T. Imai, M. Murakami, Y. Fudaka, M. Aiki, and T. Ito. Over 10,000 km straight line transmission system experiment at 2.5 Gb/s using in-line optical amplifiers. *In Opt. Amp. and Their Appl. Topical Meet*, Santa Fe, NM, 1992.

[28] H. Xu, J. Wen, J. Zweck, L. Yan, C. Menyuk, and G. Carter. The effects of Distributed PMD, PDL, and Loop scrambling on BER Distributions in a Recirculating Loop used to emulate long-haul terrestrial transmission. *In Opt. Fib. Comm.* (OFC'03), Georgia, Atlanta, 2003.

[29] N.J. Smith, N.J. Doran, F.M. Knox, and W. Forysiak. Energy-scaling characteristics of solitons in strongly dispersion managed fibres. *Opt. Lett.*, 21(24):1981-1983, 1996.

[30] N.J. Smith, F.M. Knox, N.J. Doran, K.J. Blow, and I. Bennion. Enhanced power solitons in optical fibres with periodic dispersion management. *Electron. Lett.*, 32(1):54-55, 1996.

[31] N.S. Bergano, J. Aspell, C.R. Davidson, P.R. Trischitta, B.M. Nyman, and F.W. Kerfoot. Bit error rate measurements of 14 000 km 5Gbit/s fibre amplifier transmission system using recirculating loop. *Electron. Lett.*, 27(21):1889-1890, 1991.

[32] N.S. Bergano and C.R. Davidson. Circulating loop transmission experiments for the study of long-haul transmission system using erbium doped fibre amplifiers. *IEEE J. Lightwave Technol.*, 13(5):879-888, 1995.

[33] N.A. Olsson. Lightwave systems with optical amplifiers. *IEEE Lightwave Technol.*, 7(7):1071-1082, 1989.

[34] C.J. Anderson and J.A. Lyle. Technique for evaluating system performance using Q in numerical simulations exhibiting intersymbol interference. *Electron. Lett.*, 30(1):71-72, 1994.

[35] D. Marcuse. Calculation of bit-error probability for a lightwave system with optical amplifiers and post-detection gaussian noise. *IEEE J. Lightwave Technol.* 4(4):505-513, 1991.

Chapter 3

Transmission over dispersion managed standard fibre

3.1 Introduction

So far, the theory and some of the problems of soliton propagation in optical fibre have been considered and details of the fibre itself have been assumed, with typical values for the parameters such as effective core area, nonlinearity coefficient and dispersion being used in calculations. While this approach causes no problem in rough calculations, it does have limitations; in particular it assumes that the fibre used is the same throughout the system. Increasingly this is not the case and there is currently a great deal of work

being done with dispersion managed systems [1] – [4], which uses a combination of different types of fibres to give the required average dispersion. This technique was initially mainly being used in NRZ systems [5] – [7] but it is becoming increasingly popular in RZ systems as a means of compensating the high dispersion of standard fibre [8] – [10]. Before considering this important application of dispersion management, stepwise-dispersion profiling will be briefly discussed.

3.2 Dispersion profiling

As discussed in section 1.5.1, the balance between SPM and GVD required for the stability of optical solitons is upset due to the effect of loss. The average soliton model takes account of this fact by ensuring that over one amplifier span SPM and GVD balance each other with SPM dominating in the initial high power section of the fibre and GVD dominating in the latter low power section of the fibre. An alternative method of keeping the soliton balanced is to reduce the dispersion of the fibre exponentially along the length of the system such that the decrease in the SPM due to the exponential fibre loss is matched by a decrease in GVD [11] – [13]. Although there has been some experimental evidence that such systems may be feasible, the careful design and manufacturing of this type of fibre limits the practicality of this scheme. By approximating the exponential decay of the fibre dispersion by a stepwise decrease in the fibre, the mismatch between SPM and GVD can be reduced leading to propagation regimes that are forbidden to uniform dispersion systems becoming accessible [14]. Using a dispersion profile with n steps of fibre leads to an n-fold decrease in the perturbation to the solitons and data rates and/or propagation length can be increased accordingly.

3.3 Dispersion compensation

One of the main problems encountered in long-haul soliton systems is Gordon-Haus timing jitter, which is a consequence of the dispersion of the fibre, and Equation (1.29) shows that this jitter is proportional to the dispersion. It has been shown that by including a dispersion-compensating element, which has the opposite sign of dispersion to that of the transmission fibre, at the end of the transmission fibre the jitter can be reduced since the average dispersion is reduced [15]. Since this discovery, dispersion management on a shorter length scale has led to further improvements in soliton propagation [16] – [19]. It has been discovered that by periodically alternating the sign of dispersion along the transmission line, it is possible to propagate stable pulses. However the nature of the pulse propagation is significantly different from soliton propagation [20] – [22], with the pulse dynamics being closely related to stretched pulse mode-locking in fibre cavities [23]. By using dispersion management, it is possible to achieve stable soliton-like pulses propagation over systems that have a high local dispersion (and even over systems which are predominantly normal dispersion [24] as long as the average dispersion is low and anomalous). This soliton-like pulses are also known as dispersion-managed solitons (DMS). The immediate implication of this is that by periodically including normal dispersive elements to compensate for the high anomalous dispersion of standard fibre, it may be possible to upgrade existing standard fibre links to 10s of Gbit/s date rates [12, 17, 18]. The dispersion compensation using dispersion compensating fibre is used in all of the transmission experiments in this thesis, except for section 3.4 where fibre Bragg grating had been used.

Studies of the dynamics of pulse propagation in dispersion managed systems by using numerical simulations have produced some startling results. It has been shown that

for a simple dispersion map consisting of two fibres with equal length and negligible loss, the stable pulse shape changes from the $sech^2(t)$ profile of the fundamental soliton towards a Gaussian profile as the strength of the map (i.e. the difference between the dispersions of the two fibre) is increased [21, 25]. There is also an increase in the energy of the stable pulses compared to that of the average solitons of a uniform dispersion system with the same average dispersion [21], results in increasing the signal-to-noise ratio (SNR). The energy of the stable pulses of the dispersion managed system being F times greater than the uniform dispersion average solitons with F given by [26]

$$F = 1 + \alpha \left[\frac{(\beta_{2(1)} - \beta_{2(av)})l_1 - (\beta_{2(2)} - \beta_{2(av)})l_2}{\tau_{fwhm}^2} \right] \tag{3.1}$$

The value of α has been found empirically to be ~ 0.7 with the effect of loss neglected. It is not yet certain how loss affects this energy enhancement but there is some evidence that F is reduced when loss is included. Simulations have shown that when the map strength is above a threshold value of ~4, DMS can exist stably even when the average dispersion is normal or zero. In conventional uniform dispersion system, the dispersion must be anomalous to allow soliton propagation and solitons cannot exist with zero or normal dispersion. Another obstacle to soliton transmission is the soliton interaction between adjacent pulses as mentioned in section 1.6.1. Even in DMS systems, soliton interaction is inevitable. A large overlap between adjacent pulses causes the frequency shift through cross-phase modulation (XPM) and, consequently, the adjacent pulses attract each other. In the case when a bit sequence is transmitted, this pulse-to-pulse interaction induces timing jitter and intersymbol interference, resulting in the reduction of the transmission distance. However, the influence of the soliton interaction is alleviated, to some extent, because of the low average dispersion.

In the stable state, the pulse returns to the same profile, peak power and width after each span of the dispersion. Figure 3.1 shows numerical simulation of the dispersion map, pulse width and spectral width over two map periods of DMS.

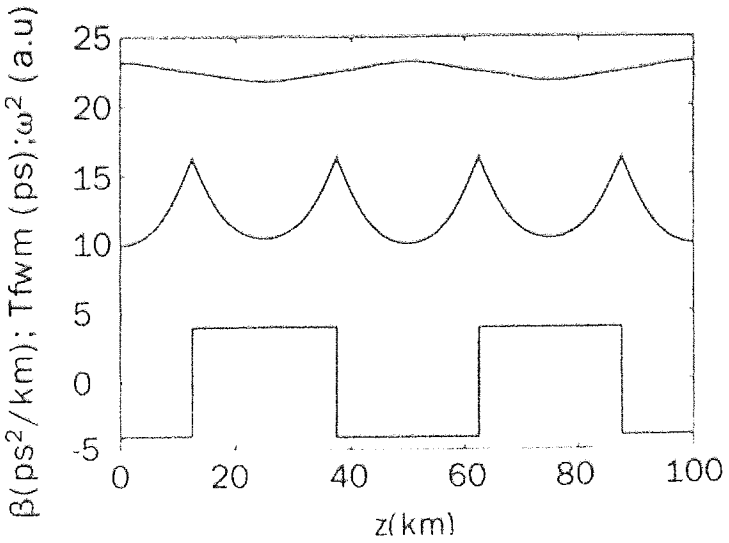

Figure 3.1: Dispersion map, pulse width and spectral width over two map periods of DMS. From reference [27]

From Figure 3.1, we can see that within each period, the pulses broaden and contract and have chirp-free minimum pulses at the centres of each section. The results of these simulations indicate that, if a transform limited pulse is launched at the start of the standard fibre, it must undergo a complex evolution before reaching the stable shape and width which is unchirped at the appropriate points in the fibres. Thus, the optimum launch position into the dispersion map for a transform limited source is not at the start of the standard fibre but at the point where the stable pulse is transform limited. When a chirped source is used, the optimum launch position is altered to match both the magnitude and the sign of the chirp of the source. An alternative way of optimising the match between the source and the dispersion map is to pre-chirp the pulses to give the required sign and magnitude before launching into the dispersion map [28].

In a real system, the lengths of the anomalous and normal dispersion fibres are unlikely to be the same and will also be likely to have different losses. A further issue that must be considered in an amplified system is the positioning of the dispersion compensating fibre in relation to the amplifier [29]. Consider the power of the pulses: at the amplifier output, the power is at the highest and nonlinearity will dominate over GVD. As the pulses propagate along the transmission fibre, the power is reduced due to the attenuation in the fibre and as in the average soliton model; there will come a point where GVD dominates [30]. For a standard fibre system, the compensating fibre will have normal dispersion and so will not be soliton supporting. The characteristics of the pulse evolution will therefore depend on which point this normal fibre is included, relative to the amplifier.

In relation to soliton propagation systems, there are other advantages of using dispersion management. In addition to an alteration in the pulse profile, the energy of the stable pulses is higher than the average soliton power [21]. This has two effects: the signal-to-noise ratio is improved since the signal power is higher and the Gordon-Haus jitter is reduced since the noise injected to each amplifier presents a smaller perturbation to the pulse [31, 32]. The fact that the stable pulse shape changes from $sech^2(t)$ towards gaussian in profile means that soliton-soliton interactions are reduced as the overlap of adjacent solitons is reduced due to the sharpening of the wings of the pulses. In WDM systems, dispersion management can help to reduce the efficiency of the four wave mixing process [33] and decrease the collision induced frequency shift between different channels [34]. These advantages and the simplicity of implementing dispersion compensated standard fibre soliton systems have lead to a rapid growth in interest in such systems.

3.3.1 40Gbit/s experimental results on dispersion managed systems (EDFA-based system)

In this section, we will demonstrate the error free transmission of a single polarisation optical time division multiplexed 40Gbit/s dispersion managed pulse data stream over 1160 km in dispersion compensated standard (non-dispersion shifted) fibre. The experimental setup is shown in Figure 3.2. The pulse source used in this experiment was a mode-locked fibre ring laser (Pritel, Inc), which produced a soliton-like pulse of 3.5ps in duration at a repetition rate of 10GHz. A 2^{31}-1 PRBS data pattern derived from an electronic pattern generator was imposed onto the 10GHz pulse stream by means of a lithium niobate amplitude modulator. A 40Gbit/s data rate was achieved by optical time division multiplexing (OTDM) the pulses using a double Mach-Zehnder type bit-interleaver (MUX) with suitable delays between the different OTDM data channels. The time-bandwidth product was 0.45 at the operating wavelength of 1557nm. An equal amplitude single polarisation 40Gbit/s output could be ensured by using polarization control in the interleaver and by positioning a fibre polariser (POL) at the MUX output. The fibre in the recirculating loop consisted of 74.6km of standard fibre and one DCF module. The DCF reduced the net average dispersion of the loop to +0.04 ps/nm/km and gave partial slope compensation resulting in a net slope of 0.017ps/nm/km. To compensate for the ~29dB loss in the loop, EDFAs were positioned before and after the DCF module. An ASE suppression filter was placed after the second EDFAs to reduce the noise. The pulses were launched into a ~27km length of standard fibre to match the input pulse and the dispersion map. The remaining 47.6km of standard fibre span was positioned after the DCF. The propagation/measurement cycle of the loop was controlled using a delay generator and two acousto-optic switches (AOM) as described in chapter 2.

After propagation, the received signal was demultiplexed to 10Gbit/s using an electro-absorption modulator (EAM) before clock recovery was performed and bit error ratio (BER) measurements or eye diagrams were taken. It has to be mentioned that for all the 40Gbit/s experiments in this thesis, we are required to use the OTDM to multiplex the signals from 10Gbit/s to 40Gbit/s, as well as using an electro-absorption modulator (EAM) or amplitude modulator before clock recovery for demultiplexing because all our the equipments were purchased about 4 to 5 years ago. During that time, this was the only way to perform 40Gbit/s transmission experiments because 40GHz components and equipments were still not available. Nowadays, we are able to purchase these 40GHz components and equipments, but their performances will be slightly difference from our results due to the differences in technologies to build these components and equipments.

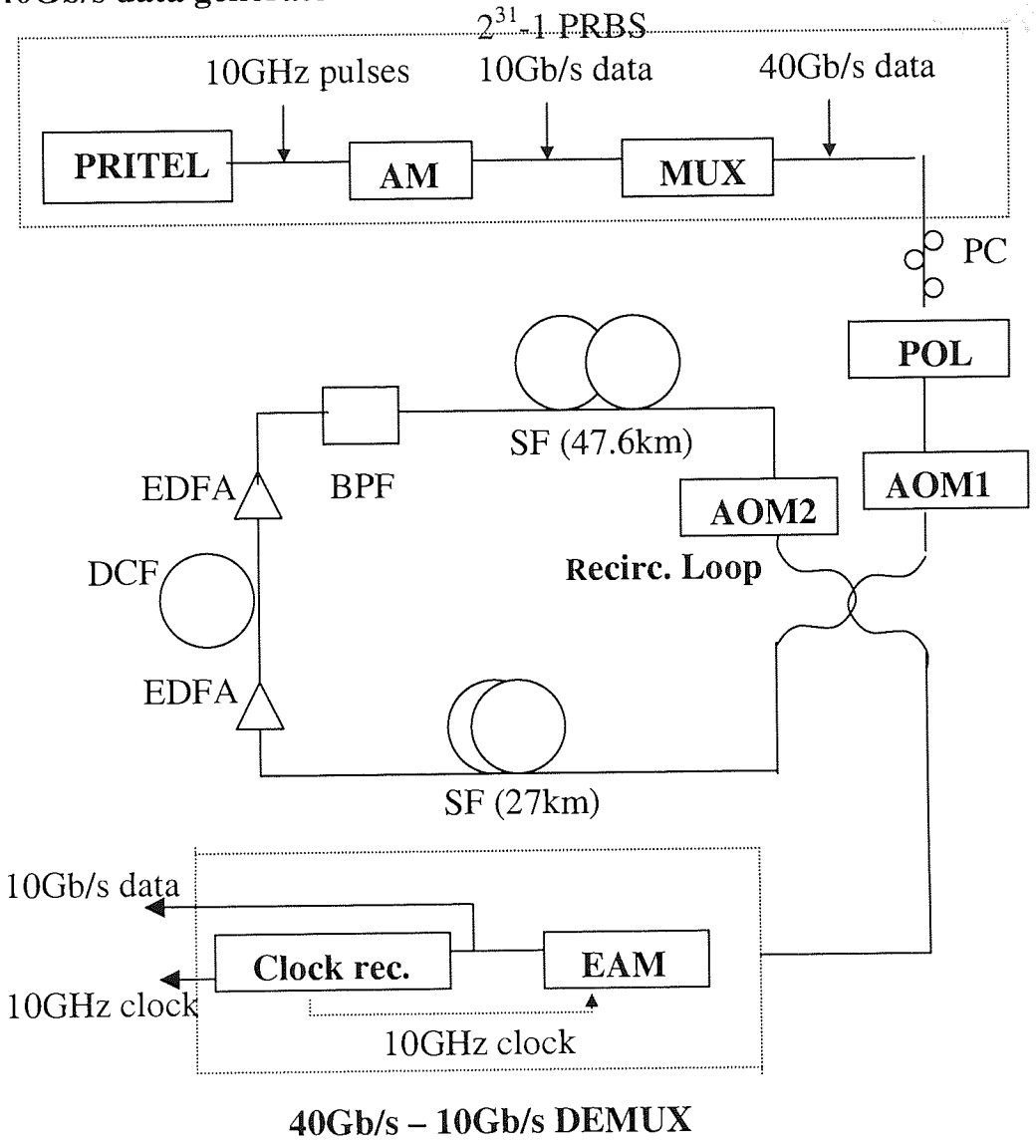

Figure 3.2: Schematic representation of the recirculating loop transmission experiment

Results of BER measurements are shown in Figure 3.3. The maximum error free distance which could be achieved with a 75km standard fibre span was 1160km. In addition to the BER results, eye diagrams of the demultiplexed 10Gbit/s data stream were taken using a sampling scope. Figure 3.4 shows eye diagrams taken for back-to-back performance and at the maximum error free distance of 1160km. These eyes show that although the propagation caused an increase in timing and amplitude jitter leading to

partial eye closure, there was no serious distortion of the pulse shape despite the strong dispersion management.

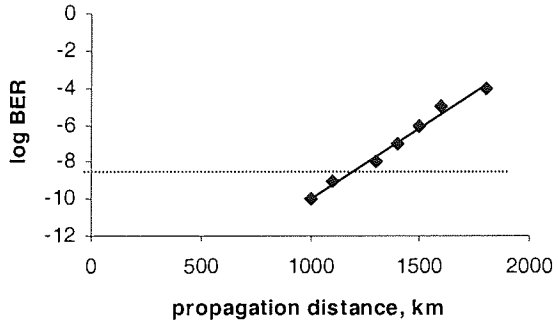

Figure 3.3: BER against propagation distance

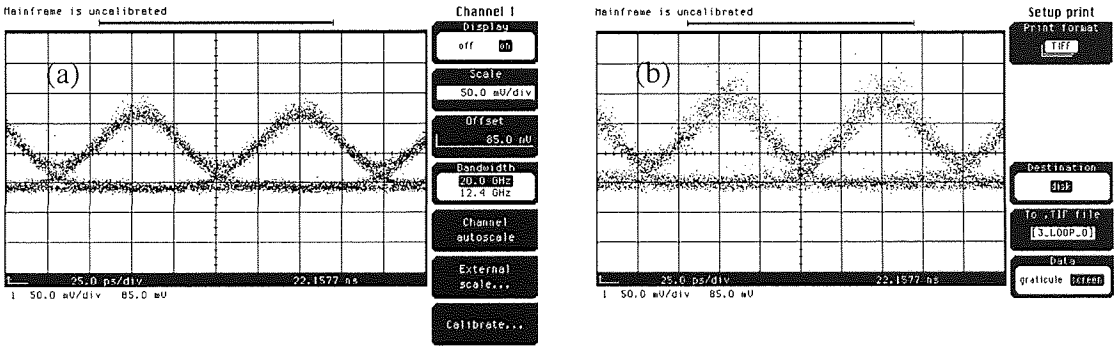

Figure 3.4: Eye diagrams of demultiplexed 10Gbit/s data patterns
(a) Back-to-back performance
(b) Propagation after 1160km

3.4 Chirped fibre Bragg grating as tunable compensator

The most advanced generation of high bit-rate optical fibre communication systems depends on precise design of dispersive components. This is mostly due to the fact that, as the bit-rate increases, the detrimental effect of higher order dispersion becomes more critical. Indeed, the dispersion tolerance of the system reduces as the square of the bit-rate. It is well known that dispersion compensation can be easily achieved by the use of suitable dispersion compensation schemes that alternate spans of anomalous dispersion

fibre (SMF) as spans of normal dispersion fibre (DCF). However, Mezentsev et al. [35] has reported that the accumulated dispersion after each period of the dispersion map is never exactly zero, even if the average dispersion is set to be zero. This is because higher order dispersion compensation is not easily addressed by the dispersion map. As a result, a residual dispersion still affects the system performance at the end of the optical link. Therefore, a post-compensating device that is able to deliver small tunable amounts of dispersion becomes essential at this point. Because of the low cost involved and compact design, a fibre Bragg grating (FBG) seems to be the most promising candidate to realise such a tunable dispersion post-compensator.

The following experiment performed by us have shown that both second and third order dispersion of a linearly chirped fibre grating can be adjusted in a predictable manner by applying a distributed strain to the FBG by the use of a mechanical multipoint bending rig. Here we refer to the photograph and schematic diagram of a multipoint rig as shown in Figure 3.5(a) and (b).

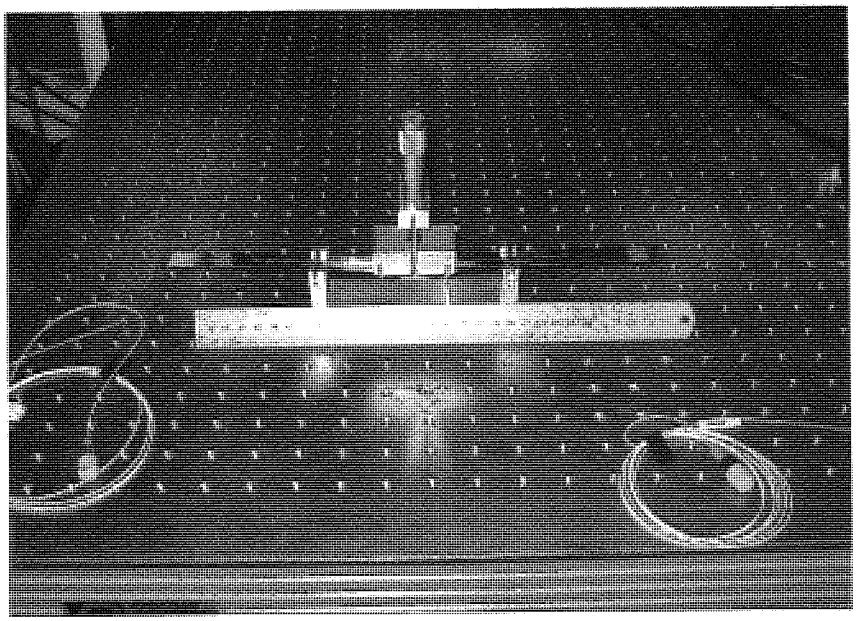

(a)

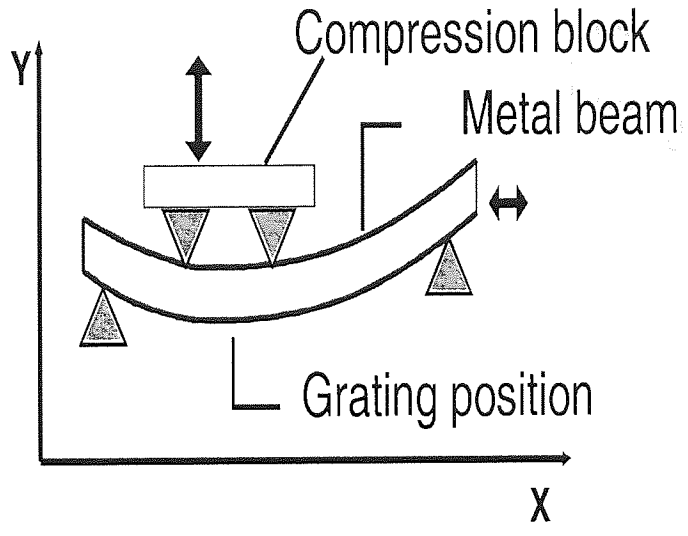

(b)

Figure 3.5 (a) Photograph and 3.5 (b) schematic diagram and working principle of the multipoint mechanical system used to change the dispersion of a linearly chirped FBG

From Figure 3.5(a), it can be seen that the multipoint mechanical system is not bulky at all. It is simply made up of a thin spring steel beam plus a tunable compression block, therefore it is very appropriate for industrial applications. The optical fibre containing the FBG is attached to one side of a thin spring steel beam. In order to eliminate any possible slippage effect, the fibre was glued onto the metal strip and a V groove was etched on the beam to minimise the amount of non-axial strain applied to the FBG.

In the experiment, a 10cm-long linearly chirped FBG was used with a bandwidth of 8 nm and initial chromatic dispersion of –130ps/nm measured at 1550nm. The linear chirped FBG was fabricated by direct exposure to UV laser beam scan by phase mask technique. The characteristic of time delay was measured earlier by using a network analyser in conjunction with a tuneable laser modulated at 1GHz under the measurement condition of the wavelength step of 5pm. From Figure 3.6, it is found that there is no large amplitude of ripple of the group delays, and the side lobe is less than -20dB.

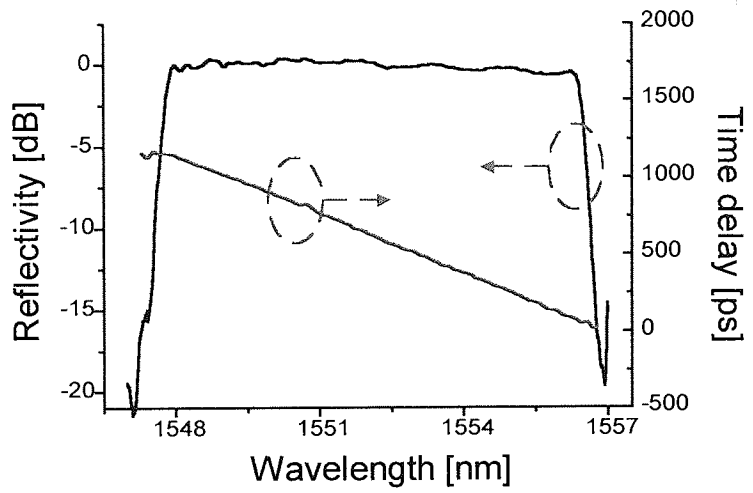

Figure 3.6: Characteristic of time delay verses wavelength of the original chirped grating

The multipoint-bending rig in Figure 3.5 was used to apply a distributed strain to the FBG. By appropriate positioning of the grating in the rig, the strain gradient can also be made variable. As a result of non-uniform strain, the grating becomes nonlinearly chirped. Therefore, both second and third order dispersion vary. More details of the bending device are given elsewhere [36, 37].

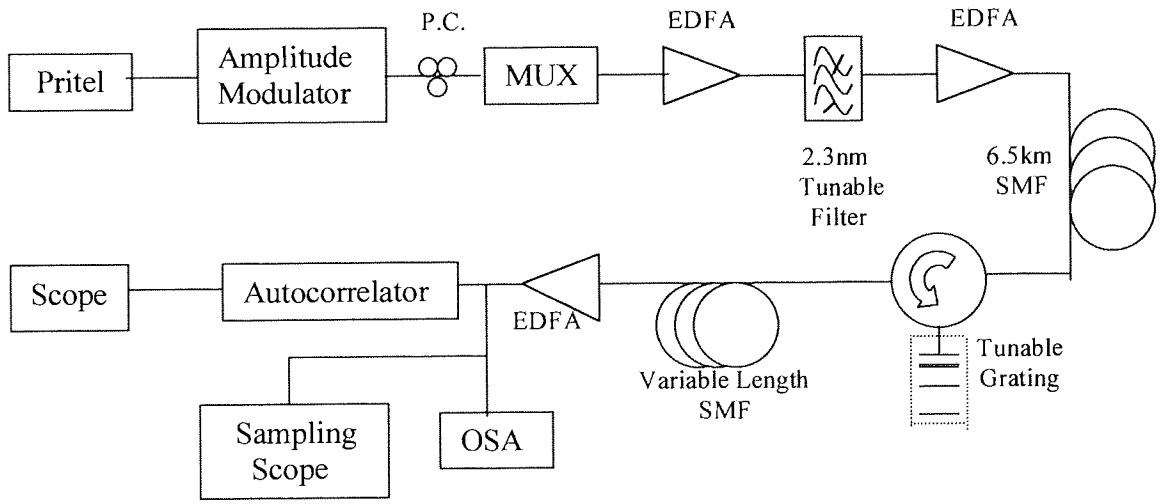

Figure 3.7: Experimental set-up used to test the recompression capability of the tuneable FBG on dispersed optical pulse streams at 10 and 40Gbit/s.

The tunability and the quality of the grating have been tested in a simple experiment using transform limited, 3ps-long pulses. The experimental set up is shown in Figure 3.7.

The pulses were broadened in a fibre delay line and subsequently recompressed in the FBG under different conditions of applied strain.

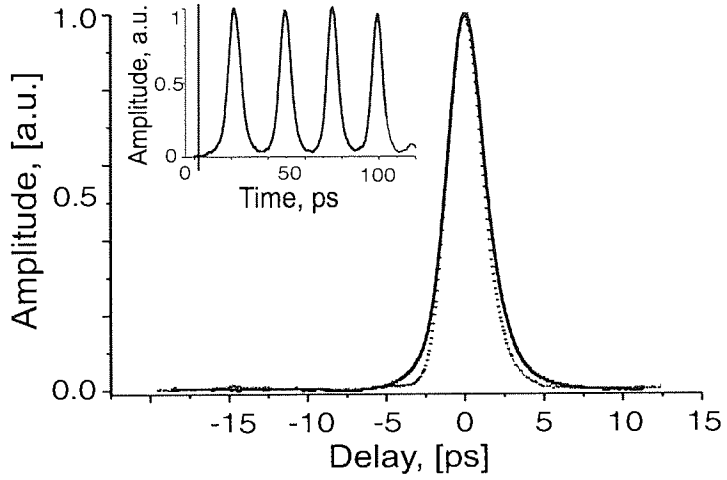

Figure 3.8: Autocorrelator traces of a 10Gbit/s pulse stream as seen from the Pritel laser (dashed line) and after optimum recompression by the tunable FBG (bold line). (Insert, the recompressed pulse stream at 40Gbit/s).

Figure 3.8 shows the autocorrelator traces of a pulse stream at 10Gbit/s from the Pritel and after recompression. Inset is the scope trace of the recompressed pulse stream at 40GHz. The experiment made use of an auxiliary span of SMF after the circulator. We used this fibre to unbalance the total dispersion of the system. When the dispersion in the system became unbalanced, the grating was tuned to the point such that the maximum recompression of the pulse was obtained again.

From results in Figure 3.8, it is clear that for any initial dispersion within the tuning range of the device, the pulse can always be recompressed to ~3.6ps. The distributed strain used for tuning the dispersion and slope of the FBG does not seem to affect its time delay ripples, i.e. the recompression capability of the device is not compromised by the imposed mechanical action. The grating has a recompression ratio of approximately 83% under any applied strain. This is also an indication of the fact that

the apodisation technique utilised to reshape the FBG's profile can actually work well to keep the amplitude of dispersion ripples low.

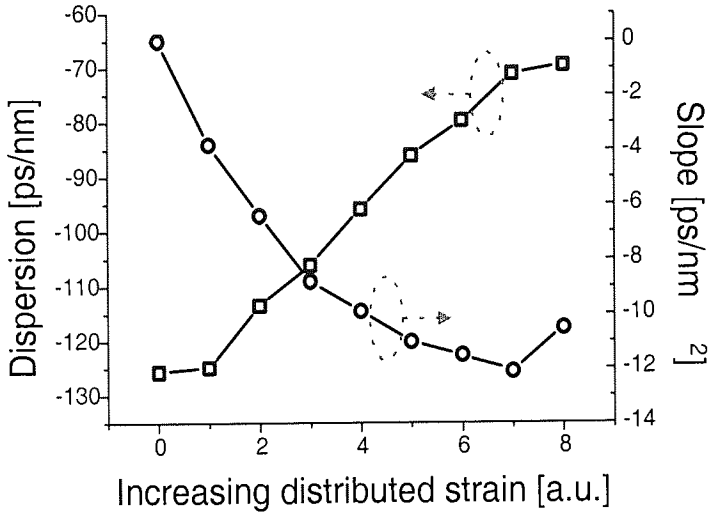

Figure 3.9: Chromatic dispersion D and dispersion slope S for the strained grating at 1550nm.

The next step has been the characterisation of the dispersion and dispersion slope that the device can deliver as a function of the applied strain using high-precision measurement in the frequency domain. The results of the low and high strains applied are shown in Figure 3.9. The measurements were made at 1550nm. A supplementary degree of freedom is offered by the displacement of the metal beam along the direction of the fibre axis. This shift would impose the maximum strain on a physically different region of the FBG, then affecting the value of dispersion and slope measured for a given wavelength. For instance, the range of variability of the chromatic dispersion at 1550nm, i.e. difference between the dispersion measured when grating is subjected to low and high strain is ~ 60ps/nm, where dispersion is –130ps/nm for low applied strain and –70ps/nm for high applied strain. The dispersion slope varies from 0 ps/nm^2 to 13 ps/nm^2.

3.5 Stimulated Raman Scattering

Stimulated Raman scattering is a nonlinear, inelastic scattering process that causes radiation propagating in the fibre to be shifted to new frequencies through interaction with optical phonons (molecular vibrations) in the fibre medium. Spontaneous Raman scattering is a linear effect and only describes the process where pump photons are scattered from the optical phonons. In stimulated Raman scattering, the scattered photons recombine with other pump photons and induce further molecular vibrations in the medium at the optical phonon frequency, thus enhancing the amount of scattered radiation.

This process was first observed in optical fibres in 1970 by Ippen et al [38] and can be described as a three wave mixing proceeds using the imaginary part of the nonlinear susceptibility. The total photon energy is not conserved in SRS since it is an inelastic scattering process. However, there is still conservation of the total energy when the optical phonons are included. If a pump photon at ω_p scatters from the optical phonons ω_o, to produce two new photons ω_{as} and ω_s, this can be written as:

$$\omega_s = \omega_p - \omega_o \tag{3.2}$$

$$\omega_{as} = \omega_p + \omega_o \tag{3.3}$$

where frequency downshifted photons (ω_s) and the frequency upshifted photon (ω_{as}) are referred to as the Stokes and anti-stokes frequencies respectively. When the process is stimulated, the Stokes radiation is amplified and the anti-Stokes radiation is attenuated. SRS is sometimes referred to as a self-phase matched process. This is because it is the pump field in combination with the scattered field which enhances oscillation of the molecules so that the field are automatically phase matched.

Neglecting the effects of loss, parametric FWM and pump depletion, the differential equation used to describe evolution of the Stokes and anti-Stokes waves are [39]:

$$\frac{dI_s}{dz} = gI_P I_s \tag{3.4}$$

and

$$\frac{dI_{as}}{dz} = -gI_P I_{as} \tag{3.5}$$

where I_p, I_s and I_{as} are the intensities at the pump, Stokes and anti-Stokes waves respectively and g is the value of the Raman gain. These equations have solutions:

$$I_s(L) = I_s(0) \exp(gI_oL) \tag{3.6}$$

$$I_{as}(L) = I_{as}(0) \exp(-gI_oL) \tag{3.7}$$

Where $I_s(0)$ and $I_{as}(0)$ are the input intensity at $z = 0$. I_o is the input intensity and L is the interaction length. The value of the Raman gain is given by the equation [40]:

$$g = \frac{\sigma_O \lambda^3}{c^2 h \xi} \tag{3.8}$$

where σ_o is the differential cross-section, c is the speed of the light, h is the plank's constant and ξ, the dielectric constant at the Stokes wavelength, λ. Typically $g = 3 \times 10^{-14}$ m/W for standard single mode fibre pumped at 1550nm [39]. The gain curve typically extends over a range of up to 40THz in bulk samples of fused quartz and in silica fibres. The Raman gain spectrum consists of a number of smaller peaks in the tails. The peak spectrum is at 13THz. An example of a typical Raman gain curve for fused silica is shown in Figure 3.10.

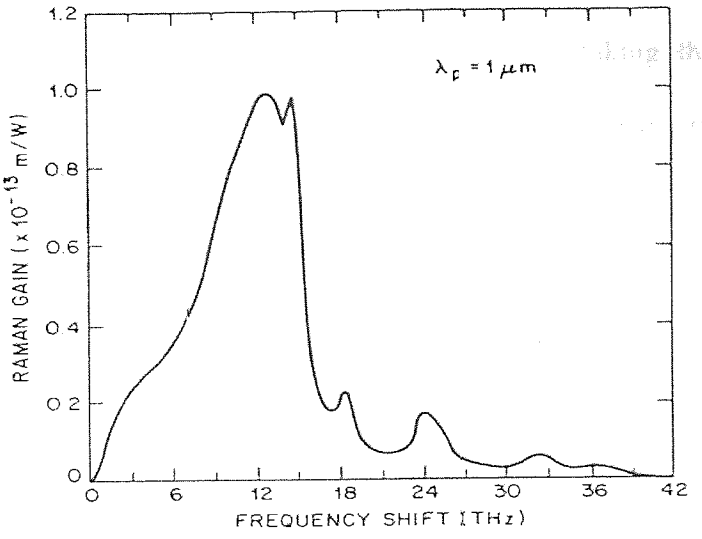

Figure 3.10: Measured Raman-gain spectrum for fused silica at a pump wavelength $\lambda p = 1$ μm. From reference [40]

The main reason for this large frequency range for silica is due to the noncrystalline nature of silica glass. In amorphous materials such as fused silica, molecular vibrational frequencies spread out into the bands that overlap and create a continuum. As a result, in contrast to most media where Raman gain is specific at well-defined frequencies, the Raman gain in silica fibres extends continuously over a broad range. Later in this chapter, we will show that optical fibre can be used as broadband amplifiers because of this feature.

This nonlinear process can greatly facilitate the generation and amplification of picosecond and femtosecond pulses as well as being useful for the generation of new frequencies. In telecommunication networks, it can also be a problem and lead to the degradation of signal information. A SRS threshold was defined by Smith et al. [41] which represents the power level at which the Stokes power equals the pump power. For the purposes of calculating the SRS thresholds, it is the main peak that contributes exclusively to the growth of the Stokes waves. The gain curve is usually assumed to

consist of a single Lorenzian peak [41]. Calculations of SRS therefore make use of the peak value of the spontaneous Raman gain spectrum g_{SRS} taking this as the gain coefficient for SRS. However, for applications such as fibre Raman amplifiers and to calculate the crosstalk in long haul WDM communication systems, the actual shape of the Raman gain curve is very important. The Raman gain coefficient is known to be inversely proportional to the pump wavelength and is dependent on the composition of the core material – varying significantly with the dopants used [42].

The SRS threshold is given by the equation:

$$P^{cr} = \frac{bKA_{eff}}{g_{SRS} L_{eff}} \tag{3.9}$$

where A_{eff} is the effective core area, g_{SRS} the Raman gain, L the effective fibre length, b is the state of polarisation and K a factor that depends on the fibre parameters. Typically this has a value of 16 (forward) – 20 (backward). As an example, for a typical single mode fibre with a length of 12.5 km, an effective core area of $50\mu m^2$ and a loss value of 0.2dB/km,

$$\text{Effective nonlinear length} = \frac{(1-\exp(-0.23*\alpha[dB/km]*L))}{0.23*\alpha[dB/km]} \tag{3.10}$$

$$= \frac{1-\exp(-0.23*0.2*12.5)}{0.23*0.2}$$

$$= 10.93\text{km}$$

Substitute this value into Equation (3.9) for critical power limit, assuming b = 2 for scrambled polarisation, $g_{SRS} = 10^{-13}$ m/W and K = 20 for backward SRS:

$$P^{cr} = \frac{2*5*10^{-11}*20}{10^{-13}*10930}$$

$$= 1.818\text{W}$$

It can be seen from Equation (3.9) that the threshold power falls significantly for longer fibres. In addition, the threshold power for backward scattering is higher than that for forward scattering. Therefore forward scattering normally dominates before the stimulated backward scattering is observed. However, it must be remembered that amplification of a backward propagating signal can also be observed since Raman amplification is independent of the relative directions of the pump and probe waves. Once the SRS threshold is reached, the power will transfer from pump power to Stokes rapidly. If the amount of Stokes radiation generated is sufficient and greater than the SRS threshold, it can also experience SRS, causing further spectral shifting of the radiation. This process of one Stokes band acting as a pump for another Stokes band is referred to as cascade Raman.

3.5.1 Feature of the fibre Raman amplifier

Until the late 1980s, researchers studied most of the fundamental features of fibre Raman amplifiers using large-scale pump laser sources [43]. Because the Raman-gain coefficient of optical fibre is small, realisation of a sufficient amount of gain over tens of kilometres of fibre requires far more than 100mW of pump power. In the early days of optical amplifier development, efficiency was paramount. Since Raman amplifiers were characterised by low efficiency, the leading role in optical communications was assumed by EDFA technology described in chapter 1. There seemed to be no place for Raman amplifiers before the explosion of Internet demands, the advent of WDM and, more importantly, the maturation of 14XX-nm high-power pump laser diodes.

It is worth recognising that the efficiency of Raman amplifiers is fundamental to their ability to function as distributed amplifiers, since the pump light propagates over a

long distance without being significantly depleted by amplified signals. Distributed amplifiers, because of their low-noise characteristics, can be essential to the enhancement of transmission performance. The fundamental process of Raman amplification occurs through the virtual upper states of a molecule. This fact implies that Raman amplification does not entail any significant absorption of signal photons. For this reason, Raman amplification generates little noise in the presence of pump light: in this case, the Raman amplifier simply becomes a passive, low-loss silica optical fibre. An EDFA, on the other hand, contains Er ions that strongly absorb signal photons in the absence of pump light generating much noise. As a result, pumping conditions must be optimised to achieve good noise performance in EDFAs.

Figure 3.11 plots signal power excursions over distance with and without a distributed gain, showing how distributed gain enhances transmission performance. In designing an optical transmission system, one should optimise the signal level in terms of noise and nonlinearity; optical amplification of lower signal level adds higher noise, whereas higher-level signals suffer more from nonlinearity in fibre. It is apparent from this figure that introducing a distributed gain increases the range of the optimal signal levels.

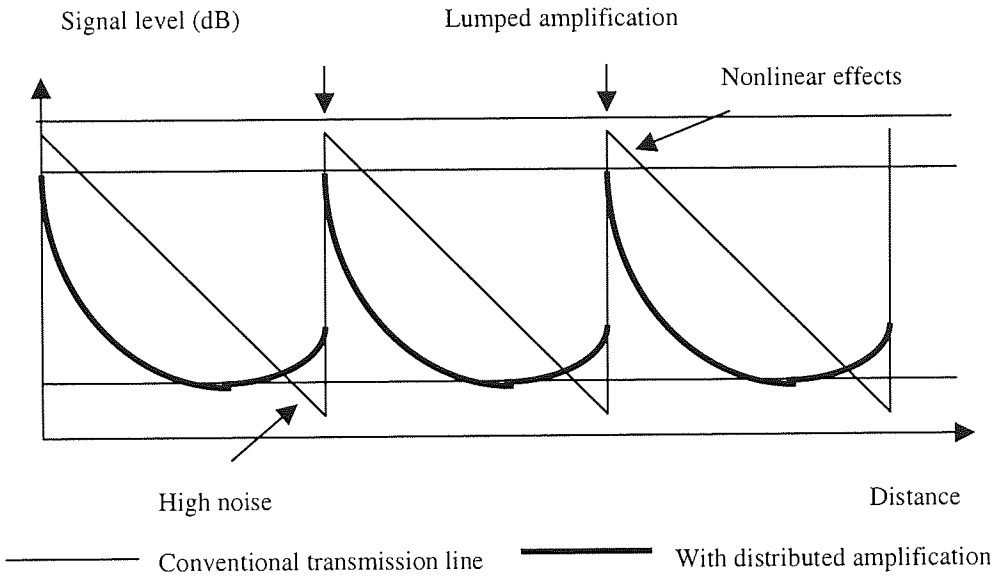

Figure 3.11: Signal excursion over distance. From reference [44]

One could also obtain extra power-budget margins by introducing distributed Raman gain. These margins could be used for various system improvements, such as increasing bit rates per channel, extending electrical regeneration distances, and enhancing spectral efficiencies.

Figure 3.12 shows a schematic of a fibre Raman amplifier. Fibre Raman amplifiers typically consist of an optical fibre as a gain medium, a counterpropagating pump light source, a wavelength-sensitive coupler to combine the pump and the signal, and an optical isolator. With the exception of the gain medium, the configuration resembles that of an EDFA. In Raman amplification, it is important to use unpolarised pump sources to avoid polarisation-dependent gain, because stimulated Raman scattering is a polarisation-sensitive process. Depolarisation, in particular, is necessary for laser diodes that emit linearly polarised light [44].

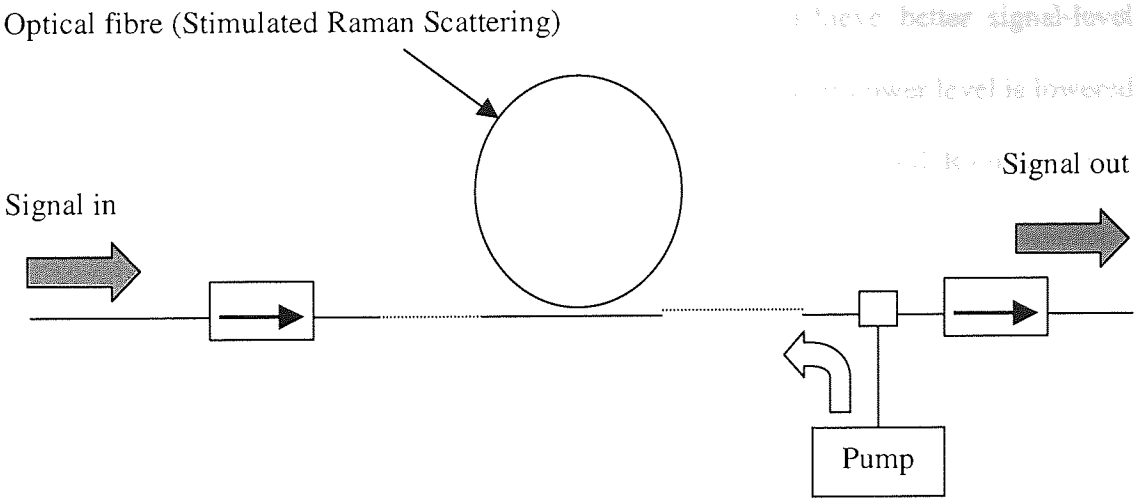

Figure 3.12: Typical scheme of fibre Raman amplifier. From reference [44]

Because of the isotropic nature of optical phonons, stimulated Raman scattering can occur for almost any orientation of pump and signal lights: since for a given range of frequency, optical phonons can have wave vectors that are almost arbitrary, they can couple with pumps and signals in any direction. In fact, fibre Raman amplifiers can be configured to be either copumped or counterpumped, maintaining in either case almost the same gain efficiency. Because the signals receive gain from both copumped and counterpumping light, the Rayleigh-backscattered signal also receives gain and does not, as happened, under unpumped conditions, decay. In this case, the nondecaying Rayleigh-backscattered portion of signal light Rayleigh backscatters again to interfere with the original signal with an indefinite amount of time delay. This phenomenon is called double-Rayleigh backscattering (DRBS) multiple-path interference (MPI) noise. Because DRBS signals travel the gain medium twice whereas the original signals travel the gain medium once, the signal-to-DRBS-MPI-noise ratio decreases when the Raman gain and the effective interaction length increase. This phenomenon translates into a limit on gain or effective length beyond which Raman amplifiers no longer improve system performance.

Counterpumped, distributed Raman amplifiers can achieve better signal-level excursion because the signals tend to be amplified only when their power level is lowered because of fibre span loss. In Figure 3.12, in which counterpumped Raman gain is assumed, it can be seen that the average path signal level is low, allowing nonlinear effects to be avoided, although the signal level fits well in the admissible transmission window. Therefore, to solve any noise issues, Raman amplifiers are usually configured as counterpumped.

Elongation of optical repeater spacing is an important issue for terrestrial long-haul optically repeated transmission system since it leads to a reduction in the number of repeaters and consequently, a lower total system cost. Distributed Raman amplification (DRA) is one of the most attractive techniques for achieving this target since DRA reduces transmission losses and thus improves the OSNR. I. Morita et al. [45] has demonstrated that by using hybrid amplification scheme using Raman amplification and an EDFA in ultra-long-distance 40Gbit/s transmission system. The same performance can be obtained by doubling the repeater spacing. The use of DRA has great promised particularly in terabit systems or better because it can be operated for any wavelength band by applying adequate pump wavelengths. Recent experimental demonstrations of ultra-high capacity WDM transmission system with aggregate capacities of more than 1 Tb/s have been based on distributed Raman amplification [46]. T.N. Nielsen et al. [47] has shown that record capacity of 3.28 Tb/s can be achieved by using dual C- and L-band hybrid Raman/ Erbium-doped inline amplifiers. S. Bigo et al. [48] has achieved 5.12Tb/s long-haul transmission experiment over 3 x 100km of Tearlight fibre. In fact, Y. Zhu et al. [49] has found that all-distributed Raman amplification allowed best

transmission performance over hybrid Raman/EDFA amplification by making a comparison between them.

Despite their many advantages, WDM-pumped Raman amplifiers are characterised by a serious problem: the effect of four-wave mixing (FWM) of pump and signal lights in small dispersion fibres. In particular, many nonzero dispersion-shifted fibres (NZDSF) have zero-dispersion wavelength in WDM pumping and signal wavelength ranges. FWM occurs around the zero-dispersion wavelength. The pump and signal lightwaves at different wavelengths around the zero-dispersion wavelength generate FWM lightwaves, which deteriorate the signals. To avoid these adverse effects, one should use a fibre with a zero-dispersion wavelength shorter than the pump wavelengths. One option is to use a dispersion-managed combination of standard single-mode fibre (SMF) and dispersion compensating fibre (DCF) [50]. Recently, other new types of non-zero dispersion shifted fibre (NZDSF) with such dispersion characteristics have also been developed [51, 52].

3.5.2 40Gbit/s experimental results on all-Raman amplified dispersion managed system

There is an increasing interest at present in techniques for upgrading installed terrestrial network that consists predominantly of standard single mode fibre (SMF) to 40Gb/s and beyond [53] – [56]. Distributed Raman amplification (DRA) is a promising technology since it can improve the optical signal-to-noise ratio (OSNR) and significantly suppress nonlinear intrachannel effects caused by severe pulse broadening due to large dispersion of SMF [57, 58]. When RZ signal of short pulse width propagating along the strong dispersion managed transmission line consists of SMF and dispersion compensation fibre (DCF), combining both dispersion management and distributed Raman amplification,

error free propagation of 40Gbit/s single channel data stream over SMF transmission line of 1300km with 36km amplification spacing was reported [58].

For terrestrial long haul transmission systems with amplification spacing of 80km or 100km SMF, high Raman pump power is needed to provide enough gain to compensate for the loss experience by data stream. However, for high Raman gains (10 – 20dB) and pumps, the multipath interference (MPI) owing to double Rayleigh backscattering of the signal (DRBS) might cause severe degradation of transmission performance [59] – [63]. Simulation results [62] and a 10Gbit/s-based NRZ transmission experiment [63] demonstrated the possibility to reduce the DRBS power and diminish MPI-caused system degradation by optimising dispersion managed fibre span configuration which consists of positive (PDF) and negative dispersion fibre (NDF). In the following experiment, a single channel 40Gbit/s signal propagating over an all Raman amplified dispersion managed SMF transmission line was investigated experimentally. In our experiments, dispersion map consisting of spans including two sections of SMF of different lengths and two DCF modules of different dispersion values. One pair of SMF and DCF formed a dispersion overcompensated subspan and another pair of SMF and DCF made a dispersion undercompensated subspan. The two subspans constructed a fully dispersion compensated span which was similar to [64]. All the four sections of fibres were Raman pumped individually. By optimising the configuration of dispersion managed fibre span and Raman pump power, one type of span configuration shows robustness to DRBS; error-free propagation of a single channel 40Gb/s over a record transmission distance of 1973km in conventional SMF with terrestrial amplification spacing has been achieved.

The experimental setup was similar to section 3.3.1 except for the fibres and EDFAs being replaced by Raman amplifiers within the recirculating loop. The parameters of fibres used in experiments are summarised in table 2. The standard single mode fibre was Corning SMF 28, with effective area of 80 $\mu m*\mu m$, Raman-gain coefficient of 7.9 x 10^{-4}/W*m. The DCF modules were OFS DK80, with effective area of 20 $\mu m*\mu m$, Raman-gain coefficient of 3.16 x 10^{-3}/W*m. Since DCF modules have smaller effective area and higher Raman-gain coefficient, the amount of pump power from the Raman to the DCF has to be controlled precisely to prevent any nonlinearity from destroying the signals. The fibre losses at 1550nm in table 2 include the connector losses and the insertion losses of Raman pump WDMs. The SMF #1 and DCF #1 constructed a dispersion overcompensated subspan. The SMF #2 and DCF #2 made dispersion undercompensated subspan. The average dispersion of the total span at 1550nm was 0.11 ps/nm/km and the average dispersion zero wavelength was about 1553.6nm. A small piece of SMF was used just before receiver to fine-tune the overall dispersion compensation after loop recirculation. Four span configurations shown in Figure 3.13 were investigated by placing SMF and DCF in different positions in the span. In all span configurations, distributed Raman amplifiers were used to compensate for the losses of SMF and DCF. The Raman pumps were counter-propagating with respect to the signal in SMF and DCF. Two Raman fibre lasers operating at 1455nm were used to pump dispersion overcompensated subspan and dispersion undercompensated subspan separately. Each Raman fibre pump laser was shared by one pair of SMF and DCF in the same subspan, the Raman pump was divided by a high power Raman fibre coupler. For each Raman coupler, there was approximately 70% pump power injected into SMF and 30% into DCF via Raman WDMs. An optical isolator was built in each Raman WDM.

Table 2: Fibre Parameters

	Length, km	Loss, dB @1550nm	Loss, dB/km @1455nm	Dispersion, ps/(nm·km) @1550nm	Dispersion slope ps/(nm^2·km) @1550nm
SMF #1	77.88	17.49	0.247	16.54	0.06
SMF #2	88.76	20.55	0.279	16.54	0.06
DCF #1	14.14	11.66	0.81	-96.11	-0.0568
DCF #2	16.33	12.12	0.87	-84.2	-0.0574

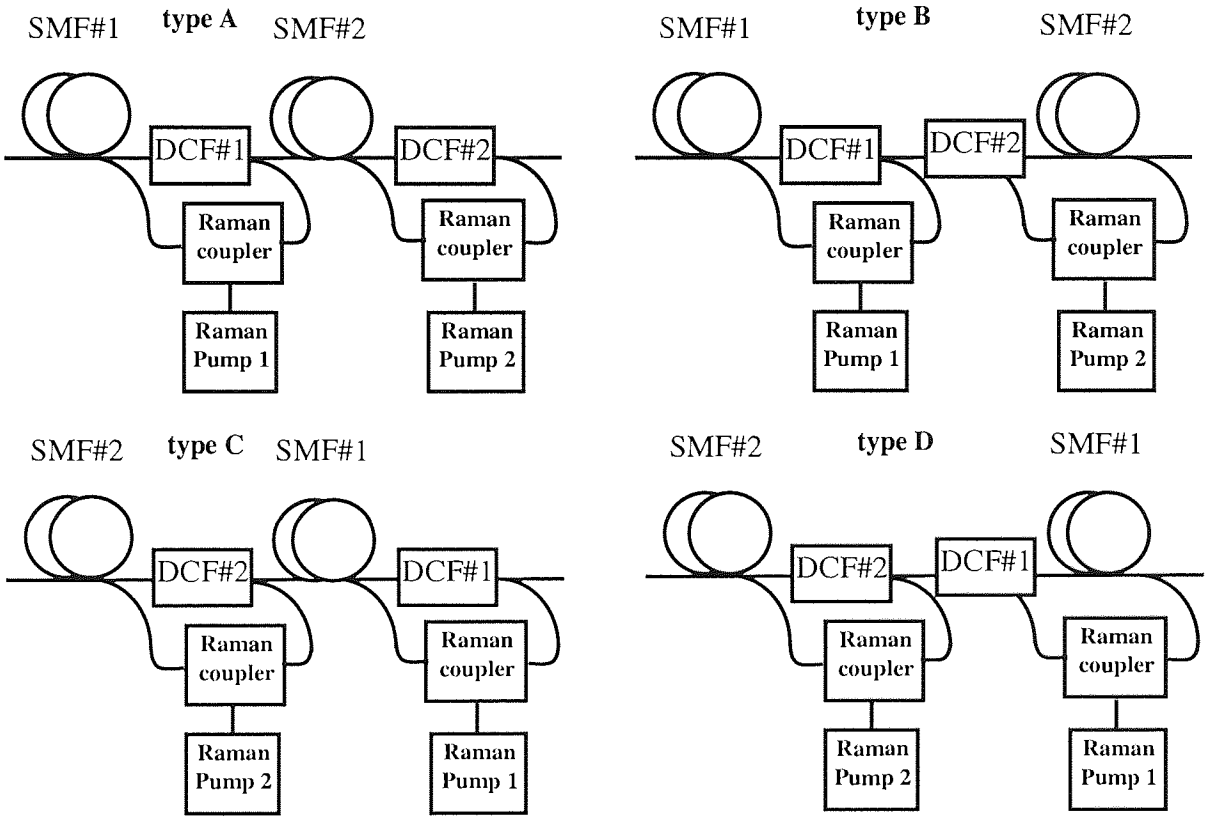

Figure 3.13: Fibre span configurations

In our experiments, Raman pump laser should provide 1.2 – 1.3W output to compensate for the total loss in each subspan. The measured OSNR degradation in 88km SMF, on the average was 5dB higher than that in 77km SMF at different Raman pump levels. There was no difference of OSNR degradation in the two DCF modules. In our later discussion, we will pay more attention on the optimisation of Raman pump for the 88km SMF dispersion undercompensated subspan. At high Raman pumps such as 1.2 – 1.3W, the MPI owing to DRBS might cause severe degradation of the electrical signal-to-noise

ratio of received data stream while the optical signal-to-noise ratio (OSNR) remains high since the spectra of the DRBS and the signal coincide [59, 61, 62]. To investigate this issue in our experiments, the Q factor and OSNR of signal after 6 circulations (approximately 1200km) in the four types of span configuration were measured. Figures 3.14(a) and 3.14(b) show the dependence of OSNR and Q factor on the output power of Raman pump 2 with different span configurations respectively, while the output of Raman pump 1 was kept at 1.3W to fully compensate the loss of the dispersion overcompensated subspan during the measurement, the Q factor was measured on a sampling oscilloscope. The optimised pulsewidth of input pulse was 3.5ps (full width half maximum, FWHM) and launch power was –2dBm. The OSNR of launched signal was 33dB. The Q factor of back-to-back signal was 15. Without MPI, OSNR and Q should have similar trend. One can easily see the Q factors first rise with pump power then drop quickly after reaching the highest value for type B to D in spite of improving of OSNR, especially for type B. But for type A, that had relative low OSNR value compared to other types shows slight Q factor degradation at high pump levels. Above results indicate that there was smallest DRBS power in type A and MPI causes slightest system degradation for type A. It also suggests that type A is more robust to the fibre nonlinearity than the other types at high Raman gain.

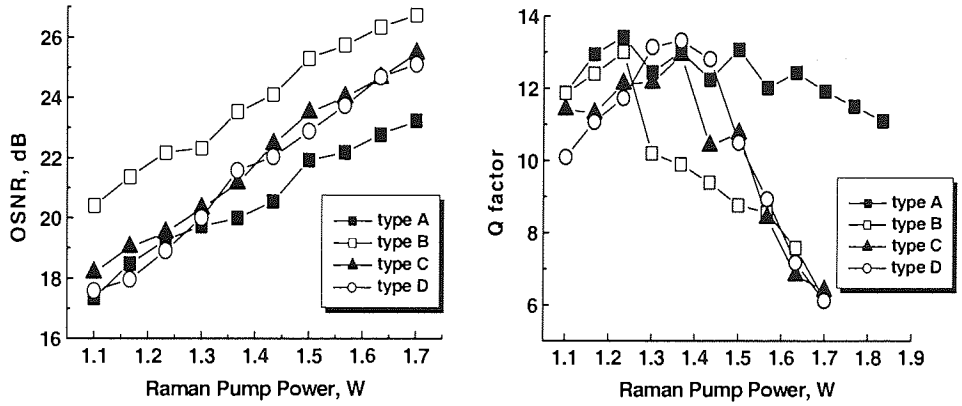

(a) (b)

Figure 3.14: (a) OSNR and (b) Q factor of signals after 6 loops of recirculation against pump power of Raman laser 2

Figure 3.15(a) shows the best transmission performance achieved for the different types of span configuration with optimised transmission conditions. The longest error free transmission distance of 1970km was achieved using type A, corresponding to 10 recirculations of the loop. Figure 3.15(b) is the OSNR evolution against propagation distance when the best transmission achieved using different types of span. It clearly shows that the OSNR remains high after long propagation distance for type A.

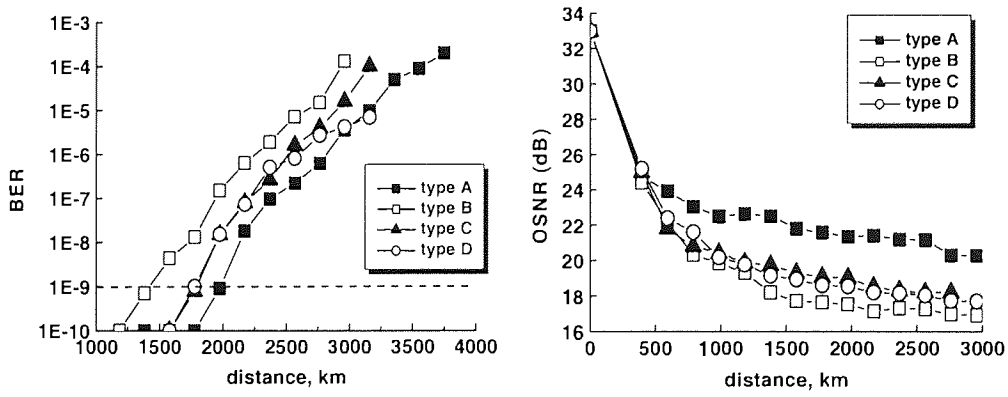

(a) (b)

Figure 3.15: (a) BER performance and (b) OSNR evolution for different types of span configuration when the longest error free propagation distance was reached

Figure 3.16 shows the eye diagrams taken for back-to-back performance and at the maximum error free distances for type A span configuration. These waveforms show that no severe timing and amplitude jitters occurred despite of the strong dispersion management even after 1973km propagation.

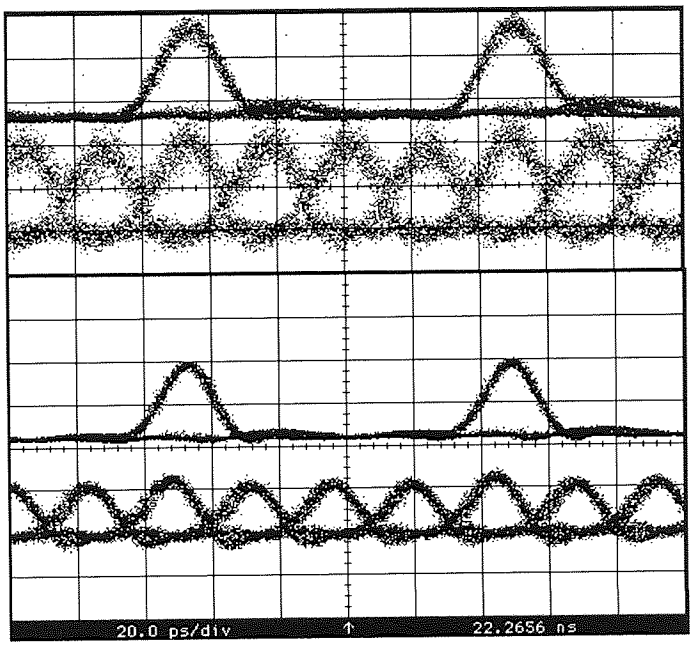

Figure 3.16: Eye diagrams of 40Gbit/s and demultiplexed 10Gbit/s data stream for type A span configuration. Upper: after 1970km propagation, Lower: back-to-back

3.6 Summary

Dispersion management techniques using both the dispersion profiling and dispersion compensation were analysed and discussed. A simple 40Gbit/s dispersion managed system experiment using the EDFAs was demonstrated. We are able to fabricate a novel chirped fibre Bragg grating-based device specifically for higher order dispersion, which will become very critical when data rates increase to 40Gbit/s or above. From our results, it shows that it is capable of compensating the second and third order dispersion by using a simple multi-point device bending the chirped fibre Bragg grating. An overview of the stimulated Raman scattering and its advantages over the erbium-doped fibre amplifiers

were illustrated. The use of Raman amplifiers in an all-Raman pumped 40Gbit/s single channel over the standard single mode fibre was built and tested. The experimental results show that if the dispersion map is not optimised correctly, detrimental effects associated with high power Raman amplification can cause degradation to the system.

References

[1] C. Kurtzke. Suppression of fibre nonlinearities by appropriates dispersion management. *IEEE Photon. Technol. Lett.*, 5(10):1250-1253, 1993.

[2] N. Edagawa, I. Morita, M. Suzuki, S.Yamamoto, H. Taga, and S. Akiba. 20Gbit/s, 8100km straight line single channel soliton based RZ transmission experiment using periodic dispersion compensation. *In Eur. Conf. on Opt. Comm.* (ECOC'95 – Brussels), pages 983-986, 1995.

[3] M. Suzuki, I. Morita, S. Yamamoto, N. Edagawa, H. Taga, and S. Akiba. Timing jitter reduction by periodic dispersion compensation in soliton transmission. *In Opt. Fib. Comm.* (OFC'95) – Washington D.C., pages PD20. OSA, 1995.

[4] M. Suzuki, I. Morita, N. Edagawa, S. Yamamoto, H. Taga, and S. Akiba. Reduction of Gordon-Haus timing jitter by periodic dispersion compensation. *Electron. Lett.*, 31(23):2027-2029, 1995.

[5] R.W. Tkach, A.R. Chraplyvy, F. Forghieri, A.H. Gnauck, and R.M. Derosier. Four-photon mixing and high-speed WDM systems. *IEEE J. Lightwave Technol.*, 13(5):841-849, 1995.

[6] L. Eskilden, P.B. Hansen, S.G. Grubb, A.M. Vengsarkar, S.K. Korotky, T.A. Strasser, J.J. Veselka, J.E.J. Alphonsus, D. Truxal, and D.J. Digiovanni. Single-fiber repeaterless transmission over 490 km at 2,488 Gbit/s using a remote preamplifier and dispersion compensation. *Electron. Lett.*, 32(18):1969-1967, 1996.

[7] N.S. Bergano and C.R. Davidson. Wavelength-division multiplexing in long-haul transmission systems. *IEEE J. Lightwave Technol.*, 14(6):1299-1308, 1966.

[8] F. Favre, D. LeGuen, M.L. Moulinard, M. Henry, G. Michaud, F. Devaux, E. Legros, B. Charbonnier, and T. Georges. Demonstration of soliton transmission at 20Gbit/s over 2200 km of standard fibre with dispersion fibre with dispersion compensation and prechirping. *Electron. Lett.*, 33(6):511-512, 1997.

[9] P. Harper, F.M. Knox, P.N. Kean, I. Bennion, and N.J. Doran. 10Gbit/s soliton propagation over 5250 km in standard fibre with dispersion compensation. *In Opt. Fib. Comm.* (OFC'97) – Dallas, pages 304-305. OSA, 1997.

[10] P. Harper, F.M. Knox, D.S. Govan, P.N. Kean, I. Bennion, and N.J.Doran. Long distance 10Gbit/s soliton transmission over standard fibre with periodic dispersion compensation. *In Eur. Conf. on Netw. And Opt Comm.* (NOC'97) – Antwerp, pages Vol2, 18-24. IOS Press, 1997.

[11] R.J. Essiambre and G.P. Agrawal. Ultrahigh-bit-rate soliton communication systems using dispersion-decreasing fibres and parametric amplifiers. *Opt. Lett.*, 21(2):116-118, 1996.

[12] K. Tajima. Compensation of soliton broadening in nonlinear optical fibres with loss. *Opt. Lett.*, 12(1):54-56, 1987.

[13] D.J. Richardson, R.P. Chamberlin, L. Dong, and D.N. Payne. High-quality soliton loss-compensation in 38 km dispersion-decreasing fibre. *Electron. Lett.*, 32(19):1681-1682, 1995.

[14] W. Forysiak, F.M. Knox, and N.J. Doran. Stepwise dispersion profiling of periodically amplified soliton systems. *IEEE J. Lightwave Technol.*, 12(8):1330-1337, 1994.

[15] W. Forysiak, K.J. Blow, and N.J. Doran. Reduction of Gordon-Haus jitter by post-transmission dispersion compensation. *Electron. Lett.*, 29(13):1225-1226, 1993.

[16] F. Favre, D. LeGuen, M.L. Moulinard, M. Henry, G. Michaud, F. Devaux, E. Legros, B. Charbonnier, and T. Georges. Demonstration of soliton transmission at 20Gbit/s over 2200 km of standard fibre with dispersion fibre with dispersion compensation and prechirping. *Electron. Lett.*, 33(6):511-512, 1997.

[17] P. Harper, F.M. Knox, P.N. Kean, I. Bennion, and N.J. Doran. 10Gbit/s soliton propagation over 5250 km in standard fibre with dispersion compensation. *In Opt. Fib. Comm.* (OFC'97) – Dallas, pages 304-305. OSA, 1997.

[18] P. Harper, F.M. Knox, D.S. Govan, P.N. Kean, I. Bennion, and N.J.Doran. Long distance 10Gbit/s soliton transmission over standard fibre with periodic dispersion compensation. *In Eur. Conf. on Netw. And Opt Comm.* (NOC'97) – Antwerp, pages Vol2, 18-24. IOS Press, 1997.

[19] F.M. Knox, Forysiak, N.J. Doran. 10Gbit/s soliton communication system over standard fibre at 1.55μm and the use of dispersion compensation. *IEEE J. Lightwave Technol.*, 13(11):1955-1962, 1995.

[20] N.J. Smith, N.J. Doran, F.M. Knox, and W. Forysiak. Energy-scaling characteristics of solitons in strongly dispersion managed fibres. *Opt. Lett.*, 21(24):1981-1983, 1996.

[21] N.J. Smith, F.M. Knox, N.J. Doran, K.J. Blow, and I. Bennion. Enhanced power solitons in optical fibres with periodic dispersion management. *Electron. Lett.*, 32(1):54-55, 1996

[22] I.R. Gabitov and S.K. Turitsyn. Average pulse dynamics in a cascaded transmission system with passive dispersion compensation. *Opt. Lett.*, 21(5):327-329, 1996.

[23] H.A. Haus, K. Tamura, L.E. Nelson, and E.P. Ippen. Stretched-pulse additive pulse mode-locking in fibre ring lasers: Theory and experiment. *IEEE J. Quantum Electron.*, 31(3):591-598, 1995.

[24] J.M. Jacob, E.A. Golovchenko, A.N. Pilipetskii, G.M. Carter, and C.R. Menyuk. Experimental demonstration of soliton transmission over 28Mm using mostly normal dispersion fibre. *IEEE Photon. Technol. Lett.*, 9(1):130-132, 1997.

[25] M. Nakazawa, H. Kubota, A. Sahara, and K. Tamura. Marked increase in the power margin through the use of a dispersion-allocated soliton. *IEEE Photon. Technol. Lett.*, 8(8):1089-1090, 1996.

[26] M.K. Chin and X.Y. Tang. Quasi-stable soliton transmission in dispersion managed fibre links with lumped amplifiers. *IEEE Photon. Technol. Lett.*, 9(4):538-540, 1997.

[27] Wladek Forysiak, Jeroen H.B. Nijhof and Nick Doran. Dispersion managed solitons: The key to terabit per second optical fibre communication systems. *Optics and Photonics News*, 11(5):35–39, 2000.

[28] T. Georges. Pre-chirping and dispersion compensation for long-haul 20 Gbit/s soliotn transmission at 1.55μm on non-dispersion-shifted fibres. *In Opt. Fib. Comm.* (OFC'97) – Dallas, pages 144-145. OSA, 1997.

[29] S. Wabnitz, I. Uzunov, and F. Lederer. Soliton transmission with periodic dispersion compensation: Effects of radiation. *IEEE Photon. Technol. Lett.*, 8(8): 1091-1093, 1996.

[30] K.J. Blow and N.J. Doran. Average soliton dynamics and operation of soliton systems with lumped amplifiers. *IEEE Photon. Technol. Lett.*, 3:369-371, 1991.

[31] N.J. Smith, W. Forysiak, and N.J. Doran. Reduced Gordon-Haus jitter due to enhanced power solitons in strongly dispersion-managed systems. *Electron. Lett.*, 32(22):2085-2086, 1996.

[32] A. Hasegawa, S. Kumar, and Y. Kodama. Reduction of collision-induced timing jitters in dispersion-managed soliton transmission systems. *Opt. Lett.*, 21(1):39-41, 1996.

[33] M.J. Ablowitz, G. Biondini, S. Chakravarty, R.B. Jenkins, and J.R. Sauer. Four-wave mixing in wavelength-division-multiplexed soliton systems: damping and amplification. *Opt. Lett.*, 21(20):1646-1648, 1996.

[34] L.F. Mollenauer, S.G. Evangelides, and J.P. Gordon. Wavelength division multiplexing with solitons in ultra-long distance transmission using lumped amplifiers. *IEEE J. Lightwave Technol.*, 9(3):362-367, 1991.

[35] V. K.Mezentsev, S.K. Turitsyn, and N.J. Doran. System optimisation of 80 Gbit/s single channel transmission over 1000 km of standard fibre. *Electron. Lett.*, 36(23):1949-1951, 2000.

[36] B.A.L. Gwandu, L. Zhang, K. Chisholm, Y. Liu, X. Shu, and I. Bennion. Compact FBG array structure for high spatial resolution distributed strain sensing. *Meas. Sci. Tech.*, 12(7):918-921, 2001.

[37] D. Giannone, Y.W.A. Lee, I.Y. Khrushchev, V.K. Mezentsev, I. Bennion, "A tuneable second and third order dispersion post-compensator by non-uniformly strained chirped fibre grating", *European patent application no. 01308203.7*, Dec 2002.

[38] R.H. Stolen, E.P. Ippen and A.R. Tynes. Raman Oscillation in glass optical waveguide. *Appl. Phys. Lett.*, vol. 20, pages 62, 1972.

[39] D. Mahgerefteh. Technique for measurement of the Raman Gain Coefficient in optical fibers. *Opt. Lett.*, 21(10):2026-2028, 1996.

[40] G.P. Agrawal. Nonlinear fibre optics. *Optics and Photonics*, Academic Press, 1995.

[41] R.G. Smith. Optical power handling capacity of low loss optical fibres as determined by stimulated Raman and Brillouin Scattering. *Appl. Opt.* 11, pages 2489-2492, 1972.

[42] F.L. Gallener. The relative Raman cross sections of vitreous SiO2, GeO2, B2O3, and P2O5. *App. Phy. Lett.*, 32(1):34-36, 1978.

[43] Y. Aoki. *Optical. and Quantum Electronics*, Vol. 21, pages 89-104, 1989.

[44] S. Namiki and Y. Emori. Ultrabroad-band Raman amplifiers pumped and gain – equalised by wavelength-division-multiplexed high power laser diodes. *IEEE J. Selected Top. Quantum Electron*, 7(1):3-16, 2001.

[45] I. Morita, K. Tanaka, and N. Edagawa. Benefit of Raman amplification in ultra-long distance 40Gbit/s-based WDM transmission using dispersion-flattened fibre span. *Electron. Lett.*, 37(8):507-509, 2001.

[46] A.K. Srivastava, S. Radic, C. Wolf, J.C. Centanni, J.W. Sulhoff, K. Kantor, and Y. Sun. Ultra-dense terabit capacity WDM transmission in L-band. *In Opt. Fib. Comm.* (OFC'2000) – Baltimore, PD23-1, OSA, 2000.

[47] T.N. Nielsen. 3.28-Tb/s (82x40Gb/s) transmission over 3x100 km nonzero-dispersion fiber using dual C- and L-band hybrid Raman/Erbium-doped inline amplifiers. *In Opt. Fib. Comm.* (OFC'2000) – Baltimore, PD23-1, OSA, 2000.

[48] S. Bigo. 5.12 Tbit/s (128 x 40 Gbit/s) transmission over 3 x 100km of Teralight fibre. *In Eur. Conf. on Opt. Comm.* (ECOC'2000), PD 1.2, ECOC 2000.

[49] Y. Zhu, C.R.S. Fludger, W.S. Lee, P. Lobb, T. Schilhabel, and A. Hadjifotiou. Experimental comparison of All-Raman and Raman/EDFA hybrid amplifications using 40 Gbit/s-based transmissions over 400 km TW-RS fibre. *Electron. Lett.*, 38(16):552-554, 2002.

[50] B. Zhu, L. Leng, L.E. Nelson, S. Knudsen, and J. Bromage. 1.6 Tb/s (40 x 42.7 Gb/s) transmission over 2000 km of fibre with 100 km dispersion-managed spans. *In Eur. Conf. of Opt. Comm.* (ECOC-2001) – Amsterdam, PD.M.1.8, IEE, 2001.

[51] L. Leng, B.Zhu, S. Stulz, and L.E. Nelson. 1.6Tb/s (40 x 40 Gb/s) transmission over 500 km of nonzero dispersion fiber with 100 km spans compensated by extra-high-slope dispersion-compensating fiber. *In Opt. Fib. Comm.* (OFC'01) – California, pages 554-555. OSA, 2001.

[52] R.E. Neuhauser, P.M. Krummrich, H. Bock, and C. Glingener. Impact of nonlinear pump interactions on broadband distributed Raman amplification. *In Opt. Fib. Comm.* (OFC'01) – California, pages MA4-1, OSA, 2001.

[53] S. B. Alleston, P. Harper, I. S. Penketh, I. Bennion, and N. J. Doran. 1220km propagation of 40Gbit/s single channel RZ data over dispersion managed standard(non-dispersion shifted) fiber. *In Opt. Fib. Comm.* (OFC 1999) - San Diego, CA, PD-3, 1999.

[54] P. Harper, S.B. Alleston, I. Bennion and N. J. Doran. 40 Gbit/s dispersion managed soliton transmission over 1160 km in standard fibre with 75 km span length. *Electron. Lett.*, 35 (24):2128-2130, 1999.

[55] R. I. Killey, H. J. Thiele, V. Mikhailov, and P. Bayvel. Reduction of intrachannel nonlinear distortion in 40Gbit/s based WDM transmission over standard fiber. *IEEE Photon. Technol. Lett.*, 12(12):1624-1626, 2000.

[56] D. S. Govan, W. Forysiak and N. J. Doran. Long-distance 40Gbit/s soliton transmission over standard fiber by use of dispersion management. *Opt. Lett.*, 23(19):1523-1525, 1998.

[57] T. Hirooka and M. J. Ablowitz. Suppression of intrachannel dispersion-managed pulse interactions by distributed amplification. *IEEE Photon. Technol. Lett.*, 14(3):316-318, 2002.

[58] I. Morita, K. Tanaka, N. Edagawa and M. Suzuki. 40Gbit/s single-channel transmission over standard singlemode fiber using distributed Raman amplification. *Electron. Lett.*, 36(25):2084-2085, 2000.

[59] Y. Zhu, C.R.S. Fludger, W.S. Lee, P. Lobb, T. Schilhabel, and A. Hadjifotiou. Experimental comparison of All-Raman and Raman/EDFA hybrid amplifications using 40 Gbit/s-based transmission over 400 km TW-RS fibre. *Electron. Lett.*, 38(16):552-554, 2002.

[60] P. M. Krummrich, R. E. Neuhauser, C. Furst, and C. Glingener. Raman plus EDFA vs. Raman only amplification in terrestrial long haul WDM transmission. *OAA'2001*, Stressa, Italy, Paper OMD5, 2001.

[61] M. Murakami, T. Matsuda, and T. Imai. Long haul WDM transmission with 20Gbit/s data channels using Raman assisted amplification. *Electron. Lett.*, 38 (1):41-43, 2002.

[62] R. Hainberger, T. Hoshida , T. Terahara, and H. Onaka. Comparison of span configurations of Raman-amplified dispersion managed fibers. *IEEE Photon. Technol. Lett.*, 14(4):471-473, 2002.

[63] M. Vasilyev, B. Szalabofka, S. Tsuda, J. M. Grochocinski, and A. F. Evans. Raman noise-figure improvement and multipath interference mitigation in effective-area-optimized dispersion-managed cable. *In Opt. Fib. Comm.* (OFC 2002), Anaheim, CA, paper ThQ4, 2002.

[64] S. G. Edirisinghe, X. Shan and A. S. Siddiqui. 40Gbit/s straight line RZ data transmission over 240km of standard fibre. *Electron. Lett.*, 36(1):19-20, 2000.

Chapter 4

Nonlinear Optical Loop Mirror (NOLM) and its applications

4.1 Introduction

The nonlinear optical loop mirror (NOLM) was first proposed as an all fibre device with potential for ultrafast signal processing by Doran et al in 1988 [1]. Operation of the device is based on a nonlinear anti-resonant ring interferometer proposed by Otsuka et al. in 1983 [2]. Although the performance of this device is similar to a Mach-Zhender interferometer, it has the advantage of being stable over long loop lengths and does not require adjustment of path lengths since each path propagates through the same length of optical fibre.

NOLMs, capable of handling ultra-short pulses, have been shown to be useful in a number of applications such as soliton switching controlled by signal power [3] – [5], all optical demultiplexing [6] – [8], passively mode-locked fibre laser systems [9] – [11], pulse shaping and pedestal suppression [12] – [14] and noise filtering in an all optical fibre communication system [15, 16]. Smith et al. [17] has proven that NOLMs can also be used as saturable absorbers in picosecond soliton transmission by removing the dispersive waves and stabilising the peak amplitude of the soliton. With future pulse width for ultra-high bit-rate transmission systems likely to be in femtosecond, NOLM is still capable of suppressing the pedestal for such a short pulse [18, 19].

The switching threshold of the NOLM can be reduced by incorporating a fibre amplifier within the loop. Such a device is referred to as the nonlinear amplifying loop mirror (NALM). Performance of the NALM has been investigated using an Nd^{3+} doped fibre amplifier within the loop [20]. Extremely low switching power (<100μW) available from the device with an erbium doped fibre amplifier incorporated within the loop [21] – [24]. These low switching powers are possible because of the high gains available from erbium doped fibre amplifiers in addition to "long" fibre loops. NALM can also be used for pulse compression from 700ps to 500ps, with a compression factor of 0.71 [25].

A NOLM can also be unbalanced by using a fibre loop in which the dispersion of the fibre is not constant but varies along the loop. This type of loop mirror is known as dispersion-imbalanced loop mirror (DILM) or nonlinear-imbalanced loop mirror (NILM). The dispersion can vary continuously as in a dispersion decreasing fibre or in a step-like fashion (using fibres with different dispersive properties connected in series). The simplest situation corresponds to the case in which the loop is made with two types of fibres. NILM is especially effective in transmitting and compressing short pulses while

rejecting cw background as well as resonant continuum [26] – [31]. Nan Chi et al. [32] has reported a new type of 2R regenerator based on high non-linear dispersion imbalanced loop mirror (HN-DILM). She shows that the increment of the extinction ratio and Q-factor could be achieved for 10Gb/s signal by using HN-DILM with carefully chosen peak input power. The fibre loop length she used was strongly reduced by applying high-nonlinear fibre (HNLF) instead of DSF, and a shorter fibre loop thus improves stability and polarisation insensitivity. NILM can also be used as a WDM 2R regenerator after transmission over 40km SMF of the WDM signals [33].

In this chapter, our main focus is on NOLM, where both NILM and NALM are built and tested for 2R regeneration in our 40Gb/s transmission system. Since we do not have any HNLF in our laboratory, we will substitute it with DSF. We will also be showing their performances as saturable absorbers and strong filters in suppressing the amplified spontaneous emission (ASE) and reducing the timing jitter and pulse-to-pulse interaction in our 10Gb/s and 40Gb/s transmission systems. Furthermore, a NOLM is built to test for its suitability in 2R regeneration for 10Gbit/s and 40Gbit/s transmission systems.

4.2 The Nonlinear Optical Loop mirror (NOLM)

The loop mirror essentially comprises of a fused fibre directional coupler with the output ports joined together with another piece of fibre, as shown in Figure 4.1.

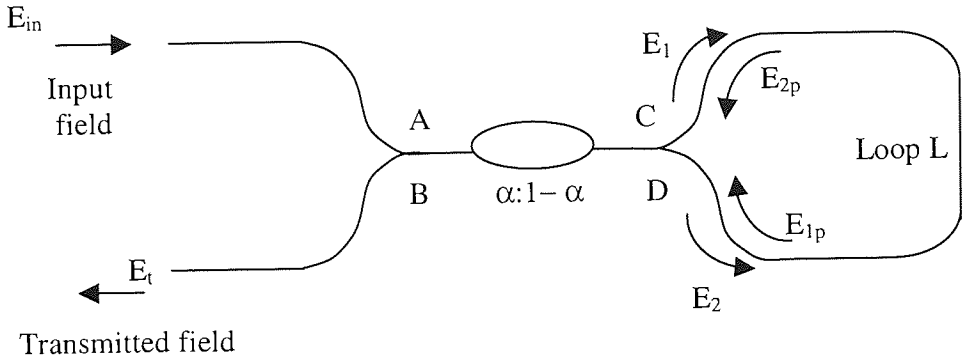

Figure 4.1 Schematic of a nonlinear optical loop mirror (NOLM) with coupling coefficient α

When $\alpha = 0.5$, where α is the coupling coefficient, the device acts as a mirror, totally reflecting the input power. The nonlinear operation can only occur when the counter-propagating radiation experiences different phase shifts (self-phase modulation due to Kerr nonlinearity) and hence this only occurs when the loop is unbalance, i.e. $\alpha \neq 0.5$. If the two couterpropagating beams are exactly in phase, they destructively interfere when they recombine at the coupler. This corresponds to minimum transmission. If, however, the beams are exactly π out of phase, they will combine constructively and give maximum transmission. Since the nonlinear phase shift experienced by the beams is power dependent, the transmissivity of the device is also power dependent. This power dependence can be seen from the graph shown in Figure 4.2.

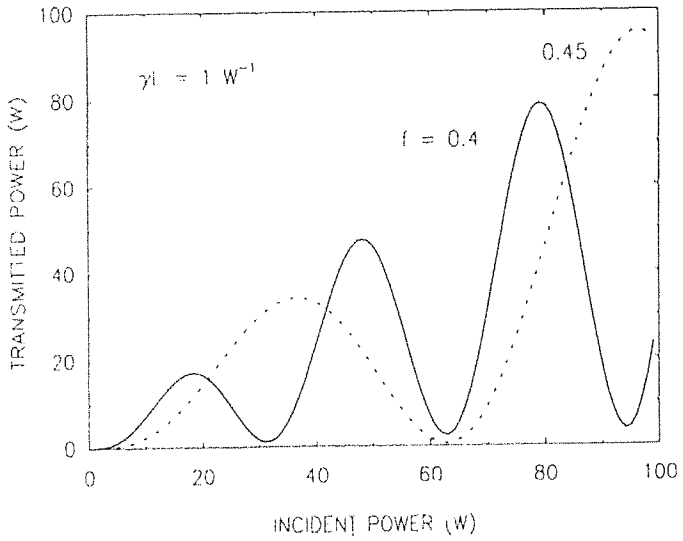

Figure 4.2: Transmitted power as a function of input power for a nonlinear fibre loop mirror (NOLM), where f = α = coupling coefficient. From reference [34]

The essential requirement for successful operation of the NOLM is that the loop must contain some asymmetry to ensure the pulses propagating in opposite direction experience a different phase change throughout the pulse. This can be done by either choosing the coupling coefficient, $\alpha \neq 0.5$, or by introducing a lumped loss or gain at some non-asymmetric position in the loop – nonlinear amplifying loop mirror (NALM). Fibres with different dispersions can also be used to cause some asymmetry – dispersion imbalanced loop mirror (DILM). The transmissions of the device will then depend on any gain or loss that may be present, as well as the input power levels and coupling ratio.

Consider a field E_{in} as the input that splits into fields E_1 and E_2 in the loop, as shown in Figure 4.1. The equations for the coupler then yield the following relations:

$$E_1 = \alpha^{1/2} E_{in} \tag{4.1}$$

$$E_2 = i\,(1-\alpha)^{1/2} E_{in} \tag{4.2}$$

These fields acquire nonlinear phase shifts ϕ_1 and ϕ_2 in the loop of length L so that the fields recombining at the coupler after propagation are [35]:

$$E_{1p} = E_1 \exp(i\phi_1) \tag{4.3}$$

$$E_{2p} = E_2 \exp(i\phi_2) \tag{4.4}$$

where the SPM-induced phase shift for each field ϕ_n is given by:

$$\phi_n = \frac{2\pi n_2 |E_n|^2 L}{\lambda} \tag{4.5}$$

where n_2 is the nonlinear (Kerr) coefficient. Using the coupler equation again, the transmitted field E_t is then given by:

$$E_t = \alpha^{1/2} E_{1p} + i (1-\alpha)^{1/2} E_{2p} \tag{4.6}$$

To calculate the output E_t, we make the transformation $E_{2p} = E_{1p}^*$ and $E_{1p} = E_{2p}^*$ and invert Equation (4.3) and (4.4) to obtain the following

$$|E_t|^2 = |E_{in}|^2 (1-2\alpha(1-\alpha)\{1 + \cos[(1-2\alpha)|E_{in}|^2 \times 2\pi n_2 L/\lambda]\}) \tag{4.7}$$

$$|E_t|^2 = |E_{in}|^2 \{1-2\alpha(1-\alpha)[1 + \cos\Delta\phi]\} \tag{4.8}$$

where $$\Delta\phi = \phi_2 - \phi_1 = (1-2\alpha)\phi \tag{4.9}$$

The transmittivity of the NOLM is the ratio of the transmitted intensity to the input intensity [34]:

$$T = 1 - 2\alpha(1-\alpha)[1 + \cos(1-2\alpha)\phi] \tag{4.10}$$

The nonlinear phase term can also be written in terms of the input power:

$$\phi = \frac{2\pi n_2 P_i L}{\lambda A_{eff}} \tag{4.11}$$

where A_{eff} is the effective core area of the fibre.

In Figure 4.2, P_t is plotted as a function of P_i for $\alpha = 0.4$, where L and $\lambda A_{eff}/n_2$ have been set to unity. At the first minima of the loop, the transmissivity is 0.04, and the loop therefore acts as a high reflector. The first switching point P_s is defined as the power at which the transmissivity is in unity (T = 1). This occurs when the argument of

the cosine term given in Equation (4.10) is equal to π and results in a power-length product given by:

$$P_s L = \frac{\lambda A_{eff}}{2n_2(1-2\alpha)} \tag{4.12}$$

If, for example, λ = 1.55μm, n_2 = 3.2 x 10-20 m^2/W and A_{eff} = 50μm^2, then the transmissivity of the loop first becomes equal to unity when the power-length product P_sL = 6.05 W.km. This would mean that for a 100m length of fibre, significant pulse shaping would be observed with peak power close to 60W. Increasing the loop length can reduce this peak power, but this will also increase the effects of fibre loss and dispersion. However, the switching threshold of a fibre-loop mirror can be reduced considerably by incorporating an optical amplifier within the loop. This will be discussed in section 4.2.2. As a consequence of the ultrafast nonlinearity of silica, the NOLM can be considered to respond instantaneously so that switching depends on the instantaneous pulse power. For non-square pulses (for example, $sech^2$ and Gaussian pulse profiles), this leads to incomplete switching and pulse shaping effects [36]. The application of the NOLM for pulse shaping, pulse compression and pedestal suppression has been demonstrated by Smith et al. [37] for $sech^2$ profiles with low normal dispersion (β_2>0). Even experimentally generated 'square' pulses will degrade slightly due to their finite rise and fall times. However, unlike non-square pulses in the normal dispersion regime, solitons have the same phase at all points across the pulse, i.e. the soliton phase is time-independent. This type of overall phase factor also exists for high-order (N>1) solitons with periodically evolving envelopes. Consequently, two solitons can have the same phase difference between all parts of the pulses if they travel different distances or experience different dispersions in identical paths, enabling complete switching in

ultrafast interferometric devices. Therefore, for our NALM experiments in sections 4.5.1 and 4.5.2, we have made use of the soliton pulses to improve our transmission results.

4.2.1 The Nonlinear-Imbalance Loop Mirror (NILM)

The response of this loop is significantly different from those of NOLM and NALM. Since dispersion acts only on pulses, cw input light of arbitrary intensity will be reflected, whereas short pulses are switched out. The idea is to construct the loop, as shown in Figure 4.3, with one segment of fibre of high anomalous dispersion, D_1, and another segment with a much lower amount of dispersion, $D_2 \approx 0$.

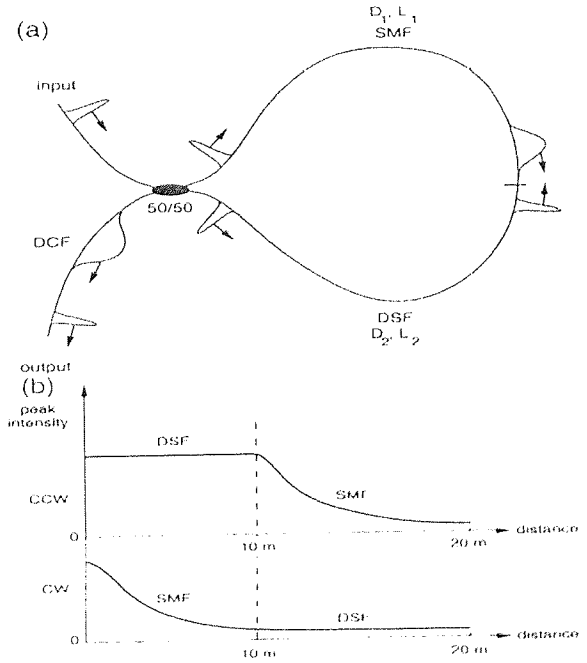

Figure 4.3: (a) Conceptual operation of a dispersion-imbalanced loop mirror (b) Plots of the peak intensity for pulse input as a function of distance along the two propagation directions, counterclockwise (CCW) and clockwise (CW). From reference [38]

In the clockwise-propagating direction inside the loop mirror, the pulse disperses quickly and then remains broad in the second segment, inducing little nonlinear phase shift. On the other hand, the counter-clockwise propagating pulse remain short for the entire first

segment, where the fibre is almost dispersionless, thus the pulse acquires a large amount of nonlinear phase shift that is both intensity dependent and proportional to L_2.

It is important to note that such a nonreciprocal phase shift exists for pulse input but not for cw input. Moreover, the suppression ratio of the input pump and signal pulses depends on the pulse width and the peak powers of the input pulses and is less than the suppression ratio obtained in cw operation. Again, we need to cancel the natural birefringence of the fibre by minimising the transmission of the loop for low-intensity cw input using the polarisation controller within the loop.

4.2.2 The Nonlinear-Amplifying Loop Mirror (NALM)

An improved exploitation of nonlinearities may be obtained by resorting to the nonlinear-amplifying loop mirror (NALM). When an amplifier with gain G, is incorporated into the loop, the output still exhibits a cosine dependence on the input power although modified by the gain term. Consider the loop shown in Figure 4.1 with a gain G inserted close to port 3. The schematic of a NOLM with an erbium doped fibre amplifier (EDFA) inside the loop is shown in Figure 4.4, where (a) and (b) represent the counter-propagating beams in the loop.

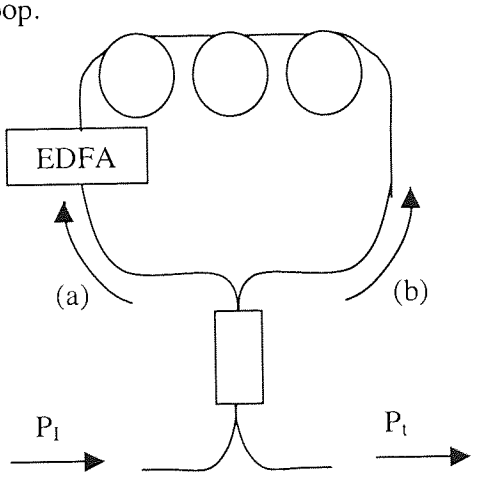

Figure 4.4: Schematic diagram of a nonlinear amplifying loop mirror (NALM), with gain from an erbium doped fibre amplifier (EDFA)

With input field E_{in}, the fields E_1', E_2' now becomes

$$E_1' = \alpha^{1/2} G^{1/2} E_{in} \exp i (G \alpha \phi) \tag{4.13}$$

$$E_2' = i (1 - \alpha)^{1/2} G^{1/2} E_{in} \exp i [(1-\alpha)\phi] \tag{4.14}$$

The transmittivity of the combined loop mirror with amplifier is now given by:

$$T = \frac{P_t}{P_{in}} = G \{1 - 2\alpha (1 - \alpha) [1 + \cos ((1 - \alpha) G - \alpha) \phi]\} \tag{4.15}$$

which results in a power length product of

$$P_s L = \frac{\lambda A_{eff}}{2n_2[(1-\alpha)G-\alpha]} \tag{4.16}$$

Now that the gain is breaking the symmetry in the loop, the coupler coefficient can be set equal to 0.5. With $\alpha = 0.5$, the switching power is inversely proportional to the gain of the amplifier in the loop. By exploiting this property, the switching power of the loop can be reduced to a few mW's (peak) power levels. For example, with $\alpha = 0.5$ and $A_{eff} = 50\mu m^2$ and a gain of 30dBm, the power – length product is approximately 2.5 mW.km. This means that for a loop length of 10km, the switching power is only 0.25mW peak power. There are several enormous advantages of using NALM since it means the pedestal suppression properties of the NOLM can be applied to the low power laser diodes typically used in optical communication system. Furthermore, NALM can be used to switch all different pulse widths, making it very flexible and convenient to use.

One other important feature of including gain in the loop mirror is that of gain saturation. This can quite dramatically change the characteristics of the device. Typically amplifiers exhibit greater stability and tolerance to fluctuations in small input power levels when operating under conditions of saturation. This is also true for NALM

and, as such, is an extremely desirable property of the device, as will be shown. Under conditions of saturation, the gain in the EDFA can be approximated by the equation [39]:

$$G = \frac{G_{ss}}{(1 + Pi / P_{sat})} + 1 \tag{4.17}$$

where G_{ss} is the small signal (unsaturated) gain and P_{sat} is the saturated power. The transmission function is now given by Equation (4.15) with a gain term G, given by Equation (4.17).

The effect that gain saturation has on the response of the amplifying loop can be seen in Figure 4.5 [39]. Here the output power of the amplifying loop is plotted as a function of the input power for a coupler coefficient of 0.5. Both L and $\lambda A_{eff}/n_2$ have been set to unity as before. This plot shows that as the power required for saturation of the EDFA is reduced, the input power required to reach the first null point is increased.

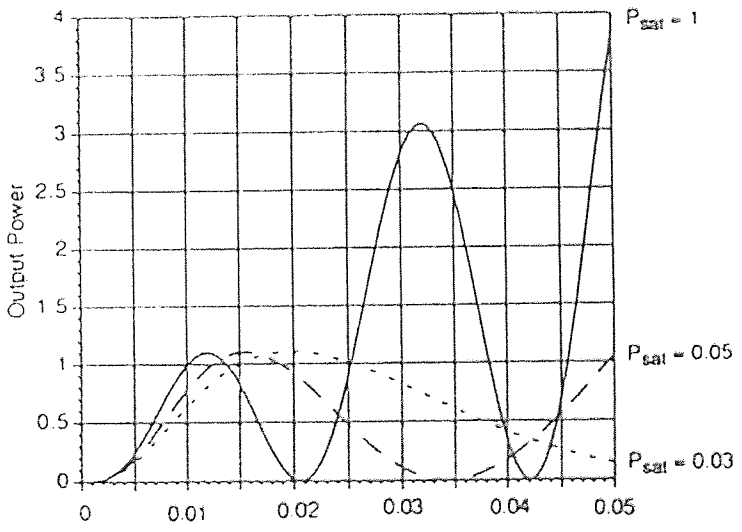

Figure 4.5: Variation of transmitted power with input power in the NALM, with Gss =20dB, α = 0.5 and L = $\lambda A_{eff}/n_2$ = 1. The saturation power Psat was 100 x Ps, 5 x Ps and 3 x Ps. From reference [39]

Pulse shaping and pedestal suppression can still be achieved when the EDFA is saturated provided the peak of the input power is close to the first switching point [39]. As the input power increases and amplifier saturates, the gain approaches unity and the relative

phase difference between the two counter-propagating beams will approach a constant value. This property helps to eliminate some of the complicated pulse shaping normally observed (there is no null point other than at zero input power) and the same time allowing pulse compression and pedestal suppression.

4.3 Autosoliton propagation over standard fibre guided by in-line NOLM

Both dispersion compensation and the use of a NOLM as a saturable absorber can improve the performance of a soliton-based communication system. As mentioned in section 3.3, dispersion compensation gives the benefits of high local and low average dispersion, while allowing pulses with higher powers to propagate, which helps to suppress Gordon-Haus timing jitter without sacrificing the optical signal-to-noise ratio (OSNR). The NOLM suppresses the build up of amplified spontaneous emission (ASE) noise and background dispersive radiation [15 – 17], which, if they are allowed to interact with the carrier pulse, can lead its breakup [16]. Therefore, solitons in a system that combines these two techniques should possess the dual advantages of being chirped (which is important for suppression of four-wave mixing in WDM transmission) and of substantially reduced ASE noise.

In this section, we demonstrate autosoliton propagation using in-line NOLMs. The transmission experiments have been carried out in a re-circulating loop. The experimental setup is shown in Figure 4.6. In the transmitter, 3.5 ps long gaussian-shaped pulses were generated at a wavelength of 1553.5nm. The signal was modulated using a 2^{31}-1 pseudo-random data pattern and subsequently optically multiplexed to 40Gbit/s.

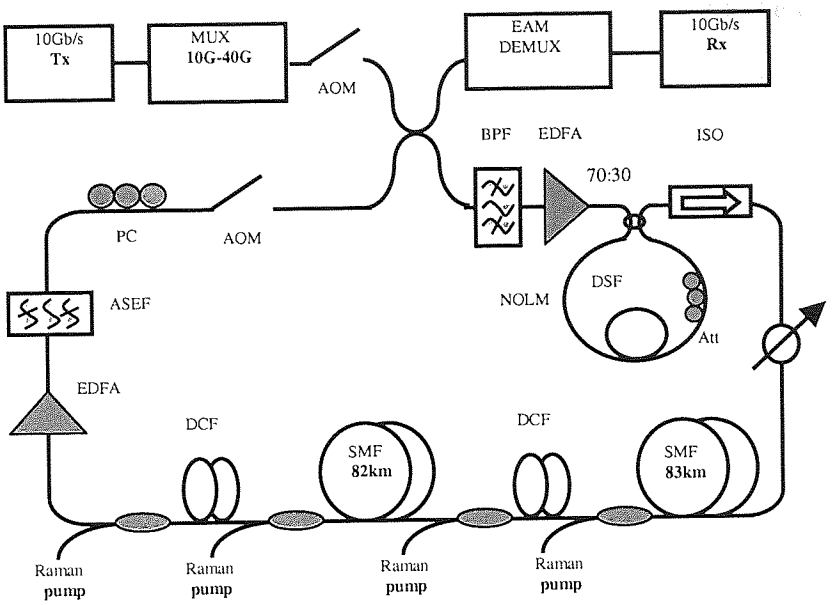

Figure 4.6: Experimental setup for NOLM to be used as 2R regenerator

At the receiver, the transmitted 40Gbit/s data stream was optically de-multiplexed to 10Gbit/s using an electro-absorption modulator (EAM). The fibre loop consisted of two spans, each including 80km of SMF (Corning SMF28) and a slope-compensating dispersion compensating module (SC-DCF). All the SMFs and SC-DCFs are backward pumped by 1455 nm Raman fibre laser.

The average dispersion of the loop was approximately 0.003 ps/nm/km at the operating wavelength. The average power of the re-circulating signal was kept below -2dBm during 40Gb/s experiments and below -9dBm during 10Gb/s experiments in order to assure quasi-linear pulse breathing in the fibre span. A bandpass filter was used to reduce the spontaneous emission noise in the system.

The NOLM was placed at the beginning of loop, and therefore regeneration was performed after each 160km round-trip. The NOLM comprised a 70:30 coupler and 2.3km of True-Wave fibre with a dispersion at the operating wavelength of +2.8 ps/nm/km. An EDFA at the NOLM input was used to boost the signal to appropriate

power level. The signal peak power at the NOLM input was adjusted to be close to the first transmission maximum of the NOLM. As a result, the NOLM efficiently suppressed the amplitude fluctuations of the input signal as well as the low-intensity spontaneous emission and the ghost pulses. The system performances in the presence and in the absence of the in-line NOLM were compared. In all measurements, the system was optimised in order to maximise the error-free transmission distance for a given configuration.

4.3.1 10Gbit/s autosoliton propagation, BER, eye-diagram and results

At 10Gb/s, the error-free propagation distance was measured to be 11,000km and 4,300km for the system with and without the in-line NOLM respectively. The eye diagrams in Figure 4.7(b) show considerably distorted eye after the non-regenerated propagation over 4,300 km. With the in-line NOLM present, a virtually clear eye diagram was observed after 11,000km (Figure 4.7(c)).

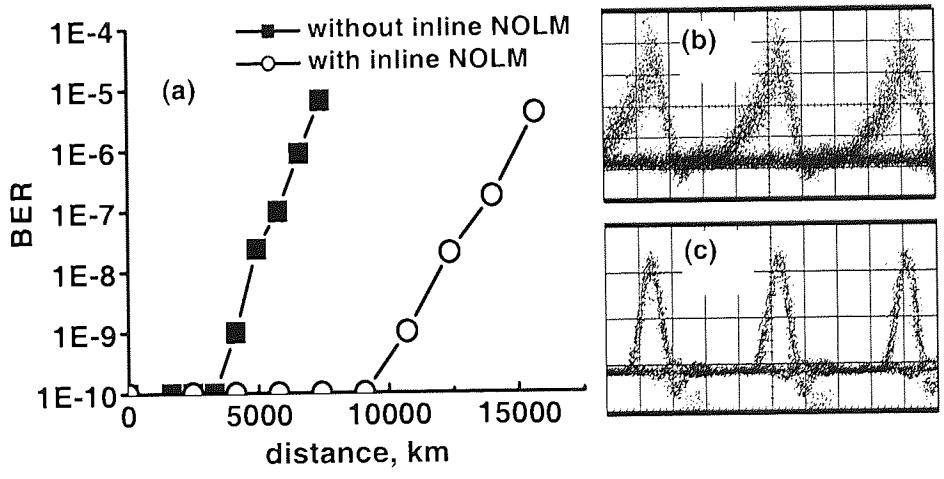

Figure 4.7: 10Gb/s experiment. (a) propagation in the system with and without the in-line NOLMs. Eye diagrams taken at (b) 4,300 km without in-line NOLM; (c) 11,000km with in-line NOLM.

The results suggest, keeping with earlier theoretical studies [40], that autosoliton transmission is supported in the system. We believe that 11,000km is the longest 'raw'

transmission distance achieved in standard fibre with terrestrial amplifier spacing without 3R regeneration.

4.3.2 40Gbit/s autosoliton propagation, BER, spectral evolution and discussion

When operated at 40Gb/s, the system initially allowed error-free transmission over a distance of 1,000 km. With the in-line NOLM acting as a 2R regenerator, the error-free distance increased to at least 4,000km (Figure 4.8(a)). With the NOLM present, no signal degradation is evident over the first 2,500km of propagation, as shown in Figure 4.8(c). Signal degradation is observed after 4,000km, although the quality of eye diagram remains reasonably high over 6,000 km and even 7,500 km (Figure 4.8(c)). The Q-factor, estimated from oscilloscope measurements, remained in range 8 – 12 up to 6,000 km, dropping below 6 after 7,500km. It must be mentioned that from Equation (2.5), Q-factor of 6 is equivalent to BER of 9. For Q-factor of 12 at 3,200 km, the BER should improve to 1.8E-33, but this will take a very long time to achieve, hence we only obtained the data for 1E-10, which is the error-free system performance.

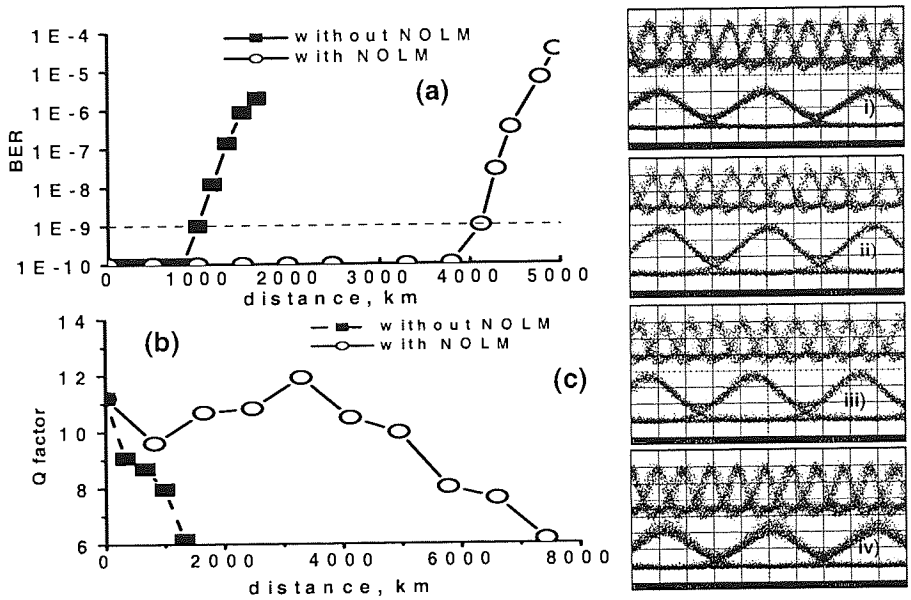

Figure 4.8: 40Gb/s measurements. (a) BER vs distance. b) Q-factor vs distance. c) Eye diagrams of received 40Gb/s and de-multiplexed 10Gb/s signal after i) 2,500km ii) 4,000km iii) 6,000km and iv) 7,500km

We believe that the difference between these two types of measurements presented above is mainly due to the environmental perturbations. The high quality of eye diagrams observe indicates that error-free propagation over transoceanic distances in excess of 7,000km is feasible after taking appropriate environmental measures. The dynamics of the 40Gb/s signal spectra, measured before the EAM, are shown in Figure 4.9. Without the loop mirror, the spectrum changes after the first round-trip as a result of in-line spectral filtering. Subsequently, the signal spectrum keeps changing during propagation in the system (Figure 4.9(a)). The situation is different when NOLM is present. In this case, the signal spectrum stabilises itself after the first round-trip and keeps unchanged up to a distance in excess of 10,000km (Figure 4.9(b)).

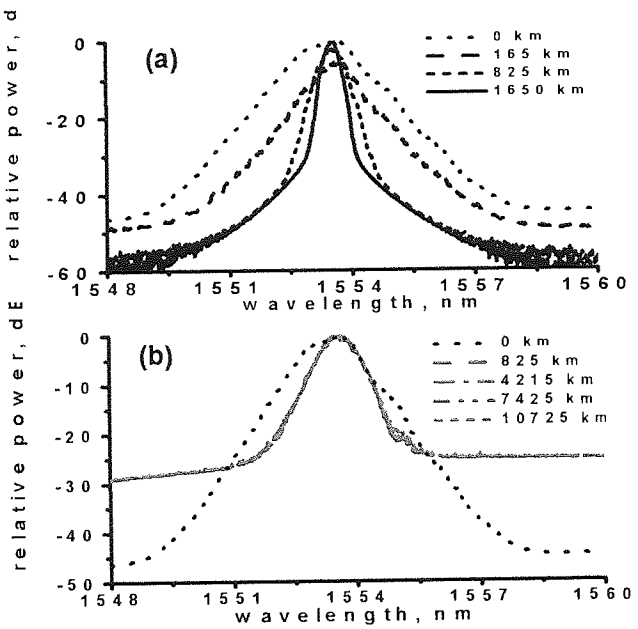

Figure 4.9: Spectral evolution of 40Gb/s signal (a) without NOLM and (b) with NOLM

The above spectral behaviour is an indicative of the system operating in the autosoliton regime in the sense that a stable pulse propagates in the system [41, 42]. The optical signal-to-noise ratio (OSNR) remains practically unchanged over 10,000km as a direct result of nonlinear filtering in the NOLM. The signal quality degradation with distance is likely to be dominated by the accumulation of timing jitter caused by strong pulse-to-pulse interaction.

4.4 NILM experiments

In a communication system with in-line optical amplifiers, the presence of amplified spontaneous emission (ASE) noise in the signal stream lowers the optical signal-to-noise ratio (OSNR) of the signal at the receiver, resulting in a higher bit error rate (BER) in transmission. We demonstrate here the possibility of using a NILM to perform noise filtering from the transmitter.

The pulse source was a mode-locked fibre ring laser (Pritel, Inc), which produced a soliton-like pulse of 3.5ps in duration at a repetition rate of 10GHz. A 2^{31}-1 PRBS data pattern derived from an electronic pattern generator was imposed onto the 10GHz pulse stream by means of a lithium niobate amplitude modulator. The time-bandwidth product was 0.45 at the operating wavelength of 1558nm. From Figure 4.10, it can be clearly seen from the eye diagrams that the noise level is being suppressed. Operating the input power after the peak of the switching curve can further reduce the slight amplitude jitter caused by the NALM

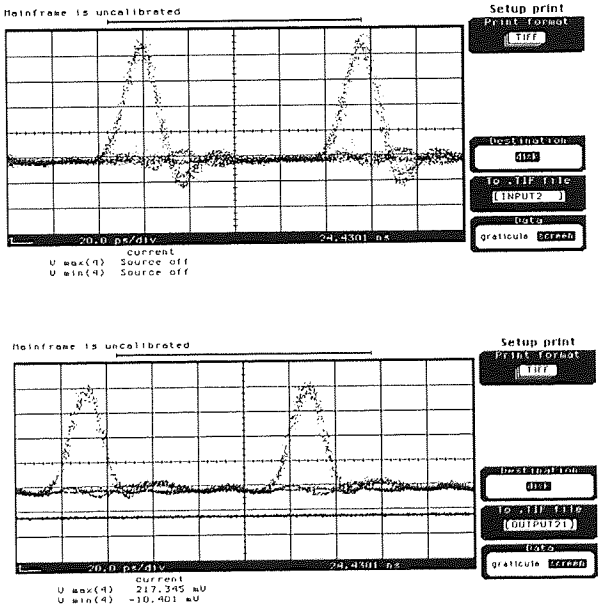

Figure 4.10: Eye diagrams for 10Gb/s signal. Top eye diagram is the input to NILM, bottom eye diagram is the output from NILM

As the bit-rate increased to 40Gb/s by passing through an optical fibre delay line multiplexer, we can observe from section 4.4.2 that the input power will not be sufficient enough to reach the peak of the switching curve and therefore the noise and amplitude jitter will not be suppressed.

4.4.1 10Gbit/s results

The pedestal suppression effect of a NILM is being implemented to our 40Gb/s single channel transmission system. A NILM comprises of 820m of DSF, 600m of DCF, a balanced 50:50 coupler and two polarisation controllers in each arm of the interferometer. The DSF gave a zero-dispersion wavelength of 1551nm and the DCF gave a dispersion of –92.4ps/nm/km at 1550nm. The switching characteristic of the NILM is shown in Figure 4.11.

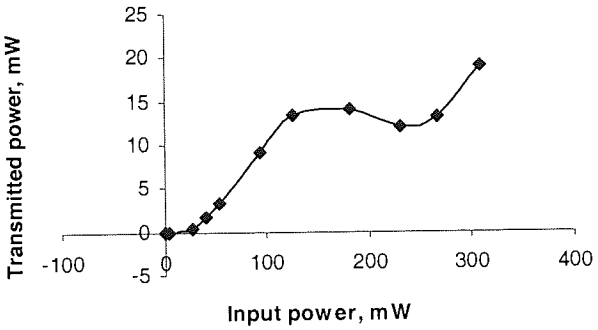

Figure 4.11: Transmission power as a function of input power for NILM

The experimental configuration is shown in Figure 4.12. The PriTel UOC-3 modelocked fibre laser source provided 3.5ps pulses at the operating wavelength of 1550nm. A 10Gbit/s 2^{31}-1 PRBS data pattern was imposed on the pulse stream by a lithium-niobate amplitude modulator (AM), and the resultant bit stream was multiplexed up to 40Gbit/s using a fibre delay line multiplexer (MUX). The polarisation of the multiplexed 10Gbit/s channels were aligned and transmitted through a polariser before splitting into the error detection and clock recovery sections by a 60:40 coupler. The 40% output was amplified by an erbium doped fibre amplifier (EDFA) and converted into an electrical signal. A 10GHz-clock signal was recovered from the incoming electrical signal by an electrical phase locked loop (PLL) based clock recovery unit as mentioned in chapter 2. The 10GHz clock was then used to drive the lithium-niobate modulator ($LiNbO_3$) and as a trigger for the measurement equipment within the error detection unit.

The 40Gbit/s data was demultiplexed to 10Gbit/s by a $LiNbO_3$ modulator. The 10Gbit/s channel was selected by varying the phase of the $LiNbO_3$ drive line by a microwave phase shifter. The resulting 10Gbit/s data stream was amplified by an EDFA before the nonlinear filtering transpired. The nonlinear filter comprised of a polarisation controller, the NILM and 2km of conventional single-mode fibre (SMF). The transmitted data from the NILM propagated through the chirp compensator to compensate for the chirp imposed by the NILM. Back reflections from the NILM were prevented by the use of isolators within the EDFA. A sampling scope observed the output of the filter and error measurements were acquired from a bit-error-ratio-test set (BERTS).

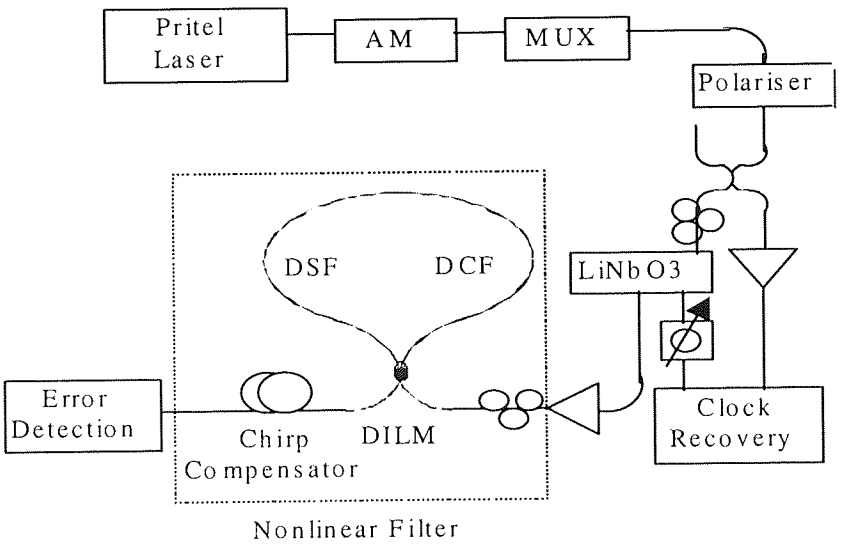

Figure 4.12: Schematic diagram of experimental setup showing the 40Gbit/s data generator, and 40Gbit/s to 10Gbit/s demultiplexer

Figure 4.13 shows the BER measurements made on the worst 10Gbit/s demultiplexed channels with and without the nonlinear filter. Initially the 40Gbit/s OTDM signal was demultiplexed without the aid of the nonlinear filter as to establish a reference of the effectiveness of the filter. At the optimum $LiNbO_3$ modulator bias, it was not possible to achieve error free demultiplexing without the nonlinear filter, only a BER of 4.3×10^{-8} was sustainable. The high error rate is due to the inability of the modulator to fully suppress

other 10Gbit/s channels. With the addition of the nonlinear filter and the polarisation states of each arm of the NILM optimised, error free demultiplexing was achieved. The output eye diagrams in Figure 4.14 shows the filtered and unfiltered outputs with the received power of the filtered output receiving a –12.6dB penalty. The diagrams clearly show the improvement gain by the addition of the filter.

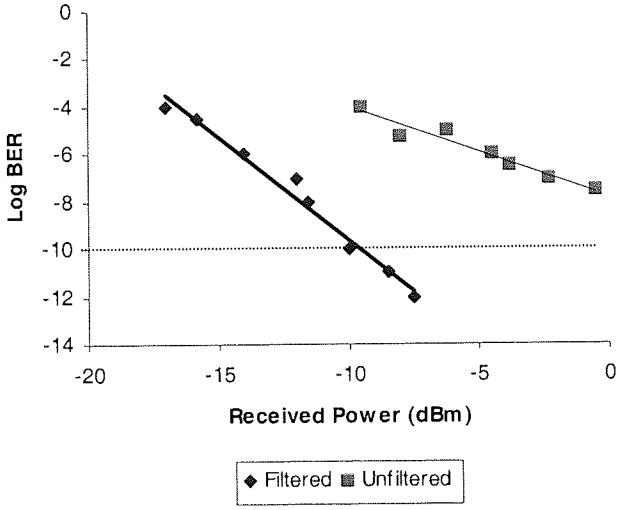

Figure 4.13: BER vs. Received Power (dBm) results for a filtered and unfiltered 10Gbit/s demultiplexed channel

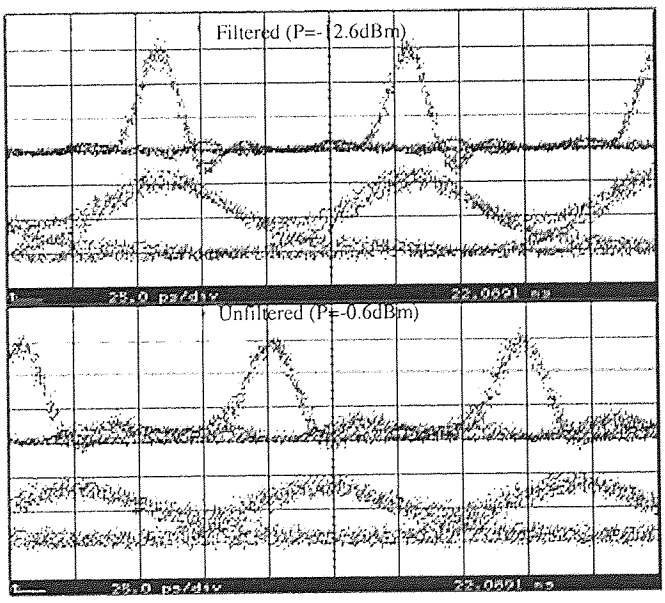

Figure 4.14: Eye diagrams result for a filtered and unfiltered 10Gbit/s demultiplexed channel

4.4.2 40Gbit/s results

The experimental setup is shown in Figure 4.15. The NILM was placed at the in-line fibre for 2R regeneration instead of after demultiplexing. The transmitted signal was modulated using 2^{31}-1 pseudo-random data pattern subsequently optically multiplexed to 40Gbit/s, then reamplified and put into the NILM to be reshaped. An ASE filter was used before the NILM to reduce the ASE noise from the amplifier to the NILM. The demultiplexing was done by using an electro-absorptive modulator (EAM) to replace the lithium-niobate modulator in section 4.4.1. Since the maximum transmission point at the output of the NILM will change as a consequence of varying the input peak power, hence the input peak power must be adjusted carefully to obtain the optimum level. Again, the best eye-diagram was observed after the peak of the switching curve [32].

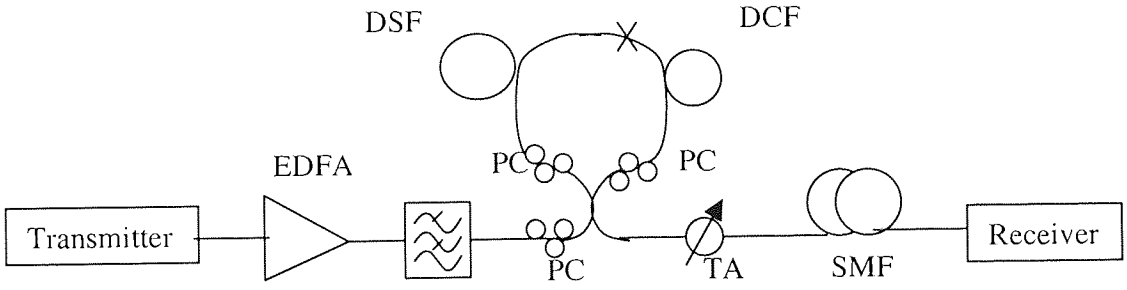

Figure 4.15: Experimental setup. PC: polarisation controller, TA: tunable attenuator, DSF: dispersion-shifted fibre, DCF: dispersion-compensating fibre.

The NILM was constructed from a 50/50 coupler and 200m of DCF and 2.3km of DSF. It acts as a nonlinear filter that transmits only pulse components with appropriate peak power and pulse duration. The zero-dispersion wavelength of the DSF is at 1579nm and the dispersion of the DCF is approximately –92.4 ps/nm/km at 1550nm. The SMF is to compensate for the large chirp after the NILM.

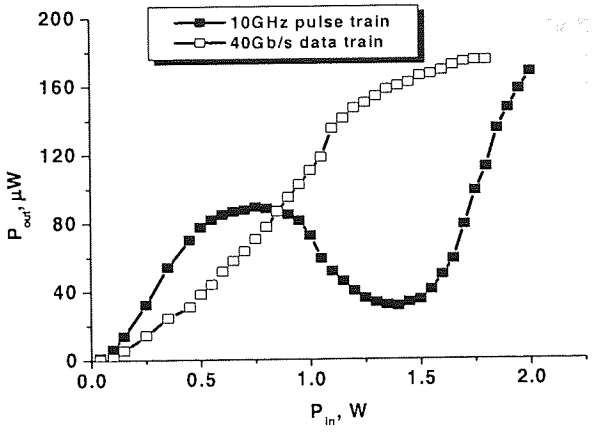

Figure 4.16: Switching curves for NILM at 10Gbit/s and 40Gb/s

From Figure 4.16, it can be seen that when the bit-rate reaches 40Gb/s, the peak of the switching curve will disappear. This is because for 40Gb/s, the peak power is not high enough to cause switching in the loop as compared to bit-rate of 10Gb/s. We have tried to maximise all the powers in the EDFAs but still could not reach the peak of the NILM. Hence no switching occurred at 40Gbit/s.

From Figure 4.17 and 4.18, it can be seen that for both back-to-back and after transmitting over a fibre span consisting of 85 km conventional SMF and 14.14 km (-96.11 ps/nm/km) DCF with backward-Raman amplification, the BER performance is not as good as without the NILM. But the extinction ratio has increased by 6dB. However, the performance of the NILM without transmission is very closed to the back-to-back performance.

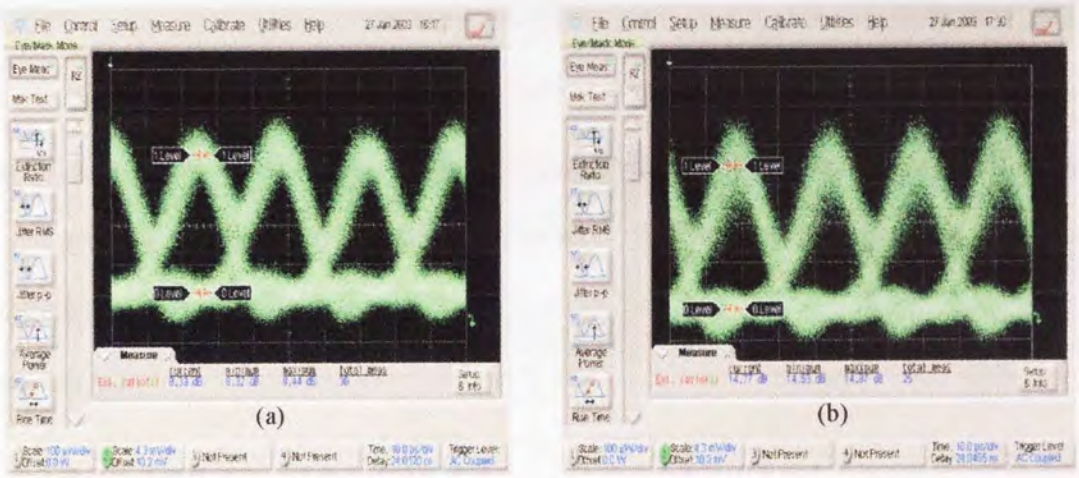

Figure 4.17: Eye diagram for 80km SMF transmission (a) without NILM and (b) with NILM.

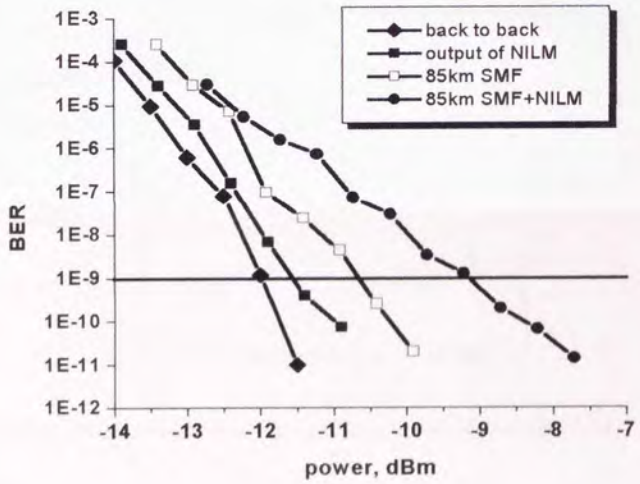

Figure 4.18: BER vs received power for back-to-back, output of DILM, 85km SMF and 85km SMF + NILM

4.5 NALM experiments

NALM is a particularly attractive configuration for telecommunication applications because it combines both intensity filtering and amplification functions. By employing the high gains typically obtained from laser-diode pumped EDFAs and 'long' fibre loops, the switching powers can be reduced to the power levels of mode-locked semiconductor lasers (~ 1mW peak). At gigahertz repetition frequencies, however, the corresponding average powers (~ 100μW) are sufficient to give rise to significant gain saturation in the

amplifier. In this section, a fast, very low threshold optical pulse switching in a NALM operating at 1550.7nm with a gain of 16.3dB is demonstrated. The NALM was built as in Figure 4.19 using a 50:50 coupler, 1 km of dispersion flattened fibre (DFF), 10m of erbium-doped fibre, a polarisation controller and a WDM coupler to allow the pump laser to pump the erbium-doped fibre.

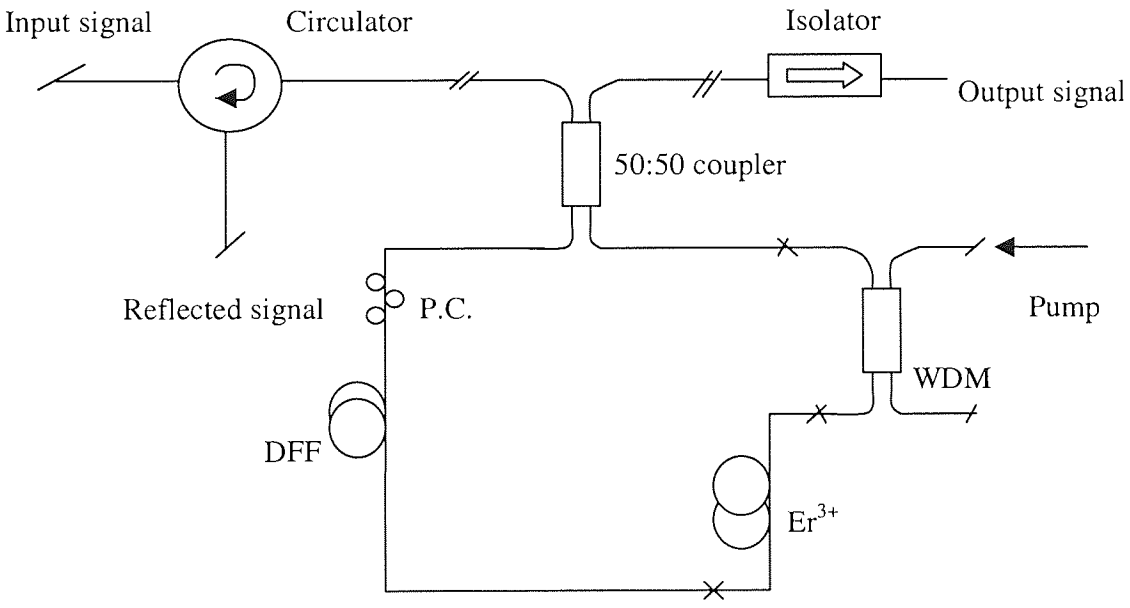

Figure 4.19: Schematic diagram of a Nonlinear-Amplifying Loop Mirror (NALM)

From the calculation,

$$\phi = P_o L \gamma \tag{4.18}$$

where Po is the input power, which is approximately 10mW. γ is the kerr nonlinear effect, which is about $3W^{-1}km^{-1}$. For switching, ϕ must be equal to π. Consider ϕ^+ as the phase in clockwise direction while ϕ^- is the phase in anti-clockwise direction. Therefore,

$$\phi^+ - \phi^- = \pi \tag{4.19}$$

$$\phi^- = P_o L \gamma / 2 \tag{4.20}$$

$$\phi^+ = P_o GL \gamma / 2 \tag{4.21}$$

where G is the gain of the amplifier, substituting Equation (4.20) and (4.21) into Equation (4.19), we obtain

$$\phi^+ - \phi^- = P_o (G-1) L \gamma / 2 = \pi$$

$$G - 1 = 2\pi / P_o L \gamma$$

$$G = 2\pi / P_o L \gamma + 1 \qquad (4.22)$$

substituting the values of P_o, L and γ into Equation (4.22), we get

$$G = 210\text{mW}$$

$$= 23.3 \text{ dB}$$

During the experiment, such a high power pump laser was not available. Therefore, in order to reduce the gain G, longer length of fibre was being used. Hence we have replaced the 1 km of DFF with a 5 km of dispersion-shifted fibre (DSF) whose zero-wavelength was at 1556nm. With this length of fibre, the gain G of the amplifier has been reduced to 16.3 dB (or 43mW). From the characteristic of the pump laser, in order to obtain 43mW, the pump current needs to be at 150mA. But taking considerations of the fibre loss in the loop, pump current of 200mA was being used instead. The switching curve for the transmitter power (mW) as a function of the input power (P_o) is shown in Figure 4.20. The bit-rate used was 40Gb/s, pulse width was 6.55ps and the wavelength as 1550.7nm.

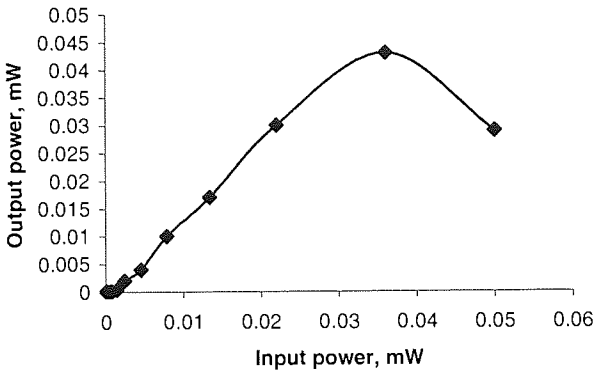

Figure 4.20: Transmitted power as a function on input power for the NALM

From Figure 4.20, the maximum input power for switching is 0.038mW and the transmission (output power / input power) is about 117%. It can clearly be seen later that this input power for switching in NALM is very much smaller compare to that of the DILM. Furthermore, the input pulse width has also been reduced from 6.55ps to 4.14ps. This shows that only the central part of the pulse is generally intense enough to experience switching, hence it is possible to remove the pedestal of an optical pulse by passing it through such a device. However, the compression factor will be relatively small since this technique works by clipping the pulse wings [20].

4.5.1 10Gbit/s results

Figure 4.21 shows the experimental setup. The transmitter consisting of 10Gbit/s data pulse with duration of 3.5ps. ISO1 and ISO2 were used to prevent any back reflection. The DSF we used has a zero-dispersion wavelength at 1510nm. The dispersion at transmitter wavelength of 1553.7nm was approximately 2.8ps/nm/km. We purposely used the anomalous fibres since we wanted to create solitons in the loop. The gain we obtained from the erbium-doped fibre was 15dB. The first thing we needed to do was to

cancel the natural birefringence of the fibre. This was performed by adjusting the polarisation controller at low-intensity cw input to minimise its transmission.

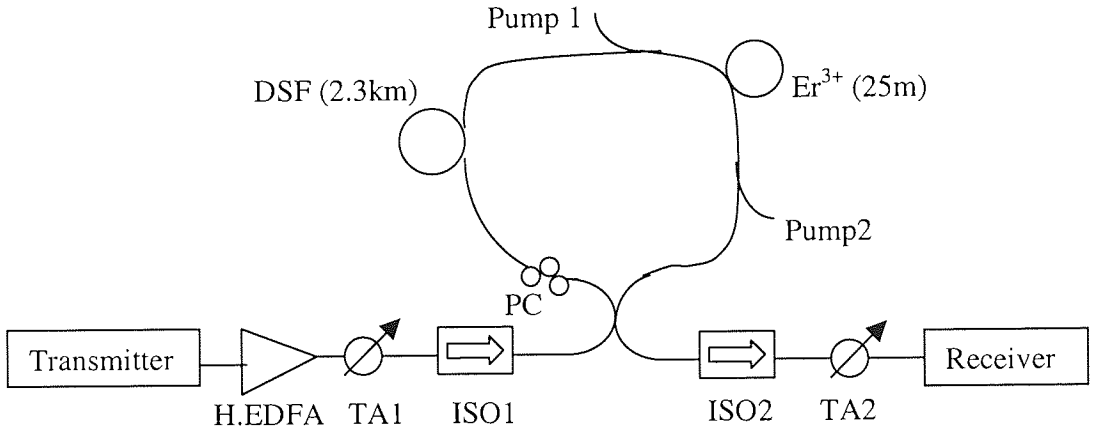

Figure 4.21: Experimental setup. PC: polarisation controller, ISO: isolator, TA: tunable attenuator, DSF: dispersion-shifted fibre, Er^{3+}: erbium-doped fibre, H.EDFA: high power erbium-doped fibre amplifier

Figure 4.22 shows the input and output spectrum. It can be seen that the wide input spectrum is due to self-phase modulation since the H.EDFA is 1.46W. The input pulse width has been compressed and becomes 1.8ps. From the output spectrum, we can observe the formation of solitons.

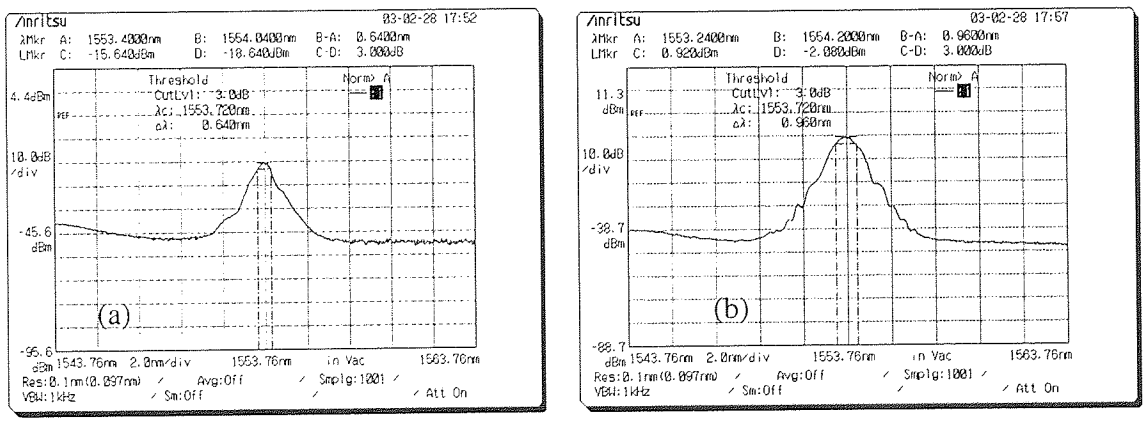

Figure 4.22: (a) Input spectrum before NALM, (b) Output spectrum after NALM

The best results are obtained after the peak of the switching curve. From Figure 4.23, it can be seen that the BER is much better with the NALM since the range of threshold voltage is much wider. The transmission experiment was not performed for this case

since in this thesis; we are more interested in high bit-rate transmission (equal or more than 40Gbit/s).

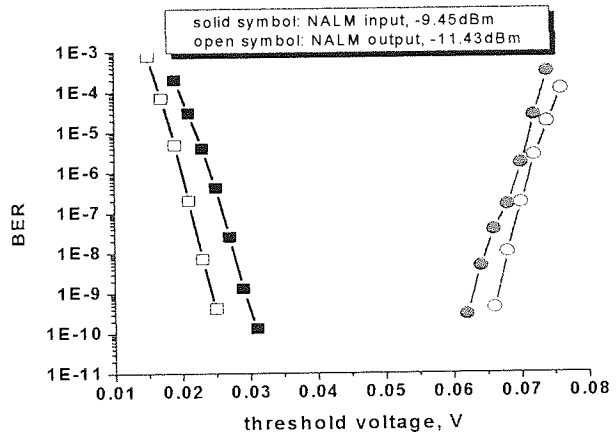

Figure 4.23: Comparison of BER vs threshold voltage for input and output of NALM

4.5.2 40Gbit/s demultiplexing

The experimental setup was similar to section 4.4.1 except that we replaced the NILM and lithium-niobate modulator with NALM and electro-absorptive modulator (EAM). Before the high power EDFA, we have inserted a 1.3nm filter to increase the optical signal-to-noise ratio (OSNR).

From Figure 4.24, we can see that the eye diagram with NALM is much better than BTB. Similarly, after propagating in the loop for one recirculation. Figure 4.25 shows that its performance is much better than without NALM due to its wider threshold voltage.

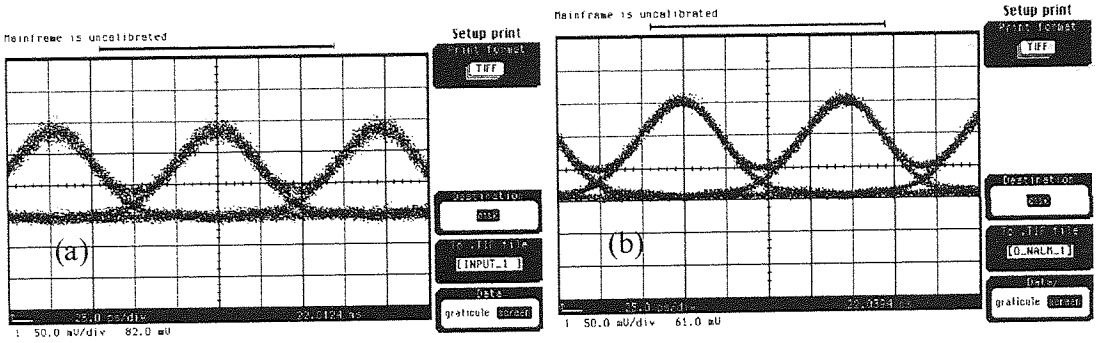

Figure 4.24: Eye diagram for (a) BTB, (b) with NALM

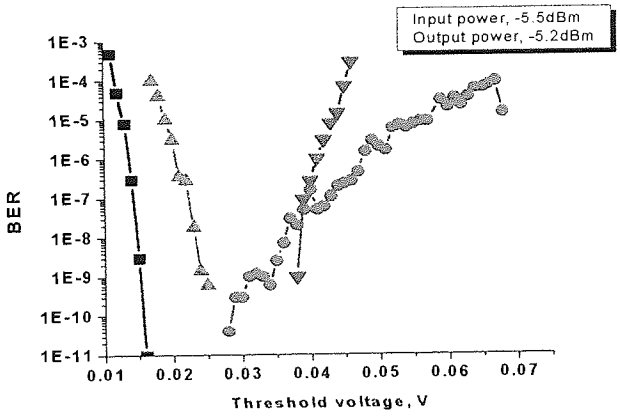

Figure 4.25: Comparison of BER vs threshold voltage for input and output of NALM (one recirculating loop, 300km), triangular – without NALM, squares and circles – with NALM

We have performed some propagation (1 – 3 recirculating loops) for this condition.

Figures 4.26 and 4.27 show the eye-diagrams and spectrums for all the three loops.

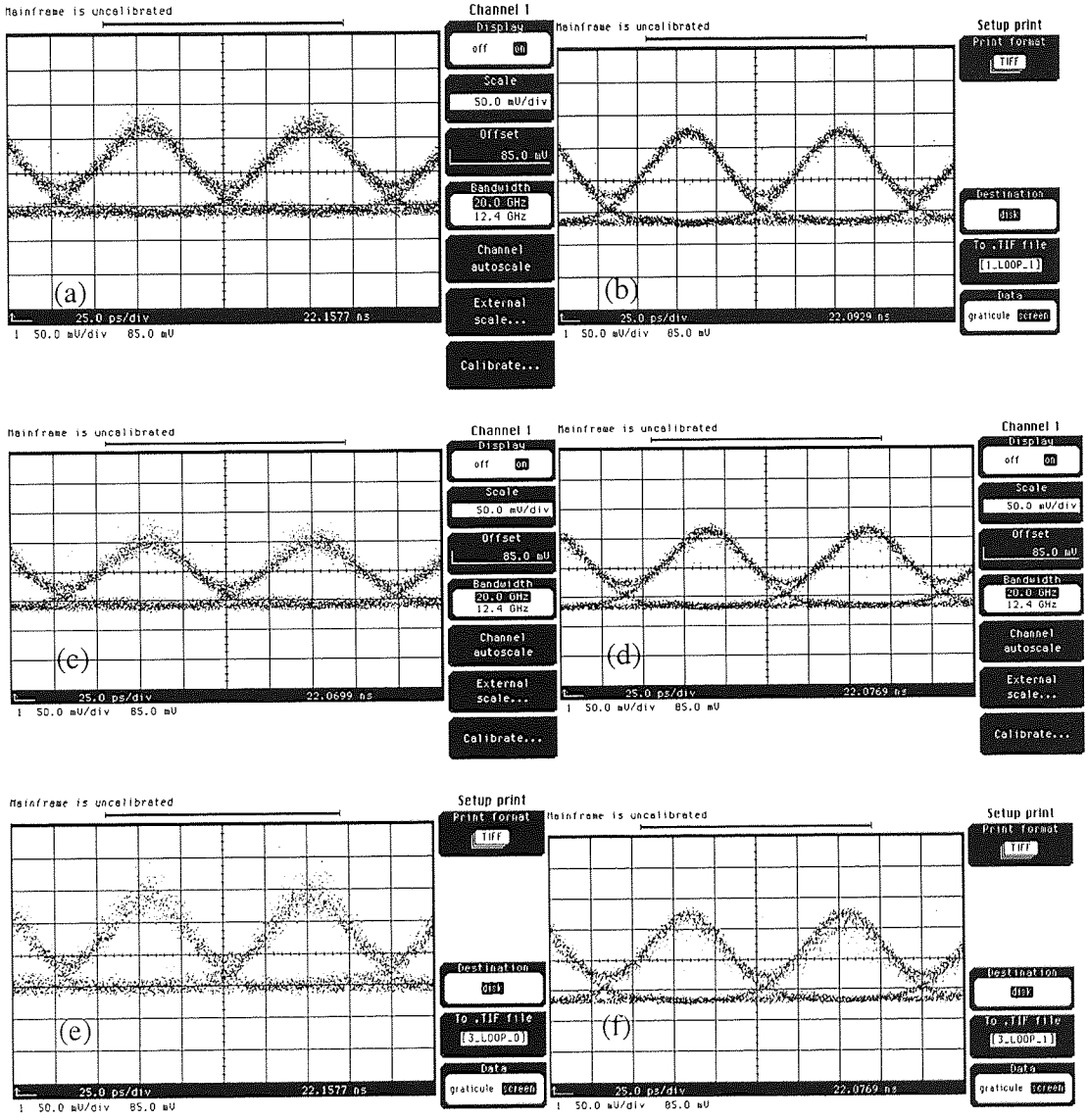

Figure 4.26: (a), (c) and (e) show the eye-diagrams for 1,2 and 3 recirculating loops without NALM. (b), (d) and (f) show the eye-diagrams for 1,2 and 3 recirculating loop with NALM

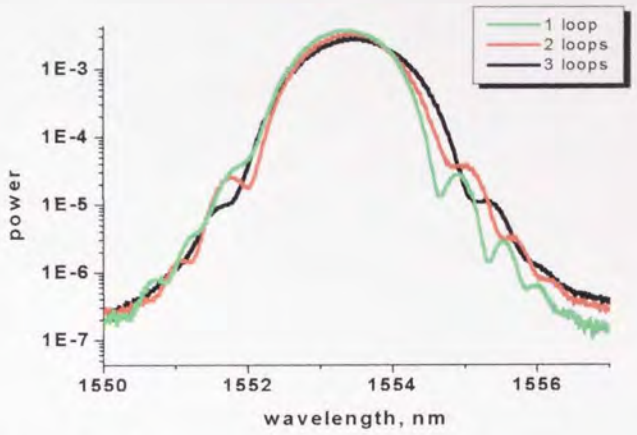

Figure 4.27: Spectrum for 1,2 and 3 recirculating loops with NALM

From Figure 4.26, we can observe that all the eye-diagrams for propagations are better with NALM. However, for the BER, only the performance of one recirculating loop is better with NALM. For two loops or greater, it is better without the NALM. As for the spectrums in Figure 4.27, we observe that as the number of recirculating loops increases, the numbers of side-lobes tend to reduce. And the solitons effect has gone after more than one recirculating loop, thus resulting in poor BER.

4.6 Summary

In this chapter, different types of loop mirrors are being described, built and studied. It started by outlining mathematically the nonlinear switching of the NOLM and its basic operating principles. It shows that the best switching occurred for soliton pulses since they have same phase across the pulse, thus preventing any incomplete switching and pulse shaping effects. The nonlinear optical loop mirror (NOLM), nonlinear-amplifying loop mirror (NALM) and nonlinear-imbalance loop mirror (NILM) have also been introduced and discussed. A NOLM was fabricated to investigate its suitability in 2R regeneration. While both NALM and NILM have been tested for their usefulness in 2R

regeneration as well as saturable absorbers at the receiving end of the transmission systems.

References

[1] N.J. Doran, and D. Wood. Nonlinear-optical loop mirror. *Opt. Lett.*, 13(1):56-58, 1988

[2] K. Otsuka. Nonlinear antiresonant ring interferometer. *Opt. Lett.*, 8(9):475-476, 1983

[3] K.J. Blow, N.J. Doran, and B.K. Nayar. Experimental demonstration of optical soliton switching in an all-fibre nonlinear Sagnac interferometer. *Electron. Lett.*, 26(14):962-964, 1990

[4] M.N. Islam, E.R. Sunderman, R.H. Stolen, W. Pleibel, and J.P. Simpson. Soliton switching in a fibre nonlinear loop mirror. *Opt. Lett.*, 14(15):811-813, 1989

[5] J.L.S. Lima, and A.S.B. Sombra. Soliton and quasi-soliton switching in nonlinear optical loop mirror constructed from dispersion decreasing fibre. *Opt. Commun.*, vol. 163, 292-300, 1999.

[6] K.J. Blow, N.J. Doran, B.P. Nelson. Demonstration of the nonlinear fibre loop mirror as an ultrafast all-optical demultiplexer. *Electron. Lett.*, 26(14):962-964, 1990.

[7] T. Yamamoto, E. Yoshida, and M. Nakazawa. Ultrafast nonlinear optical loop mirror for demultiplexing 640Gb/s TDM signals. *Electron Lett.*, 34(10):1013-1014, 1998.

[8] E. Yamada, K. Suzuki, and M. Nakazawa. Subpicosecond optical demultiplexing at 10GHz with zero-dispersion, dispersion-flattened, nonlinear fibre loop mirror controlled by 500fs gain-switched laser diode. *Electron. Lett.*, 30(23):1966-1968, 1994.

[9] W. Shu, S. Jefferson, and L.F. Richard. High-power passively mode-locked Er-doped fibre laser with a nonlinear fibre loop mirror. *Opt. Lett.*, 18(17):1444-1446, 1993.

[10] D.J. Richardson, R.I. Laming, D.N. Payne, V. Matsas, and M.W. Phillips. Amplification of femtosecond pulses in a passive, all fibre soliton source. *Opt. Lett.*, 17(22):1596-1598, 1992.

[11] I.N. Duling. Subpicosecond all-fibre erbium laser. *Electron. Lett.*, 27(6):544-545, 1991.

[12] J. Wu, Y. Li, C. Lou, and Y. Gao. Optimisation of pulse compression with an unbalance nonlinear optical loop mirror. *Opt. Commun.*, 180(1):43-47, 2000.

[13] A.L. Steele. Pulse compression by an optical fibre loop mirror constructed from two different fibre. *Electron. Lett.*, 29(22):1972-1974, 1993.

[14] K. Smith, N.J. Doran, and P.G. Wigley. Pulse compression, and pedestal suppression employing a nonlinear optical loop mirror. *Opt. Lett.*, 15(22):1294-1296, 1990.

[15] B. Olsson, and P.A. Andrekson. Noise filtering with the nonlinear optical loop mirror. *IEEE J. Lightwave Tech.*, 13(2):213-215, 1995.

[16] M. Matsumoto, H. Ikeda, and A. Hasegawa. Suppression of noise accumulation bandwidth-limited soliton transmission by means of nonlinear loop mirrors. *Opt. Lett.*, 19(3):183-185, 1994.

[17] K. Smith, and N.J. Doran. Picosecond soliton propagation using nonlinear optical loop mirrors as intensity filters. *Electron. Lett.*, 30(13):1084-1085, 1994.

[18] L. Chusseau, and E. Delevaque. 250fs optical pulse generation by simultaneously soliton compression and shaping in a nonlinear optical loop mirror including a weak attenuation. *Opt. Lett.*, 19(10):734-736, 1994.

[19] M.D. Pelusi, Y. Matsui, and A. Suzuki. Pedestal suppression from compressed femtosecond pulses using a nonlinear fibre loop mirror. *IEEE J. Quantum Electron.*, 35(6):867-874, 1999.

[20] M.E. Fermann, F. Harberl, M. Hofer, and H. Hochreiter. Nonlinear amplifying loop mirror. *Opt. Lett.*, 15(13):752-754, 1990.

[21] K. Smith, E.J. Greer, N.J. Doran, D.M. Bird, and K.H. Cameron. Pulse amplification and shaping using a nonlinear loop mirror that incorporates a saturable gain. *Opt. Lett.*, 17(6):408-410, 1992.

[22] D.J. Richardson, R.I. Laming, and D.N. Payne. Very low threshold sagnac switch incorporating an erbium doped fibre amplifier. *Electron. Lett.*, 26(21):1779-1781, 1990.

[23] K. Rottwitt, W. Margulis, and J.R. Taylor. Spectral filtering of solitons by means of a nonlinear amplifying loop mirror. *Opt. Lett.*, 20(15):1601-1603, 1995.

[24] G.W. Pearson, R. Zanoni, and J. Krasinski. Analysis of ultra-short pulse propagation in a fibre nonlinear amplifying loop mirror. *In Opt. Commun.*, vol. 103, pp. 507-518, 1993.

[25] R.A. Betts, S.J. Frisken, C.A. Telford. All-optical pulse compression using amplifying sagnac loop. *Electron. Lett.*, 27(10):858-860, 1991.

[26] W.S. Wong, S. Namiki, M. Margalit, H.A. Haus, and E.P. Ippen. Self-switching of optical pulses in dispersion-imbalanced nonlinear loop mirrors. *Opt. Lett.*, 22(15):1150-1152, 1997.

[27] I.Y. Khrushchev, I.H. White, and R.V. Penty. Femtosecond pulse generation from a gain-switched laser diode by means of a dispersion-imbalanced loop mirror. Proc. 5th Int. *Workshop on Femtosecond Technol.*, pp. 73, 1997.

[28] I.Y. Khrushchev, I.H. White, and R.V. Penty. High-quality laser diode pulse compression in dispersion-imbalanced loop mirror. *Electron. Lett.*, 34(10):1009-1010, 1998.

[29] K.R. Tamura, and M. Nakazawa. A polarization-maintaining pedestal-free femtosecond pulse compressor incorporating an ultrafast dispersion-imbalanced nonlinear optical loop mirror. *IEEE Photon Techno. Lett.*, 13(5):526-528, 2001.

[30] I.Y. Khrushchev, I.D. Philips, A.D. Ellis, R.J. Manning, D. Nesset, D.G. Moodie, R.V. Penty, I.H. White. OTDM applications of dispersion-imbalanced fibre loop mirror. *Electron. Lett.*, 35(14):1183-1185, 1999.

[31] K.R. Tamura, and M. Nakazawa. Spectral-smoothing and pedestal reduction of wavelength tunable quasi-adiabatically compressed femtosecond solitons using a dispersion-flattened imbalanced loop mirror. *IEEE Photon. Technol. Lett.*, 11(2):230-232, 1999.

[32] N. Chi, L. Xu, L. Oxenlowe, T. Tokle, and P. Jeppesen. 2R regenerator based on high nonlinear dispersion-imbalanced loop mirror. *Opt. Commun.*, vol. 206, pp. 295-300, 2002.

[33] N. Chi, B. Carlsson, and P. Jeppesen. 2R regeneration based on dispersion-imbalanced loop mirror and its applications in WDM systems. *IEEE J. Lightwave Technol.*,20(10):1809-1817, 2002.

[34] G.P. Agrawal. Nonlinear fibre optics. *Optics and Photonics*, Academic Press, 1995.

[35] E.G.Bryant, S.F. Carter, A.D. Ellis, W.A. Stallard, J.V. Wright and R. Wyatt. Unrepeatered 2.4 Gb/s transmission over 250 km of step index fibre using erbium power amplifier. *Electron. Lett.*, 26(8): 528-529, 1990.

[36] K.J. Blow, N.J. Doran, and B.K. Nayar. Experimental demonstration of optical soliton switching in an all-fibre nonlinear Sagnac interferometer. *Electron. Lett.*, 26(14):962-964, 1990.

[37] K. Smith, N.J. Doran, and P.G. Wigley. Pulse compression, and pedestal suppression employing a nonlinear optical loop mirror. *Opt. Lett.*, 15(22):1294-1296, 1990.

[38] W.S. Wong, S. Namiki, M. Margalit, H.A. Haus, and E.P. Ippen. Self-switching of optical pulses in dispersion-imbalanced nonlinear loop mirrors. *Opt. Lett.*, 22(15):1150-1152, 1997.

[39] K. Smith, E.J. Greer, and N.J. Doran. Square pulse amplification using nonlinear loop mirror incorporating saturable gain. *Electron. Lett.*, 27(22):2046-2048, 1991.

[40] S. Boscolo, J. H. B. Nijhof and S. K. Turitsyn, "Auto-soliton transmission in dispersion-managed systems guided by in-line nonlinear optical loop mirrors", *Opt. Lett.*, 25(17):1240-1242, 2000.

[41] S. Boscolo and S. K. Turitsyn and K. J. Blow, "All-optical passive regeneration of 40 Gbit/s soliton data stream using dispersion management and in-line NOLMs", *Electron. Lett.*, 37(2):112-113, 2001.

[42] I. Morita, K. Tanaka, N. Edagawa and M. Suzuki. 40Gbit/s single-channel transmission over standard singlemode fiber using distributed Raman amplification. *Electron. Lett.*, 36(25):2084-2085, 2000.

Chapter 5

Thesis Conclusion

This thesis has investigated several advanced optical techniques to improve the performance of high capacity (10Gbit/s and 40Gbit/s) transmission system. Since all the transmission experiments were performed using the recirculating loop, hence its principles of operations, design considerations, advantages and disadvantages have all been discussed.

Dynamic dispersion compensation (DC) is becoming paramount in high-speed transmission systems, operating at 40Gbit/s and beyond. At these high bit rates,

dispersion tolerances become small enough that variations in dispersion, which are negligible in slower systems, can severely influence transmission performance. In such systems, the amount of dispersion compensation required at the receiver to maintain optimum system performance may also vary in time. We have fabricated such a tunable dispersion compensator by using non-uniformly strained the linear chirped fibre Bragg gratings. Experimental results have shown that it is capable of compensating for both second and third order dispersions. Such a device has also been tested in the recirculating loop but the results are very poor. The main reason for this is due to the fact that the FBG suffered from delay ripples and the use of a single span recirculating loop highlighted this problem. Hence the best position to place this device is at the receiver to compensate for the unpredictable residual dispersion. Future work could be done to use this device for higher bit rate (>40Gbit/s). Since FBGs have low insertion loss and polarisation sensitivity, these reasons should be sufficient to ensure that research continues into this application.

As the ever-increasing demand for extra capacity and longer transmission distance pushes the technologies to the limit, there is a growing interest in addressing some of the system impairments of the transmission fibre. The concept of dispersion managed transmission span, consisting of both positive and negative dispersion fibres offers the promise of highly accurate in-line chromatic dispersion control. In conjunction with distributed Raman amplification, it offers the possibility of a simpler and cost-effective system solution. In our experiment, we have shown that by carefully optimising the dispersion map of a standard fibre transmission system, the system degradation caused by double Rayleigh back scattering (DRBS) could be minimised, resulting in increasing the transmission distance. Distributed Raman amplification (DRA) has many advantages

over the lumped erbium amplifier: such as relaxing the constraint on the amplifier location within the dispersion map, improving the optical signal-to-noise ratio (OSNR) to accommodate add/drop sites, and adds only very little noise. Furthermore, it also enables signal transmission over a single flat ultra-wide band and lowers the cost of a system by having a reduced number of components. With these huge advantages, the advancements and challenges of Raman amplification will continue to grow rapidly, even for ultra long-haul submarine systems.

The advantages of all-optical signal processing for high bit rate systems are increasingly being recognised and have stimulated interest in the demonstration of all-optical switching and logic operations. The nonlinear optical loop mirror (NOLM) has gained wide acceptance as an ultra fast all optical data processing devices since its nonlinearity is ultra fast and losses are low. Although it may have many applications, in this thesis we have investigated its usage as saturable absorbers in removing low-power background dispersive waves through saturable absorption and as a tool for signal re-amplification and re-shaping (2R) in data transmission systems. The first experiment involves building a NOLM for 2R regeneration for both 10Gbit/s and 40Gbit/s transmission systems. It shows that by using autosoliton transmission in a dispersion-managed system with in-line NOLM, error-free propagation over 1100km at 10Gbit/s and 4000km at 40Gbit/s have been achieved in standard fibre without Forward Error Correction (FEC). This performance can be further improved by taking appropriate environmental measures.

Both the nonlinear-imbalance loop mirror (NILM) and nonlinear amplifying loop mirror (NALM) were also been built and tested for this purpose. The bit rate we used was 40Gbit/s. The NILM does not provide good results since both the eye diagrams and

BER are poorer than without the DILM. Moreover, we cannot locate the switching peak of the curve. Basically there are a few reasons for these poor results. Firstly, the length of the anomalous DSF and the normal DCF in the loop must be optimised. During the experiment, we did not perform any simulation but tried changing both fibre lengths randomly. Secondly, the anomalous DSF can be replaced by highly nonlinear fibres (HNLF) to enhance system performance by shortening the loop length, which will improve system stability and polarisation insensitivity. Thirdly, the anomalous DSF can also be replaced by polarisation maintaining fibres (PMF) to improve stability and receiver sensitivity. In the case of NALM, as we were using solitons in the loop, it required very high power to maintain the solitons. For 40Gbit/s bit-rate, the peak power is four times lower than 10Gbit/s. Therefore, although we have maximised all our power in all the EDFAs, we still did not have enough power to support the existence of solitons at 40Gbit/s, hence we could not manage to reach the peak of the switching curve. This means that the NALM is not being switched at all, resulting in poor performances. We believe that by changing the erbium-doped fibre within the NALM to one that has a higher gain, or using polarisation maintaining fibre (PMF) instead of DSF in the NALM to increase its stability, system performance can be improved. If we were able to obtain good results for regeneration, the propagating distance will be greatly increased since after every loop, we will be able to regenerate the signal, hence greatly increasing the results, similar to the situation for NOLM.

Next, both the NILM and NALM were placed near the receiver (after the demultiplexer) as saturable absorber to compare with the back-to-back performance. For the case of NILM, without any propagation, its performance is better than back-to-back. However, when propagating experiments were taken, the NILM tends to degrade the

system performance since it is very sensitive to input pulse width and it only works well for chirped-free input pulses. For recirculating loop experiments, with every propagating loop, the output pulse width and chirp will be slightly changed. Hence results after the NILM will be affected. Moreover, the peak of the switching curve was lost for this case due to poor switching from the NILM. In fact, we have tried to compress the pulse by using the dispersion-flattened fibre (DFF) before sending the signals into the recirculating loop, but as the pulse width and chirp still varied after every propagating loop, it was impossible to compress the signal after every loop.

It must be mentioned that the switching peak of every loop mirror is very important since best results will only be obtained at the position immediately after this peak. This applies to both NALM and NILM applications. We have introduced something new to the NALM by increasing the input power and using the anomalous dispersion-shifted fibres (DSF) in the NALM. The purpose was to create solitons in the loop. From the theory of nonlinear optical loop mirror technique, it is found that hyperbolic secant pulses or solitons are the best pulse shapes for complete switching since they have the same phase at all point across the pulse. The experimental results show that it does make a difference. Both the threshold voltage and eye-diagram for one recirculating loop looked better with NALM. However, for two loops or more, the BER started to deteriorate due to one or all of the following reasons. Firstly, the dispersion after each loop is not perfectly matched. Secondly, we did not have enough power to cause the solitons in more than one (or the first) loop, thus causing switching imperfection. Thirdly, the input signal to the NALM after one loop was quite noisy such that even with a NALM, it was not enough to recover the signal. We have even tried to increase the length of DSF in the NALM so that the soliton period will be reduced. But

this did not help the results since we needed more power to compensate for the dispersion from the DSF, causing further degradation of the signals. Therefore, we conclude that loop mirrors are better used as regenerators than saturable absorber at the receiver.

Future work that could be done to follow-up on this work on nonlinear optical loop mirrors include demonstration of all-optical fibre signal processing at 40Gbit/s. This involves wavelength conversion, 2R regeneration, OTDM demultiplexing and saturable absorbers at the receiver of the transmission system. Furthermore, its use as a WDM regenerator can also be explored and challenged. It must be emphasised that proper simulations need to be performed before building any of the loop mirrors to ensure efficient results.

Although the growth of fibre optics communication has slowed down considerably, due to the current world economy crisis, we believe that this work will produce a breakthrough if the future work explores and investigates the use of more advanced optical techniques to further enhance the systems performance in this exciting field.

Appendix A

Publications and patent

1) Z. Huang, A. Gray, Y.W.A. Lee, I.Y. Khrushchev, I. Bennion, "40Gbit/s transmission over transoceanic distance in a nonlinear switched-guided standard fibre link", *Optics Letter*, waiting for acceptance.

2) Z. Huang, A. Gray, Y.W.A. Lee, I.Y. Khrushchev, I. Bennion, "40Gbit/s transmission over 4000km of standard fibre using in-line nonlinear optical loop mirror", *European Conference on Optical Communication (ECOC 2003)*, Rimini, Italy, Sep 2003.

3) Z. Huang, A. Gray, Y.W.A. Lee, I.Y. Khrushchev, I. Bennion, "All-Raman amplified transmission at 40Gbit/s in standard single mode fibre", *European Conference on Lasers and Electro-Optics (CLEO EUROPE 2002)*, Munich, Germany, July 2003.

4) D. Giannone, Y.W.A. Lee, I.Y. Khrushchev, V.K. Mezentsev, and I. Bennion, "A tuneable second and third order dispersion post-compensator by non-uniformly strained chirped fibre grating", *European patent application no. 01308203.7*, Dec 2002.

5) D. Giannone, Y.W.A. Lee, I.Y Khrushchev, V.K. Mezentsev and I. Bennion, "Tunable compensation of second and third order dispersion by non-uniformly strained chirped fibre Bragg grating", *European Conference on Optical Communication (ECOC 2002)*, Copenhagen, Denmark, Sep 2002.

6) D. Giannone, Y.W.A. Lee, I.Y. Khrushchev, V.K. Mezentsev, I. Bennion, "A tuneable FBG-based dispersion compensator for high bit-rate optical transmission", *Photon 2002*, Cardiff, Wales, Sep 2002.

7) D. Giannone, Y.W.A. Lee, I.Y. Khrushchev, V.K. Mezentsev, I. Bennion, "Dispersion and slope compensation by mechanically tuned fiber Bragg grating", *IQEC/LAT 2002*, Moscow, Russia, Jun 2002.

8) D. Giannone, Y.W.A. Lee, I.Y. Khrushchev, V.K. Mezentsev, I. Bennion, "Tuneable compensator of dispersion and slope using non-uniformly strained chirped fibre grating", *Conference on Lasers and Electro-Optics (CLEO 2002)*, Long Beach, California, May 2002.

9) R.A. Ibbotson, Y.W.A. Lee, S.A. Feiven, I.Y. Khrushchev and K.J. Blow, "Robust 40 to 10 Gbit/s demultiplexer comprising a lithium niobate modulator and a passive non-linear fibre switch", *Non-Linear Guided Waves (NLGW2001)*, Clearwater, Florida, Mar 2001.